The Thesis committee for Noble Ariel Hatten
Certifies that this is the approved version of the following thesis:

A Critical Evaluation of Modern Low-Thrust, Feedback-Driven Spacecraft Control Laws

APPROVED BY

SUPERVISING COMMITTEE:

Cesar Ocampo, Supervisor

Maruthi Akella

A Critical Evaluation of Modern Low-Thrust, Feedback-Driven Spacecraft Control Laws

by

Noble Ariel Hatten, B.S.

THESIS

Presented to the Faculty of the Graduate School of

The University of Texas at Austin

in Partial Fulfillment

of the Requirements

for the Degree of

MASTER OF SCIENCE IN ENGINEERING

THE UNIVERSITY OF TEXAS AT AUSTIN

December 2012

For all those who made this possible.

Acknowledgments

First and foremost, I would like to thank my adviser, Dr. Cesar Ocampo, whose teaching first drew me to orbital mechanics as an undergraduate and whose direction led me to the topic discussed in this thesis. Also, I would like to thank Dr. Maruthi Akella for serving as a member of my thesis committee.

I am indebted to many for their generous help in the development of this document. In particular, Ricardo Leon Restrepo Gomez's Gradient Tuning Algorithm was an invaluable validation tool, and Nicholas Bradley participated in countless helpful discussions on topics ranging from Fortran bugs to thesis document organization to college football. Dr. Stefano Campagnola at the Japan Aerospace Exploration Agency, Dr. Anastassios Petropoulos at the Jet Propulsion Laboratory, and Nitin Arora at the Georgia Institute of Technology were also helpful in results verification.

I thank my family and friends for all they have done for me, both during the process of writing this thesis and in the years that preceded it. They gave me the opportunity and motivation to do all that I have done.

Finally, to my fiancee Gabby: I apologize for all those times I was grouchy when you walked in on me while I was working. Thank you for putting up with all of my frustrated outbursts.

A Critical Evaluation of Modern Low-Thrust, Feedback-Driven Spacecraft Control Laws

Noble Ariel Hatten, M.S.E.
The University of Texas at Austin, 2012

Supervisor: Cesar Ocampo

Low-thrust spacecraft trajectory optimization is often a difficult and time-consuming process. One alternative is to instead use a closed-loop, feedback-driven control law, which calculates the control using knowledge of only the current state and target state, and does not require the solution of a nonlinear optimization problem or system of nonlinear equations. Though generally suboptimal, such control laws are attractive because of the ease and speed with which they may be implemented and used to calculate feasible low-thrust maneuvers.

This thesis presents the theoretical foundations for seven modern low-thrust control laws based on control law "blending" and Lyapunov control theory for a particle spacecraft operating in an inverse-square gravitational field. The control laws are evaluated critically to determine those that present the best combinations of thoroughness of method and minimization of user input required. The three control laws judged to exhibit the most favorable

characteristics are then compared quantitatively through three numerical simulations. The simulations demonstrate the effectiveness of feedback-driven control laws, but also reveal several situations in which the control laws may perform poorly or break down altogether due to either theoretical shortcomings or numerical difficulties. The causes and effects of these issues are explained, and methods of handling them are proposed, implemented, and evaluated. Various opportunities for further work in the area are also described.

Table of Contents

Acknowledgments **v**

Abstract **vi**

List of Tables **xii**

List of Figures **xiv**

Chapter 1. Introduction **1**

1.1 Motivation 1

1.2 Problem Statement 4

1.3 Thesis Organization 5

Chapter 2. Orbital Mechanics **7**

2.1 Introduction 7

2.2 Coordinate System Definitions 8

2.2.1 Central Body Centered Inertial (CBCI) Coordinate System 8

2.2.2 VUW Coordinate System 8

2.2.3 $R\theta H$ Coordinate System 9

2.2.4 Transformations Between Coordinate Systems 10

2.2.4.1 Transformation Between VUW System and CBCI System 11

2.2.4.2 Transformation Between $R\theta H$ System and CBCI System 11

2.3 Thrust Direction Unit Vector and Angle Definitions 12

2.4 Keplerian Orbits 13

2.5 Variational Equations 17

2.6 Optimization of Variational Equations for Classical Orbital Elements 22

2.6.1 Semi-major Axis 23
2.6.2 Eccentricity 24
2.6.3 Inclination 24
2.6.4 Right Ascension of the Ascending Node 25
2.6.5 Argument of Periapsis 26
2.6.6 True Anomaly 28
2.7 Optimization of Variational Equations for Equinoctial Orbital Elements 28
2.7.1 Semi-major Axis 29
2.7.2 P_1 29
2.7.3 P_2 30
2.7.4 Q_1 30
2.7.5 Q_2 31
2.7.6 True Longitude 32
2.8 Minimization of Element Rates 32

Chapter 3. Descriptions and Qualitative Analyses of Low-Thrust Control Laws 33

3.1 Introduction 33
3.2 Lyapunov Control 34
3.2.1 LaSalle's Invariance Theorem 37
3.3 Petropoulos Control and Joseph Control 38
3.3.1 Petropoulos Control 38
3.3.2 Joseph Control 46
3.4 Naasz Control 49
3.5 Kluever Control and Ruggiero Control 55
3.5.1 Kluever Control 55
3.5.2 Ruggiero Control 57
3.6 Bombrun Control 59
3.7 Chang Control 61
3.8 Summary 64

Chapter 4. Numerical Simulation of Low-Thrust Control Laws 66
4.1 Introduction 66
4.2 Control Laws Modeled 66
4.3 Spacecraft State Propagation 67
4.4 Modifications to Control Laws 69
4.4.1 Modifications to Naasz Control 70
4.4.2 Modifications to Joseph Control 71
4.4.3 Modifications to Petropoulos Control 72
4.5 Coast Segments 72
4.6 Defining Convergence 75

Chapter 5. Numerical Results 78
5.1 Introduction 78
5.2 Equatorial Orbit to Polar Orbit Transfer 79
5.3 Low-Earth Orbit to Geosynchronous Orbit Transfer 88
5.4 Geostationary Transfer Orbit to Molniya Orbit Transfer 101
5.5 Summary 113

Chapter 6. Conclusions and Recommendations for Further Study 116
6.1 Conclusions 116
6.2 Recommendations for Further Study 122

Appendices 126

Appendix A. Supplemental Expressions 127
A.1 Derivatives of Classical Element Variational Equations with Respect to True Anomaly 127
A.2 Derivatives of Petropoulos's Penalty Function with Respect to the Classical Orbital Elements 129
A.3 Derivatives of Petropoulos's Scaling Function with Respect to the Classical Orbital Elements 129
A.4 Naasz's Fixed-Step State Propagator 130
A.5 Edelbaum's Low-Thrust Orbit Transfer Analysis 131

Appendix B. MATLAB Scripts **134**

B.1 Petropoulos Control: Derivatives of V_P with Respect to the Classical Element Set 134

Bibliography **140**

List of Tables

3.1 Summary of low-thrust control laws. 64
3.2 Summary of low-thrust control law weighting parameters and selection methods. 65

5.1 Control law abbreviations. 79
5.2 Equatorial orbit to polar orbit maneuver elements. 79
5.3 Equatorial orbit to polar orbit maneuver characteristics. . . . 80
5.4 Equatorial orbit to polar orbit maneuver convergence tolerances. 80
5.5 Equatorial orbit to polar orbit maneuver comparisons: continuous control application. 80
5.6 Equatorial orbit to polar orbit maneuver comparisons: absolute effectivity coasting criteria. 81
5.7 Equatorial orbit to polar orbit maneuver comparisons: relative effectivity coasting criteria. 81
5.8 Equatorial orbit to polar orbit maneuver comparisons: Naasz coasting criterion. 82
5.9 LEO-to-GEO maneuver elements. 88
5.10 LEO-to-GEO maneuver characteristics. 88
5.11 LEO-to-GEO maneuver convergence tolerances. 88
5.12 LEO-to-GEO maneuver comparisons: continuous control application. 89
5.13 LEO-to-GEO maneuver comparisons: absolute effectivity coasting criteria. 90
5.14 LEO-to-GEO maneuver comparisons: relative effectivity coasting criteria. 91
5.15 LEO-to-GEO maneuver comparisons: Naasz coasting criteria. 91
5.16 GTO-to-Molniya maneuver elements. 101
5.17 GTO-to-Molniya maneuver characteristics. 101
5.18 GTO-to-Molniya maneuver convergence tolerances. 102

5.19 GTO-to-Molniya maneuver comparisons: continuous control application. 105
5.20 GTO-to-Molniya maneuver comparisons: absolute effectivity coasting criteria. 105
5.21 GTO-to-Molniya maneuver comparisons: relative effectivity coasting criteria. 106
5.22 GTO-to-Molniya maneuver comparisons: Naasz coasting criteria. 106

List of Figures

2.1 The CBCI, VUW, and $R\theta H$ coordinate systems. 10

2.2 Angles used to describe the spacecraft control direction in the VUW system and the $R\theta H$ system. 13

5.1 Equatorial orbit to polar orbit maneuver comparisons: semi-major axis evolution, continuous control application. Note: Only two curves are visible because all evolutions but P are identical. 85

5.2 Equatorial orbit to polar orbit maneuver comparisons: inclination evolution, continuous control application. Note: Only two curves are visible because all evolutions but P are identical. . . 86

5.3 Equatorial orbit to polar orbit maneuver comparisons: eccentricity evolution, continuous control application. Note: Only two curves are visible because all evolutions but P are identical. 87

5.4 LEO-to-GEO maneuver comparisons: semi-major axis evolution, continuous control application. 94

5.5 LEO-to-GEO maneuver comparisons: inclination evolution, continuous control application. 95

5.6 LEO-to-GEO maneuver comparisons: eccentricity evolution, continuous control application. 96

5.7 LEO-to-GEO maneuver comparisons: semi-major axis evolution, $\eta_{a_{threshold}} = 0.9$. 97

5.8 LEO-to-GEO maneuver comparisons: inclination evolution, $\eta_{a_{threshold}} = 0.9$. 98

5.9 LEO-to-GEO maneuver comparisons: eccentricity evolution, $\eta_{a_{threshold}} = 0.9$. 99

5.10 LEO-to-GEO maneuver comparisons: propellant mass usage evolution, $\eta_{a_{threshold}} = 0.9$. 100

5.11 GTO-to-Molniya maneuver comparisons: semi-major axis evolution, continuous control application. 108

5.12 GTO-to-Molniya maneuver comparisons: inclination evolution, continuous control application. 109

5.13 GTO-to-Molniya maneuver comparisons: eccentricity evolution, continuous control application. 110
5.14 GTO-to-Molniya maneuver comparisons: right ascension of the ascending node evolution, continuous control application. Note that Petropoulos's control law yields convergence to $\Omega = -180°$, which is equivalent to $\Omega = 180°$. 111
5.15 GTO-to-Molniya maneuver comparisons: argument of periapsis evolution, continuous control application. 112

Chapter 1

Introduction

1.1 Motivation

The problem of calculating the control required to perform a low-thrust[1] orbit transfer maneuver has historically proved very difficult [21]. It is desirable to optimize these trajectories with respect to one or more performance indices, often required fuel mass or required maneuver time. However, even as computing capabilities continue to improve, producing an optimal low-thrust trajectory, either by a direct or indirect method, is far from routine and can still be a difficult and time-consuming ordeal. Direct optimization methods – which, as the name suggests, search directly for control directions that optimize a performance index – are adversely affected by the long time span required by low-thrust maneuvers. For example, a direct method may allow for the control direction to be piecewise-constant in time and change discontinuously at predetermined points in time. Each of these control directions becomes a variable that must be optimized; for a maneuver that may last years, this can lead to a very large number of variables and long computation

[1]The term "low-thrust" is difficult to define, but generally refers to propulsion systems that provide significantly smaller thrust-to-weight ratios than those of traditional chemical propulsion systems and remain active for significant percentages of maneuver times (e.g. ion thrusters).

times if the solution is to have sufficient resolution. Furthermore, many standard optimization techniques require that an initial guess of each optimization variable be provided by the user as a starting point for an iterative solution method, and the provision of inaccurate initial guesses often causes algorithms to fail. Determination of a sufficiently accurate initial guess for, say, a control direction midway through a maneuver that requires hundreds of revolutions about a central body can itself be a laborious and time-consuming matter.

Indirect optimization methods, on the other hand, are based on the calculus of variations [11] and so do not require the use of very large numbers of optimization variables. However, this does not necessarily result in an easier problem, as indirect methods *do* require the optimization of the notoriously difficult-to-guess costates. The costates determine the control direction at every time on the transfer trajectory, and because they are propagated in time just like the actual spacecraft states, the costates can only be optimized at a single point along each trajectory segment. Since a low-thrust maneuver generally consists of a single trajectory segment many days in length, the terminal spacecraft states are very highly dependent on the values of the costates at the point of optimization. Thus, the indirect problem's extreme sensitivity to initial guesses of the optimization variables makes its solution difficult and time consuming, as well.

One alternative to either direct or indirect optimization methods is a closed-loop, feedback-driven (CLFD) control law. In general, a maneuver prescribed by this type of control law is suboptimal. Nevertheless, a CLFD

control law is often a desirable method of generating a low-thrust transfer trajectory for several reasons. First, unlike direct and indirect optimization methods, a CLFD control law requires knowledge of only the current spacecraft state and the target spacecraft state in order to determine the control that should be applied. Second, most CLFD spacecraft control laws do not require the solution of a system of nonlinear equations in order to determine the control. This means that the use of an iterative nonlinear solver and the determination of accurate initial guesses for variables are unneeded. Together, these two facts mean that:

1. Because no iteration is required, a maneuver using a CLFD control law requires significantly less time to simulate numerically than a maneuver using an optimization technique. This makes CLFD control laws particularly suitable to preliminary trajectory design in which trade studies comparing large numbers of possible maneuvers must be performed.

2. Because no variables need be guessed, a well-designed CLFD control law requires less up-front user effort than an optimization technique. (As will be explored in this thesis, however, this generally does not mean that analyst discretion is eliminated entirely from the trajectory design process.)

Thus, given the advantages of CLFD control laws and the difficulties in computing optimal low-thrust trajectories, coupled with the ever-increasing

utility of low-thrust spacecraft propulsion systems, it is no surprise that considerable attention has been paid to the development of low-thrust CLFD control laws. The goal of this thesis is to provide a thorough, critical comparison of a representative sampling of modern low-thrust CLFD control laws from two points of view: first, a qualitative comparison of the theoretical foundations and the strengths and weaknesses of the control laws, and, second, a quantitative comparison of the performance of several of the most promising control laws discussed by means of multiple numerical simulations.

1.2 Problem Statement

The problem explored by this thesis may be described in its most basic form as: Given a spacecraft capable of producing control acceleration in a known elliptical orbit about a central body, how should the control be directed in order to maneuver the spacecraft to a different, known elliptical orbit about the same central body?

Within this framework, the problem may be detailed further by the following assumptions and restrictions:

1. The gravitational attraction between the central body and the spacecraft and the control force of the spacecraft are the only forces that act on the spacecraft. Other forces, such as non-spherical-central-body effects and solar radiation pressure, are not considered.

2. The state of the spacecraft at the beginning of the maneuver is fully

defined, but only the target orbit is specified – the location of spacecraft arrival within the target orbit is free.

3. The maneuver flight time is free in the sense that no equality constraints are placed on the time of flight. However, from a practical standpoint, maximum flight times are sometimes imposed to prevent excessively time-consuming maneuvers.

4. The central body and the spacecraft are both modeled as point masses.

5. The mass of the spacecraft is assumed to be negligible in comparison to the mass of the central body.

6. The control acceleration produced by the spacecraft is constrained to be "low-thrust," as discussed in Section 1.1.

7. The spacecraft propulsion system is thrust-limited and has a constant specific impulse.

8. The manner in which the control acceleration is calculated is restricted to be a CLFD control law, as discussed in Section 1.1.

1.3 Thesis Organization

Chapter 2 introduces the background theory necessary to develop the control laws discussed in this thesis. Topics covered include coordinate system definitions, the variational equations for a spacecraft in a two-body gravita-

tional field experiencing a disturbing acceleration, and the determination of the disturbing acceleration required to extremize the variational equations.

Chapter 3 describes the theoretical and algorithmic bases for seven low-thrust, CLFD spacecraft control laws. The strengths and weaknesses of each control law are evaluated. Because several of the control laws are derived using control Lyapunov functions, the chapter commences with a brief description of Lyapunov control theory.

Three of the control laws introduced in Chapter 3 are also compared quantitatively through numerical simulations. Chapter 4 discusses the methods used to implement the control laws and several modifications made to facilitate direct comparison and optimal performance. Chapter 5 then presents the results of using the control laws to perform three orbit transfer maneuvers. The performances of the control laws – from the perspectives of both maneuver optimality and algorithm ease-of-use – are discussed and compared against one another. Causes of poor performance – or even failure – are also discussed, and several remedies to improve performance in these situations are suggested.

Finally, Chapter 6 presents conclusions that may be drawn from this thesis and several recommendations for extensions of this work.

Chapter 2

Orbital Mechanics

2.1 Introduction

This chapter presents the orbital mechanics necessary to derive the low-thrust control laws presented in Chapter 3. First, all coordinate systems used in this thesis are defined, as are the unit vectors and angles used to define the spacecraft control direction. Next, several methods of characterizing Keplerian orbits are summarized, each of which is used by at least one of the control laws discussed in this thesis. The variational equations that govern the evolution of Keplerian orbits in the presence of a disturbing acceleration – in this case due to the spacecraft's control system – are then introduced for each of these characterizations. Finally, the variational equations are extremized with respect to both control direction and location on an orbit to obtain the optimal rates of change of orbital parameters and the corresponding control directions, quantities important to the development of several of the control laws discussed in Chapter 3.

2.2 Coordinate System Definitions

2.2.1 Central Body Centered Inertial (CBCI) Coordinate System

The origin of the central body centered inertial (CBCI) coordinate system is located at the center of mass of the central body. (Since the central body is assumed to be approximated by a point mass throughout this thesis, the origin coincides with the location of the point mass.) The third axis points in the direction of the north pole of the body, and the first axis and second axis lie in the equatorial plane and are perpendicular to one another in such a manner that the system is right-handed. Unit vectors for the CBCI system are $\hat{\boldsymbol{e}}_i$, $\hat{\boldsymbol{e}}_j$, and $\hat{\boldsymbol{e}}_k$ for the first, second, and third axes, respectively. It may be noted that, if the central body is assumed to be the earth and $\hat{\boldsymbol{e}}_i$ is aligned with the vernal equinox direction, the CBCI system becomes identical to the commonly used Earth centered inertial (ECI) system. However, because the analysis presented in this thesis does not require that the central body be the earth, the name CBCI system is used instead of ECI system.

2.2.2 VUW Coordinate System

The origin of the VUW system is the center of mass of the spacecraft. (Since the spacecraft is assumed to be approximated by a point mass throughout this thesis, the origin coincides with the location of the point mass.) The first axis points in the direction of the instantaneous spacecraft velocity vector, and the third axis points in the direction of the instantaneous spacecraft angular momentum vector. The second axis is defined such that the system

is right-handed. The unit vectors for the VUW system are $\hat{\boldsymbol{e}}_v$, $\hat{\boldsymbol{e}}_u$, and $\hat{\boldsymbol{e}}_w$ for the first, second, and third axes, respectively.

2.2.3 $R\theta H$ Coordinate System

The origin of the $R\theta H$ or polar coordinate system is the center of mass of the spacecraft. The first axis points in the direction of the instantaneous spacecraft position vector (relative to the central body), and the third axis points in the direction of the instantaneous spacecraft angular momentum vector. The second axis is defined such that the system is right-handed. The unit vectors for the $R\theta H$ system are $\hat{\boldsymbol{e}}_r$, $\hat{\boldsymbol{e}}_\theta$, and $\hat{\boldsymbol{e}}_h$. The unit vectors of the CBCI, VUW, and $R\theta H$ coordinate systems are shown in Figure 2.1, in which $\boldsymbol{r}$ is the position vector of the spacecraft relative to the central body.

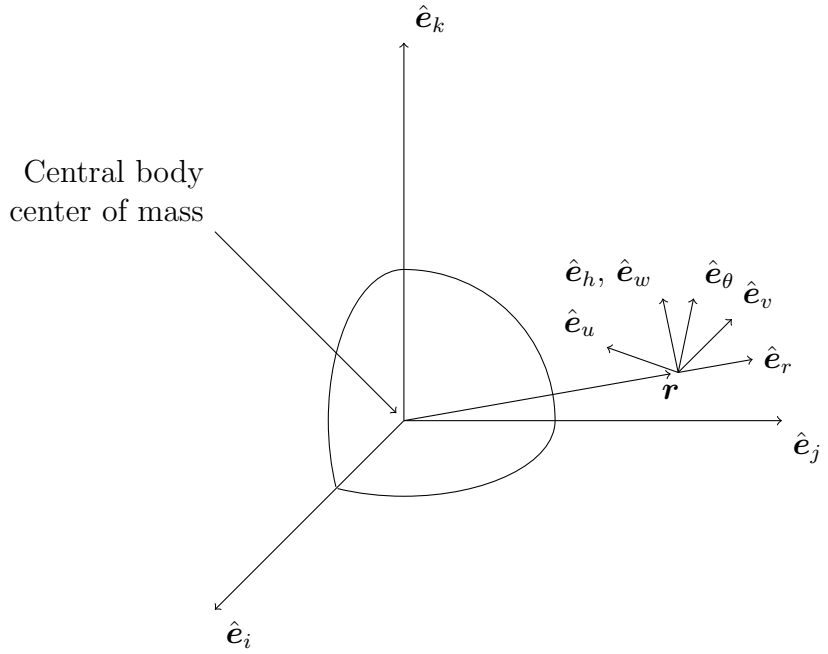

Figure 2.1: The CBCI, VUW, and $R\theta H$ coordinate systems.

2.2.4 Transformations Between Coordinate Systems

Rotation matrices are used to express a vector given in one system in a different system. A generic vector $\boldsymbol{\zeta}$, expressed in a generic ABC coordinate system, may be expressed as $\boldsymbol{\zeta}'$ in a second generic system, the DEF system, by performing

$$\boldsymbol{\zeta}' = \boldsymbol{R}^{ABC \to DEF} \boldsymbol{\zeta}, \tag{2.1}$$

where $\boldsymbol{R}^{ABC \to DEF}$ is a square matrix whose dimensions are each equal to the dimension of $\boldsymbol{\zeta}$ [2]. Because transformation matrices are orthonormal, the

inverse operation is simply

$$\boldsymbol{\zeta} = \left(\boldsymbol{R}^{ABC\rightarrow DEF}\right)^T \boldsymbol{\zeta}'. \tag{2.2}$$

2.2.4.1 Transformation Between VUW System and CBCI System

The transformation matrix used to express a vector given in the VUW system in the CBCI system is given by

$$\boldsymbol{R}^{VUW\rightarrow\text{CBCI}} = \begin{pmatrix} \frac{\boldsymbol{v}^T\hat{\boldsymbol{e}}_i}{v} & \frac{(\boldsymbol{h}\times\boldsymbol{v})^T\hat{\boldsymbol{e}}_i}{|\boldsymbol{h}\times\boldsymbol{v}|} & \frac{\boldsymbol{h}^T\hat{\boldsymbol{e}}_i}{h} \\ \frac{\boldsymbol{v}^T\hat{\boldsymbol{e}}_j}{v} & \frac{(\boldsymbol{h}\times\boldsymbol{v})^T\hat{\boldsymbol{e}}_j}{|\boldsymbol{h}\times\boldsymbol{v}|} & \frac{\boldsymbol{h}^T\hat{\boldsymbol{e}}_j}{h} \\ \frac{\boldsymbol{v}^T\hat{\boldsymbol{e}}_k}{v} & \frac{(\boldsymbol{h}\times\boldsymbol{v})^T\hat{\boldsymbol{e}}_k}{|\boldsymbol{h}\times\boldsymbol{v}|} & \frac{\boldsymbol{h}^T\hat{\boldsymbol{e}}_k}{h} \end{pmatrix}, \tag{2.3}$$

where $\boldsymbol{v}$ is the spacecraft velocity vector with respect to the central body and $\boldsymbol{h} = \boldsymbol{r} \times \boldsymbol{v}$ is the spacecraft's specific angular momentum vector. (The operator "$\times$" represents the matrix cross product.) The notation $|\boldsymbol{\zeta}|$ represents the Euclidean norm of a vector, and is also represented more succinctly by $\zeta = |\boldsymbol{\zeta}| = \left(\boldsymbol{\zeta}^T\boldsymbol{\zeta}\right)^{\frac{1}{2}}$.

2.2.4.2 Transformation Between $R\theta H$ System and CBCI System

The transformation matrix used to express a vector given in the $R\theta H$ system in the CBCI system is given by

$$\boldsymbol{R}^{R\theta H\rightarrow \text{CBCI}} = \begin{pmatrix} \frac{\boldsymbol{r}^T\hat{\boldsymbol{e}}_i}{r} & \frac{(\boldsymbol{h}\times\boldsymbol{r})^T\hat{\boldsymbol{e}}_i}{|\boldsymbol{h}\times\boldsymbol{r}|} & \frac{\boldsymbol{h}^T\hat{\boldsymbol{e}}_i}{h} \\ \frac{\boldsymbol{r}^T\hat{\boldsymbol{e}}_j}{r} & \frac{(\boldsymbol{h}\times\boldsymbol{r})^T\hat{\boldsymbol{e}}_j}{|\boldsymbol{h}\times\boldsymbol{r}|} & \frac{\boldsymbol{h}^T\hat{\boldsymbol{e}}_j}{h} \\ \frac{\boldsymbol{r}^T\hat{\boldsymbol{e}}_k}{r} & \frac{(\boldsymbol{h}\times\boldsymbol{r})^T\hat{\boldsymbol{e}}_k}{|\boldsymbol{h}\times\boldsymbol{r}|} & \frac{\boldsymbol{h}^T\hat{\boldsymbol{e}}_k}{h} \end{pmatrix}. \tag{2.4}$$

2.3 Thrust Direction Unit Vector and Angle Definitions

The direction of the spacecraft thrust vector in three-dimensional space may be defined either by a unit vector or by a set of two angles. Two primary pairs of angles are used in this thesis: α_{VUW} and β_{VUW}, defined by their relationship with the control direction unit vector in the VUW system; and $\alpha_{R\theta H}$ and $\beta_{R\theta H}$, defined by their relationship with the control direction unit vector in the $R\theta H$ system. The relationships between the unit vectors and thrust angles are

$$\hat{\boldsymbol{u}}_{VUW} = \begin{pmatrix} \cos(\alpha_{VUW})\cos(\beta_{VUW}) \\ \sin(\alpha_{VUW})\cos(\beta_{VUW}) \\ \sin(\beta_{VUW}) \end{pmatrix} \tag{2.5}$$

$$\hat{\boldsymbol{u}}_{R\theta H} = \begin{pmatrix} \sin(\alpha_{R\theta H})\cos(\beta_{R\theta H}) \\ \cos(\alpha_{R\theta H})\cos(\beta_{R\theta H}) \\ \sin(\beta_{R\theta H}) \end{pmatrix}. \tag{2.6}$$

The angle α_{VUW} is the control angle in the instantaneous orbital plane, measured from $\hat{\boldsymbol{e}}_v$ and positive toward the positive $\hat{\boldsymbol{e}}_u$ axis; its domain is $\alpha_{VUW} \in [0, 2\pi)$. β_{VUW} is the out-of-plane control angle, measured off the instantaneous orbital plane and positive in the direction of the instantaneous angular momentum; its domain is $\beta_{VUW} \in [-\frac{\pi}{2}, \frac{\pi}{2}]$. $\alpha_{R\theta H}$ is also a measurement of the

control angle in the instantaneous orbital plane. However, it is measured from $\hat{\boldsymbol{e}}_\theta$, positive toward the positive $\hat{\boldsymbol{e}}_r$ axis. $\beta_{R\theta H}$ is equivalent to β_{VUW}. The control angles are depicted in Figure 2.2.

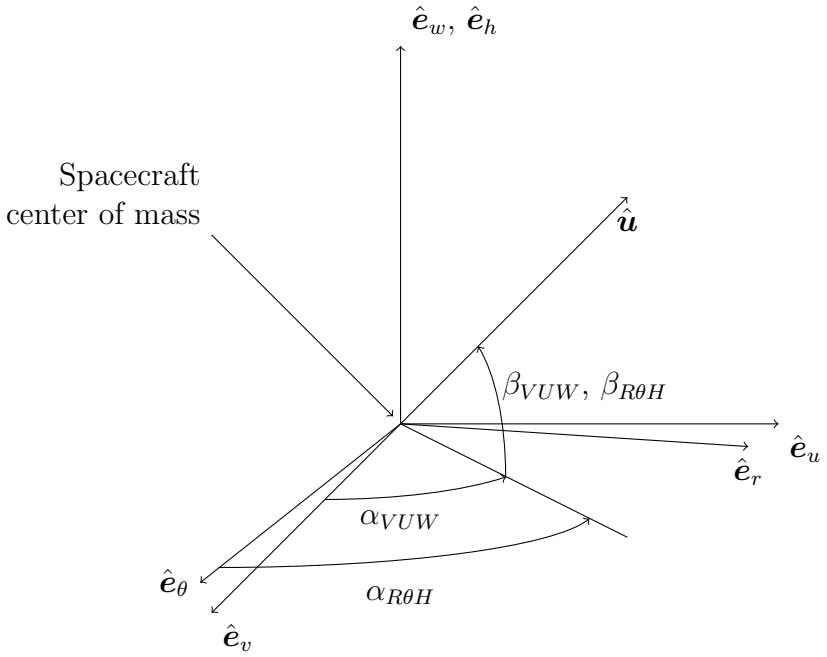

Figure 2.2: Angles used to describe the spacecraft control direction in the VUW system and the $R\theta H$ system.

2.4 Keplerian Orbits

The equation of motion of a particle subject only to the gravitational force of a central gravitational field may be written as [2]

$$\ddot{\boldsymbol{r}} = -\frac{GM_{CB}}{r^3}\boldsymbol{r} = -\frac{\mu}{r^3}\boldsymbol{r}, \tag{2.7}$$

under the assumption that the mass of the particle is insignificant compared to the mass of the central body. In (2.7), $\ddot{\boldsymbol{r}}$ is the second time derivative of $\boldsymbol{r}$, G is the universal gravitational constant, M_{CB} is the mass of the central body, and $\mu = GM_{CB}$ is the gravitational parameter of the central body. In such a force field, closed orbits take the form of ellipses, which may be characterized in several ways. Three methods are of interest in this thesis: the Keplerian or classical orbital element set, the equinoctial orbital element set, and the angular momentum vector and eccentricity vector. The classical element set is comprised of semi-major axis a, eccentricity e, inclination i, right ascension of the ascending node Ω, and argument of periapsis ω. Another element, such as true anomaly ν, is required to specify the particle's location within a particular orbit [2].

A drawback of the classical element set is its lack of robustness for all types of orbits [2, 3]. For circular orbits ($e = 0$), ω and ν are undefined; for equatorial orbits ($i = 0$), Ω and ω are undefined. One method of eliminating these deficiencies is to use instead the equinoctial element set [3]: a, P_1, P_2, Q_1, and Q_2, which may be related to the classical element set by

$$a = a \tag{2.8}$$

$$P_1 = e\sin(\varpi) \tag{2.9}$$

$$P_2 = e\cos(\varpi) \tag{2.10}$$

$$Q_1 = \tan\left(\frac{1}{2}i\right)\sin(\Omega) \tag{2.11}$$

$$Q_2 = \tan\left(\frac{1}{2}i\right)\cos(\Omega), \tag{2.12}$$

where $\varpi = \Omega + \omega$ is the longitude of periapsis. Recovery of the classical element set from the equinoctial set is achieved through the relations [3, 17]

$$a = a \tag{2.13}$$

$$e = \sqrt{P_1^2 + P_2^2} \tag{2.14}$$

$$i = 2\ \text{atan}\left(\sqrt{Q_1^2 + Q_2^2}\right) \tag{2.15}$$

$$\Omega = \text{atan}\left(\frac{Q_1}{Q_2}\right) \tag{2.16}$$

$$\omega = \text{atan}\left(\frac{P_1}{P_2}\right) - \text{atan}\left(\frac{Q_1}{Q_2}\right). \tag{2.17}$$

The equinoctial elements only exhibit singularities for the case in which $i = 180°$ [17].

A third method of characterizing an orbit is through the use of the specific angular momentum vector $\boldsymbol{h}$ and eccentricity vector $\boldsymbol{e}$, given by [3]

$$\boldsymbol{h} = \boldsymbol{r} \times \boldsymbol{v} \tag{2.18}$$

$$\boldsymbol{e} = \frac{1}{\mu}[\boldsymbol{v} \times (\boldsymbol{r} \times \boldsymbol{v})] - \frac{\boldsymbol{r}}{r}. \tag{2.19}$$

The vectors $\boldsymbol{h}$ and $\boldsymbol{e}$ are constant on a Keplerian orbit and together define that orbit, although, as with the classical and equinoctial element sets, another parameter is required to specify the particle's location within that orbit.[1] This method of orbit classification encounters no singularities. Transformation between $\boldsymbol{h}$ and $\boldsymbol{e}$ and the classical element set is accomplished via the relations [2, 18]

$$a = \frac{|\boldsymbol{h}|^2}{\mu(1 - |\boldsymbol{e}|^2)} \tag{2.20}$$

$$e = |\boldsymbol{e}| \tag{2.21}$$

$$i = \text{atan}\left(\frac{\sqrt{(\boldsymbol{h}^T\hat{\boldsymbol{e}}_i)^2 + (\boldsymbol{h}^T\hat{\boldsymbol{e}}_j)^2}}{\boldsymbol{h}^T\hat{\boldsymbol{e}}_k}\right) \tag{2.22}$$

$$\Omega = \text{atan}\left(\frac{\boldsymbol{n}^T\hat{\boldsymbol{e}}_j}{\boldsymbol{n}^T\hat{\boldsymbol{e}}_i}\right) \tag{2.23}$$

$$\omega = \pm\text{atan}\left(\frac{|\boldsymbol{n} \times \boldsymbol{e}|}{\boldsymbol{n}^T\boldsymbol{e}}\right), \tag{2.24}$$

where $\boldsymbol{n} = \hat{\boldsymbol{e}}_k \times \boldsymbol{h}$ is the node vector and the sign of ω is set equal to the sign of $(\boldsymbol{n} \times \boldsymbol{e})^T\boldsymbol{h}$.

[1] It should be noted that $\boldsymbol{h}$ and $\boldsymbol{e}$ comprise six variables while the classical and equinoctial element sets require only five variables to define an orbit. This discrepancy is rectified by recalling that $\boldsymbol{h}$ and $\boldsymbol{e}$ are not independent: $\boldsymbol{h}$ is perpendicular to the orbital plane and $\boldsymbol{e}$ lies in the orbital plane so that $\boldsymbol{h}^T\boldsymbol{e} = 0$.

While the equinoctial element set and the $\boldsymbol{h}$ and $\boldsymbol{e}$ orbit representation improve on the classical element set by introducing fewer potential singularities, a significant drawback of both of these orbit characterizations when considering them for use in an orbit transfer scheme is the coupling exhibited when transforming between these elements and the classical element set. If a full orbit transfer is desired – that is, the target orbit is completely specified – this produces no problem. However, it is very often the case that a mission requires the targeting of only a subset of the classical element set. For example, a mission may require achieving a specified a, e, and i but have no requirements on Ω and ω. In this situation, using the equinoctial element set or the $\boldsymbol{h}$ and $\boldsymbol{e}$ set to define the target orbit places unnecessary restrictions on the target values of Ω and ω that will likely increase propellant mass and/or time required to achieve the target orbit.

2.5 Variational Equations

The equation of motion of a particle subject to a disturbing acceleration in a central gravitational field may be written as [3]

$$\ddot{\boldsymbol{r}} + \frac{\mu}{r^3}\boldsymbol{r} = \boldsymbol{a}_d, \tag{2.25}$$

where $\boldsymbol{a}_d$ is the disturbing acceleration vector. For the control laws presented in this thesis, the disturbing acceleration is always taken to be the spacecraft control acceleration. Therefore, in the derivation of control laws, the disturbing

acceleration is written as $\boldsymbol{u}$. For generality, however, the notation $\boldsymbol{a}_d$ is used for the derivation of the variational equations themselves.

If $\boldsymbol{a}_d$ is written in the $R\theta H$ coordinate system, then the time derivatives of the classical orbital elements are collectively referred to as Gauss's form of the Lagrange Planetary Equations [3, 17]:

$$\frac{\mathrm{d}\Omega}{\mathrm{d}t} = \frac{r\sin(\omega+\nu)}{h\sin(i)}a_{dh} \tag{2.26}$$

$$\frac{\mathrm{d}i}{\mathrm{d}t} = \frac{r\cos(\omega+\nu)}{h}a_{dh} \tag{2.27}$$

$$\frac{\mathrm{d}\omega}{\mathrm{d}t} = \frac{1}{he}\left[-p\cos(\nu)a_{dr} + (p+r)\sin(\nu)a_{d\theta}\right] - \frac{r\sin(\omega+\nu)\cos(i)}{h\sin(i)}a_{dh} \tag{2.28}$$

$$\frac{\mathrm{d}a}{\mathrm{d}t} = \frac{2a^2}{h}\left(e\sin(\nu)a_{dr} + \frac{p}{r}a_{d\theta}\right) \tag{2.29}$$

$$\frac{\mathrm{d}e}{\mathrm{d}t} = \frac{1}{h}\{p\sin(\nu)a_{dr} + [(p+r)\cos(\nu) + re]a_{d\theta}\} \tag{2.30}$$

$$\frac{\mathrm{d}\nu}{\mathrm{d}t} = \frac{h}{r^2} + \frac{1}{he}[p\cos(\nu)a_{dr} - (p+r)\sin(\nu)a_{d\theta}] \tag{2.31}$$

$$\frac{\mathrm{d}\nu_0}{\mathrm{d}t} = \frac{1}{he}[p\cos(\nu)a_{dr} - (p+r)\sin(\nu)a_{d\theta}] \tag{2.32}$$

$$\frac{\mathrm{d}M}{\mathrm{d}t} = \sqrt{\frac{\mu}{a^3}} + \frac{b}{ahe}\left[(p\cos(\nu) - 2re)a_{dr} - (p+r)\sin(\nu)a_{d\theta}\right] \tag{2.33}$$

$$\frac{\mathrm{d}M_0}{\mathrm{d}t} = \frac{b}{ahe}\left[(p\cos(\nu) - 2re)a_{dr} - (p+r)\sin(\nu)a_{d\theta}\right], \tag{2.34}$$

where $p = a(1-e^2)$ is the semi-latus rectum, $b = a\sqrt{1-e^2}$ is the semi-minor axis, and M is the mean anomaly. The quantities ν_0 and M_0 are the true anomaly at epoch and mean anomaly at epoch, respectively, and are introduced to remove the secular terms from (2.31) and (2.33). This is accomplished by setting the epoch time to the time of periapsis passage.

For utilization in low-thrust control laws, it is convenient to express these equations in a matrix-vector form. If each of the variational equations is written as

$$\frac{\mathrm{d}\mathcal{O}}{\mathrm{d}t} = \dot{\mathcal{O}}_r a_{dr} + \dot{\mathcal{O}}_\theta a_{d\theta} + \dot{\mathcal{O}}_h a_{dh}, \quad \mathcal{O} = a, e, i, \Omega, \omega, M_0, \tag{2.35}$$

then Gauss's form of the Lagrange Planetary Equations (using M_0 to define location on the orbit) may be rewritten as

$$\begin{pmatrix} \dot{a} \\ \dot{e} \\ \dot{i} \\ \dot{\Omega} \\ \dot{\omega} \\ \dot{M}_0 \end{pmatrix} = \boldsymbol{A}\boldsymbol{a}_d, \tag{2.36}$$

where the elements of the matrix $\boldsymbol{A}$ are the coefficients of the disturbing acceleration terms in the variational equations.

In the implementation of several control laws, it is necessary to obtain the derivatives of the variational equations for the slow-moving classical elements with respect to true anomaly; these expressions are given in Appendix A.1.

The time derivatives of the equinoctial elements may be written as [3]

$$\frac{\mathrm{d}a}{\mathrm{d}t} = \frac{2a^2}{h}\left[(P_2\sin(L) - P_1\cos(L))a_{dr} + \frac{p}{r}a_{d\theta}\right] \tag{2.37}$$

$$\begin{aligned}\frac{\mathrm{d}P_1}{\mathrm{d}t} = \frac{r}{h}\Big\{&-\frac{p}{r}\cos(L)a_{dr} + \left[P_1 + \left(1+\frac{p}{r}\right)\sin(L)\right]a_{d\theta} - \cdots \\ &\cdots - P_2(Q_1\cos(L) - Q_2\sin(L))a_{dh}\Big\}\end{aligned} \tag{2.38}$$

$$\begin{aligned}\frac{\mathrm{d}P_2}{\mathrm{d}t} = \frac{r}{h}\Big\{&\frac{p}{r}\sin(L)a_{dr} + \left[P_2 + \left(1+\frac{p}{r}\right)\cos(L)\right]a_{d\theta} + \cdots \\ &\cdots + P_1(Q_1\cos(L) - Q_2\sin(L))a_{dh}\Big\}\end{aligned} \tag{2.39}$$

$$\frac{\mathrm{d}Q_1}{\mathrm{d}t} = \frac{r}{2h}\left(1+Q_1^2+Q_2^2\right)\sin(L)a_{dh} \tag{2.40}$$

$$\frac{\mathrm{d}Q_2}{\mathrm{d}t} = \frac{r}{2h}\left(1+Q_1^2+Q_2^2\right)\cos(L)a_{dh} \tag{2.41}$$

$$\begin{aligned}\frac{\mathrm{d}l}{\mathrm{d}t} = n - \frac{r}{h}\Bigg\{&\left[\frac{a}{a+b}\left(\frac{p}{r}\right)(P_1\sin(L) + P_2\cos(L)) + \frac{2b}{a}\right]a_{dr} + \cdots \\ &\cdots + \frac{a}{a+b}\left(1+\frac{p}{r}\right)(P_1\cos(L) - P_2\sin(L))a_{d\theta} + \cdots \\ &\cdots + (Q_1\cos(L) - Q_2\sin(L))a_{dh}\Bigg\}\end{aligned} \tag{2.42}$$

$$\begin{aligned}\frac{\mathrm{d}l_0}{\mathrm{d}t} = -\frac{r}{h}\Bigg\{&\left[\frac{a}{a+b}\left(\frac{p}{r}\right)(P_1\sin(L) + P_2\cos(L)) + \frac{2b}{a}\right]a_{dr} + \cdots \\ &\cdots + \frac{a}{a+b}\left(1+\frac{p}{r}\right)(P_1\cos(L) - P_2\sin(L))a_{d\theta} + \cdots \\ &\cdots + (Q_1\cos(L) - Q_2\sin(L))a_{dh}\Bigg\},\end{aligned} \tag{2.43}$$

where $L = \varpi + \nu$ is the true longitude, $b = a\sqrt{1-P_1^2-P_2^2}$, $l = \varpi + M$ is the mean longitude, and $n = \sqrt{\frac{\mu}{a^3}}$ is the mean motion. The mean longitude at epoch, $l_0 = \varpi + M_0$, is introduced to remove the secular term in (2.42). As was done with the classical element set, the matrix-vector form of the equinoctial variational equations may be written as

$$\begin{pmatrix} \dot{a} \\ \dot{P}_1 \\ \dot{P}_2 \\ \dot{Q}_1 \\ \dot{Q}_2 \\ \dot{l}_0 \end{pmatrix} = \boldsymbol{B}\boldsymbol{a}_d, \tag{2.44}$$

where the elements of the matrix $\boldsymbol{B}$ are the coefficients of the disturbing acceleration terms in the variational equations.

The variational equations for $\boldsymbol{h}$ and $\boldsymbol{e}$ may be written as [3]

$$\frac{\mathrm{d}\boldsymbol{h}}{\mathrm{d}t} = \boldsymbol{r} \times \boldsymbol{a}_d \tag{2.45}$$

$$\mu\frac{\mathrm{d}\boldsymbol{e}}{\mathrm{d}t} = \boldsymbol{a}_d \times (\boldsymbol{r} \times \boldsymbol{v}) + (\boldsymbol{a}_d \times \boldsymbol{r}) \times \boldsymbol{v}. \tag{2.46}$$

(Note that the gravitational parameter μ is assumed to be constant in time and is therefore removed from the differentiation.)

Like those of the orbital element sets, the variational equations for $\boldsymbol{h}$ and $\boldsymbol{e}$ may also be written in matrix-vector form:

$$\begin{pmatrix} \dot{\boldsymbol{h}} \\ \mu\dot{\boldsymbol{e}} \end{pmatrix} = \begin{pmatrix} 0 & -r_3 & r_2 \\ r_3 & 0 & -r_1 \\ -r_2 & r_1 & 0 \\ -(r_2v_2 + r_3v_3) & (2r_1v_2 - r_2v_1) & (2r_1v_3 - r_3v_1) \\ (2r_2v_1 - r_1v_2) & -(r_1v_1 + r_3v_3) & (2r_2v_3 - r_3v_2) \\ (2r_3v_1 - r_1v_3 & (2r_3v_2 - r_2v_3) & -(r_1v_1 + r_2v_2) \end{pmatrix} \begin{pmatrix} a_{d_1} \\ a_{d_2} \\ a_{d_3} \end{pmatrix}. \tag{2.47}$$

In (2.47), the non-specific subscripts 1, 2, and 3 are used to denote the components of $\boldsymbol{r}$, $\boldsymbol{v}$, and $\boldsymbol{a}_d$ because the equation is valid regardless of the choice of coordinate frame.

2.6 Optimization of Variational Equations for Classical Orbital Elements

In order to complete an orbit transfer maneuver efficiently, it is natural to attempt to extremize the time rates of change given by the variational equations. Several control laws discussed in this thesis employ some form of this strategy; a summary of the results is presented here [20, 21, 23]. For these derivations, the control acceleration is represented by (2.6); the subscripts on $\alpha_{R\theta H}$ and $\beta_{R\theta H}$ are dropped for conciseness.

The control angles at which the time rates of change of the classical orbital elements are maximized[2] are found by invoking the first-order necessary conditions for optimality [11]:

$$\frac{\partial \dot{\mathcal{O}}}{\partial \alpha} = 0 \tag{2.48}$$

$$\frac{\partial \dot{\mathcal{O}}}{\partial \beta} = 0 \tag{2.49}$$

and solving for α and β. (The symbol $\mathcal{O}$ represents a, e, i, Ω, and ω in turn.) The optimal location (in terms of ν) on a given orbit for applying control to

[2]Minimization of element rates is discussed in Section 2.8.

change each element is found similarly, by setting

$$\frac{\partial \dot{\mathcal{O}}}{\partial \nu} = 0 \tag{2.50}$$

and solving for ν.

2.6.1 Semi-major Axis

The optimal control angles for increasing a are given by

$$\alpha = \text{atan}\left(\frac{e\sin(\nu)}{1 + e\cos(\nu)}\right) \tag{2.51}$$

$$\beta = 0. \tag{2.52}$$

The optimal location on an orbit at which to increase a is periapsis; that is,

$$\nu = 0, \tag{2.53}$$

which gives a maximum $\dot{a}$ over an orbit of

$$\dot{a} = 2a_d\sqrt{\frac{a^3(1+e)}{\mu(1-e)}}, \tag{2.54}$$

where a_d is the magnitude of the control acceleration.

2.6.2 Eccentricity

The optimal control angles for increasing e are given by

$$\alpha = \text{atan}\left(\frac{\sin(\nu)}{\cos(\nu) + \cos(E)}\right) \tag{2.55}$$

$$\beta = 0, \tag{2.56}$$

where E is the eccentric anomaly. The optimal location on an orbit at which to increase e is apoapsis; that is,

$$\nu = \pi, \tag{2.57}$$

which gives a maximum $\dot{e}$ over an orbit of

$$\dot{e} = \frac{2pa_d}{h}. \tag{2.58}$$

2.6.3 Inclination

Inclination may only be changed by out-of-plane control acceleration, so the control angle α is meaningless when i is changed optimally. The optimal out-of-plane control angle for increasing i is given by

$$\beta = \text{sign}[\cos(\omega + \nu)]\frac{\pi}{2}. \tag{2.59}$$

The values of ν that satisfy first-order optimality conditions for being the location on an orbit at which the maximum $\dot{i}$ occurs are

$$\nu = -\text{asin}(e\sin(\omega)) - \omega. \tag{2.60}$$

The quadrant ambiguity created by the presence of the inverse sine function may be resolved by substituting both possible values of ν into the variational equation for i; the ν that yields the larger value of $\dot{i}$ is the solution. The maximum $\dot{i}$ over an orbit is then

$$\dot{i} = \frac{pa_d}{h\left(\sqrt{1-e^2\sin^2(\omega)} - e|\cos(\omega)|\right)}. \tag{2.61}$$

2.6.4 Right Ascension of the Ascending Node

Right ascension of the ascending node may only be changed by out-of-plane control acceleration, so the control angle α is meaningless when Ω is changed optimally. The optimal out-of-plane control angle for increasing Ω is given by

$$\beta = \text{sign}[\sin(\omega+\nu)]\frac{\pi}{2}. \tag{2.62}$$

The values of ν that satisfy first order optimality conditions for being the location on an orbit at which the maximum $\dot{\Omega}$ occurs are

$$\nu = \text{acos}(-e\cos(\omega)) - \omega. \tag{2.63}$$

The quadrant ambiguity created by the presence of the inverse sine function may be resolved by substituting both possible values of ν into the variational equation for Ω; the ν that yields the larger value of $\dot{\Omega}$ is the solution. The maximum $\dot{\Omega}$ over an orbit is then

$$\dot{\Omega} = \frac{pa_d}{h\sin(i)\left(\sqrt{1-e^2\cos^2(\omega)} - e|\sin(\omega)|\right)}. \tag{2.64}$$

2.6.5 Argument of Periapsis

Argument of periapsis is unique among the classical elements because it is the only one whose value may be changed by both in-plane and out-of-plane control acceleration, a characteristic that complicates the derivation of the optimal control angles. One solution is to simply use a numerical optimization algorithm. However, it is also possible to find an approximate analytical solution. Petropoulos [20, 21] did so by treating the in-plane and out-of-plane rates of change separately. This yields, for in-plane control, optimal control angles of

$$\alpha_i = \text{atan}\left(\frac{-p\cos(\nu)}{(p+r)\sin(\nu)}\right) \tag{2.65}$$

$$\beta_i = 0, \tag{2.66}$$

and an optimal orbit location of

$$\nu_i = \operatorname{acos}\left\{ \left[\frac{1-e^2}{2e^3} + \sqrt{\frac{1}{4}\left(\frac{1-e^2}{e^3}\right)^2 + \frac{1}{27}} \right]^{\frac{1}{3}} - \cdots \right.$$
$$\left. \cdots - \left[-\frac{1-e^2}{2e^3} + \sqrt{\frac{1}{4}\left(\frac{1-e^2}{e^3}\right)^2 + \frac{1}{27}} \right]^{\frac{1}{3}} - \frac{1}{e} \right\}. \tag{2.67}$$

The quadrant ambiguity for ν_i created by the presence of the inverse cosine function may be resolved by comparing the values of $\dot{\omega}_i$ obtained at the two possible values of ν_i. As the correct ν_i maximizes $\dot{\omega}_i$, the ν_i that yields a larger value of $\dot{\omega}_i$ must necessarily be the ν_i at which the optimal $\dot{\omega}_i$ occurs. The maximum $\dot{\omega}_i$ over an orbit is then

$$\dot{\omega}_i = \frac{a_d}{eh}\sqrt{p^2\cos^2(\nu_i) + (p+r_i)^2(1-\cos^2(\nu_i))}, \tag{2.68}$$

where r_i is the distance between the spacecraft and the central body evaluated at ν_i.

If instead only out-of-plane control is considered, the optimal control angles are

$$\alpha_o = 0 \tag{2.69}$$

$$\beta_o = \operatorname{sign}\left[-\sin(\nu+\omega)\cos(i)\right]\frac{\pi}{2}. \tag{2.70}$$

The location over an orbit at which the maximum $\dot{\omega}_o$ occurs is

$$\nu_o = \text{acos}(-e\cos(\omega)) - \omega. \tag{2.71}$$

The quadrant ambiguity created by the presence of the inverse sine function may be resolved by substituting both possible values of ν_o into the variational equation for ω using $\alpha = 0$ and the optimal value of β; the ν_o that yields the larger value of $\dot{\omega}_o$ is the solution. The maximum $\dot{\omega}_o$ over an orbit is then

$$\dot{\omega}_o = \frac{pa_d|\cos(i)|}{h\sin(i)\left(\sqrt{1-e^2\cos^2(\omega)} - e|\sin(\omega)|\right)}. \tag{2.72}$$

2.6.6 True Anomaly

Because the goal of the control laws discussed in this thesis is not to correct errors in location within an orbit, the control angles and orbit location that extremize $\dot{\nu}$ are unneeded and are not presented.

2.7 Optimization of Variational Equations for Equinoctial Orbital Elements

The rates of change of the equinoctial elements may be extremized in much the same manner as the rates of change of the classical elements were extremized in Section 2.6.

2.7.1 Semi-major Axis

The quantities associated with extremizing $\dot{a}$ are the same as those given in Section 2.6.1.

2.7.2 P_1

As was the case with ω of the classical element set, P_1 and P_2 of the equinoctial element set may be changed by both in-plane and out-of-plane control acceleration. In Section 2.6.1, expressions were obtained for the extremizing values of $\dot{\omega}$ for the case in which the control acceleration is purely in-plane and the case in which the control acceleration is purely out-of-plane. Here, however, because analytical expressions for $\max(\dot{P}_1)$ and $\max(\dot{P}_2)$ are not required for the control law discussed in this thesis that utilizes these values [12], a numerical optimization technique is used instead. Following the derivations given in [12], the global maximum of $\dot{P}_1$ over an osculating orbit is found by recognizing that the first possible maximum occurs when $\cos(L) = -1$ and control acceleration is directed purely in the $\hat{\boldsymbol{e}}_r$ direction. Under these circumstances,

$$\dot{P}_1 = \frac{p}{h}. \tag{2.73}$$

A numerical search method (Joseph uses the Golden search method [12]) is then used to find the maximum values of $\dot{P}_1$ that may be achieved over an osculating orbit via application of control acceleration purely in the $\hat{\boldsymbol{e}}_\theta$ direction

and purely in the $\hat{\boldsymbol{e}}_h$ direction. (Note that, because $\dot{P}_1$ is trigonometric in L, two local maxima may exist for each of the functions maximized numerically. Both must be calculated.) The global maximum of $\dot{P}_1$ is the greatest of the five $\dot{P}_1$ values found by this procedure.

2.7.3 P_2

The maximum value of $\dot{P}_2$ is found in exactly the same manner in which the maximum value of $\dot{P}_1$ is determined (Section 2.7.2), except that the one possible maximum determined through application of control acceleration purely in the $\hat{\boldsymbol{e}}_r$ direction occurs at $\sin(L) = 1$ rather than at $\cos(L) = -1$. (The value of $\dot{P}_2$ at this location is $\dot{P}_2 = \frac{p}{h}$.)

2.7.4 Q_1

Q_1 is only affected by out-of-plane control acceleration, so the in-plane control angle α is meaningless when Q_1 is changed optimally, and the optimal out-of-plane control angle for increasing Q_1 is

$$\beta = \text{sign}(\sin(L))\frac{\pi}{2}. \tag{2.74}$$

The value of L at which the maximum $\dot{Q}_1$ occurs on an osculating orbit is given by

$$L = -\text{acos}(P_2). \tag{2.75}$$

The quadrant ambiguity in (2.75) may be resolved by evaluating $\dot{Q}_1$ at both possible values of L; the value of L that yields the larger $\dot{Q}_1$ is the solution. The maximum value of $\dot{Q}_1$ is then found by substituting the optimal L into (2.40).

2.7.5 Q_2

Q_2 is only affected by out-of-plane control acceleration, so the in-plane control angle α is meaningless when Q_2 is changed optimally, and the optimal out-of-plane control angle for increasing Q_2 is

$$\beta = \text{sign}(\cos(L))\frac{\pi}{2}. \tag{2.76}$$

The value of L at which the maximum $\dot{Q}_2$ occurs on an osculating orbit is given by

$$L = -\text{asin}(P_1). \tag{2.77}$$

The quadrant ambiguity in (2.77) may be resolved by evaluating $\dot{Q}_2$ at both possible values of L; the value of L that yields the larger $\dot{Q}_2$ is the solution. The maximum value of $\dot{Q}_2$ is then found by substituting the optimal L into (2.41).

2.7.6 True Longitude

Because the goal of the control laws discussed in this thesis is not to correct errors in location within an orbit, the control angles and orbit location that extremize $\dot{l}$ are unneeded and are not presented.

2.8 Minimization of Element Rates

The preceding derivations give the conditions that achieve *maximum* rates of change of the classical elements and equinoctial elements and the corresponding maxima. No further derivation is required to obtain the minima because of the following relations [20]:

$$\min(\dot{\mathcal{O}}) = -\max(\dot{\mathcal{O}}) \tag{2.78}$$

$$\alpha_{min} = \alpha_{max} + \pi \tag{2.79}$$

$$\sin(\beta_{min}) = -\sin(\beta_{max}). \tag{2.80}$$

Chapter 3

Descriptions and Qualitative Analyses of Low-Thrust Control Laws

3.1 Introduction

In this chapter, algorithmic descriptions and qualitative analyses of seven distinct low-thrust control laws are presented. While each control law is different, all those discussed in this thesis share several important characteristics:

1. All laws require the initial spacecraft state to be fully defined; the location of the spacecraft within an orbit at the start of the maneuver is fixed.

2. All laws use some form of the variational equations presented in Section 2.5.

3. All laws are intended for use in global transfer problems; no law relies on knowledge of a reference transfer trajectory from which the controlled trajectory is perturbed.

4. All laws are capable of performing both in-plane and out-of-plane maneuvers.

In the interests of brevity and unambiguity, each of the control laws described in this thesis is referenced by the name of the first author of the source in which the control law is described.

3.2 Lyapunov Control

The majority of the control laws studied in this thesis are based on Lyapunov control theory. To avoid repetition, the theory is presented generally first, then discussed as it applies to individual control laws.

Lyapunov's Second Theorem [9] states that, for a system

$$\dot{\boldsymbol{Z}} = \boldsymbol{f}(\boldsymbol{Z}), \quad \boldsymbol{Z} = \boldsymbol{X} - \boldsymbol{X}_T, \tag{3.1}$$

the equilibrium point $\boldsymbol{X}_T$ is globally asymptotically stable[1] if there exists a scalar function $V(\boldsymbol{Z})$ (called a Lyapunov function) such that

1. $V(\mathbf{0}) = 0$, where $\mathbf{0}$ is an appropriately dimensioned vector of zeros.
2. $V(\boldsymbol{Z}) > 0 \quad \forall \boldsymbol{Z} \neq \mathbf{0}$.
3. $\dot{V}(\boldsymbol{Z}) < 0 \quad \forall \boldsymbol{Z} \neq \mathbf{0}$.
4. $\lim_{|\boldsymbol{Z}| \to \infty} V(\boldsymbol{Z}) = \infty$.

[1] It is important to note that stability in the sense of Lyapunov by itself does not guarantee a successful orbit transfer maneuver, particularly for the case in which the target orbit is only partially defined. For example, a transfer for which the target eccentricity is free may result in the osculating eccentricity approaching unity, leading to a non-elliptical orbit.

For the problem considered by this thesis, $\boldsymbol{X}$ is taken to be a vector of values that define the current osculating orbit of the spacecraft, and $\boldsymbol{X}_T$ contains the target values of each of those elements, such that $\boldsymbol{Z} = \boldsymbol{X} - \boldsymbol{X}_T = \boldsymbol{0}$ if the spacecraft is on the target orbit. Thus, by the first condition of Lyapunov's Second Theorem, the goal of the Lyapunov-based control laws is to direct the spacecraft control such that the value of the Lyapunov function is driven to zero. Furthermore, for an efficient orbit transfer, it is desirable to direct the control such that the osculating orbit is driven to the target orbit as quickly as possible; that is, for a given spacecraft state and target state, the control should be directed such that $\dot{V}$ is as negative as possible. This is achieved [17] by noting that the equations of motion for the spacecraft may be written in the form

$$\dot{\boldsymbol{X}} = \boldsymbol{g}(\boldsymbol{X}, \boldsymbol{a})\boldsymbol{u}, \tag{3.2}$$

where $\boldsymbol{g}(\boldsymbol{X}, \boldsymbol{a})$ is a matrix that relates $\dot{\boldsymbol{X}}$ to the control $\boldsymbol{u}$, and $\boldsymbol{a}$ is a vector of parameters independent of $\boldsymbol{X}$. For an autonomous system,

$$\dot{V}(\boldsymbol{Z}) = \dot{V}(\boldsymbol{X} - \boldsymbol{X}_T) = \frac{\partial V}{\partial \boldsymbol{X}}\dot{\boldsymbol{X}} = \frac{\partial V}{\partial \boldsymbol{X}}\boldsymbol{g}\boldsymbol{u}. \tag{3.3}$$

Making $\dot{V}$ as negative as possible is then a simple matter of directing the control such that

$$\boldsymbol{u} = -\boldsymbol{g}^T \left(\frac{\partial V}{\partial \boldsymbol{X}} \right)^T , \tag{3.4}$$

and the resulting $\dot{V}$ is

$$\dot{V} = -\left| \left(\frac{\partial V}{\partial \boldsymbol{X}} \right)^T \boldsymbol{g}^T \right|^2 . \tag{3.5}$$

In summary, the steps required to apply a Lyapunov-type spacecraft control scheme are:

1. Determine the elements of $\boldsymbol{X}$. These must be selected such that a Lyapunov function that accurately captures a "distance" between the current state and the target state may be written as a function of $\boldsymbol{X}$ and $\boldsymbol{X}_T$. For example, in the low-thrust spacecraft control problem, a possibility is $\boldsymbol{X} = (a \quad e \quad i \quad \Omega \quad \omega)^T$, which allows for the targeting of the five classical orbital elements.

2. Write the dynamics of the system as $\dot{\boldsymbol{X}} = \boldsymbol{g}(\boldsymbol{X}, \boldsymbol{a})\boldsymbol{u}$. For the preceding example, $\boldsymbol{g}$ is given by rows one through five of the matrix in (2.36), $\boldsymbol{u}$ is given by (2.6), and the only element of $\boldsymbol{a}$ is true anomaly.

3. Find a suitable Lyapunov function $V(\boldsymbol{Z}) = V(\boldsymbol{X} - \boldsymbol{X}_T)$ such that the system is stable in the sense of Lyapunov. There is no hard-and-fast

approach capable of generating a Lyapunov function for all dynamic systems [17]; however, a popular choice in the low-thrust spacecraft control problem [5, 6, 12, 17, 20, 21] takes the form of

$$V(\boldsymbol{Z}) = \sum_{i=1}^{n} K_i Z_i^2, \tag{3.6}$$

where $\boldsymbol{Z}$ is $n \times 1$ and all $K_i \geq 0$. The key to the formulation of a good Lyapunov function of this form is the method of the determination of the K_i, which weight the error terms in V.

4. Determine $\frac{\partial V}{\partial \boldsymbol{X}}$ to find the optimal control $\boldsymbol{u}$ for a given $\boldsymbol{X}$ and $\boldsymbol{X}_T$.

3.2.1 LaSalle's Invariance Theorem

A useful tool for proving stability in the sense of Lyapunov for an autonomous system for which $\dot{V}$ is *not* strictly less than zero for all $\boldsymbol{Z} \neq \boldsymbol{0}$ is LaSalle's Invariance Theorem [9, 17], which states that $\boldsymbol{Z} = \boldsymbol{0}$ is a globally uniformly asymptotically stable point if

1. $V(\boldsymbol{Z}) > 0 \quad \forall \boldsymbol{Z} \neq \boldsymbol{0}$.
2. $\lim_{|\boldsymbol{Z}| \to \infty} V(\boldsymbol{Z}) = \infty$.
3. $\dot{V} \leq 0$ and $\dot{V} \neq 0$ along any solution to the system except $\boldsymbol{Z} = \boldsymbol{0}$.

LaSalle's Invariance Theorem is used to prove stability in the sense of Lyapunov for several of the control laws presented in this thesis [5, 6, 17]

because the corresponding Lyapunov functions do not meet the third condition for Lyapunov stability (Section 3.2) but do meet all conditions to satisfy LaSalle's Invariance Theorem.

3.3 Petropoulos Control and Joseph Control

Control laws presented by Petropoulos [20, 21] and Joseph [12] are presented together because Joseph's method is based on that of Petropoulos. However, the two control laws are not identical, and the differences between the algorithms produce interesting and important differences in the results that may be obtained through their application.

3.3.1 Petropoulos Control

The refined version of Petropoulos's control law [21], also known as the Q-law, is based on a Lyapunov function given by

$$V_P = (1 + W_P P) \sum_{\mathcal{O}} W_{\mathcal{O}} S_{\mathcal{O}} \left(\frac{\delta \mathcal{O}}{\max_\nu(\dot{\mathcal{O}})} \right)^2, \quad \mathcal{O} = a, e, i, \Omega, \omega, \tag{3.7}$$

where W_P is a weighting function, P is a penalty function, $W_{\mathcal{O}}$ is a weighting function, $S_{\mathcal{O}}$ is a scaling function, and $\delta\mathcal{O}$ is an error metric given by

$$\delta\mathcal{O} = \begin{cases} \mathcal{O} - \mathcal{O}_T, & \mathcal{O} = a, e, i \\ \text{acos}(\cos(\mathcal{O} - \mathcal{O}_T)), & \mathcal{O} = \Omega, \omega \end{cases}. \tag{3.8}$$

The use of the cosine and inverse cosine functions in (3.8) has the effect of returning the principle value for $\delta\mathcal{O}$ ($\delta\mathcal{O} \in [0, \pi]$). This allows the control law to take advantage of the continuity of Ω and ω at 0 and 2π. Were $\delta\Omega$ and $\delta\omega$ defined simply as $\Omega - \Omega_T$ and $\omega - \omega_T$, respectively, the control law would not "know" that, for example $\Omega = 10°$ is "near" $\Omega = 350°$. The control law would thus call to increase Ω rather than decrease it, creating inefficiency in the maneuver.

For a, e, i, and Ω, the value $\max_\nu(\dot{\mathcal{O}})$ refers to the maximum rate of change of each classical element over the current osculating orbit. (Expressions for these values are presented in Section 2.6.) The expression for $\max_\nu(\dot{\omega})$ is more complicated, however, because an analytical expression is not available the maximum rate of change of ω over an orbit. Instead, a weighted average of the maximum $\dot{\omega}$ achievable through purely in-plane control on the current osculating orbit and the maximum $\dot{\omega}$ achievable through purely out-of-plane control on the current osculating orbit is used, so that

$$\max_\nu(\dot{\omega}) = \frac{\max_\nu(\dot{\omega}_i) + b\, \max_\nu(\dot{\omega}_o)}{1 + b}, \tag{3.9}$$

where b is a parameter, nominally set to $b = 0.01$.

The purpose of the penalty function P is to enforce mission constraints. Petropoulos gives an example penalty function whose goal is to create a minimum periapsis distance for the transfer trajectory:

$$P = \exp\left[k\left(1 - \frac{r_p}{r_{p_{min}}}\right)\right], \tag{3.10}$$

where k is a parameter, nominally set to 100, r_p is the osculating periapsis distance, and $r_{p_{min}}$ is the minimum allowable periapsis distance. (Implementation of the penalty function requires calculation of the derivatives of P with respect to the orbital elements; the necessary expressions are given in Appendix A.2.) The penalty weighting function W_P is nominally set to unity if the penalty function is active and zero otherwise. Similarly, the classical element weighting functions $W_{\mathcal{O}}$ are nominally set to unity if the corresponding element is targeted and zero if its final value is free.

The scaling function $S_{\mathcal{O}}$ is nominally set to

$$S_{\mathcal{O}} = \begin{cases} \left[1 + \left(\frac{a - a_T}{m a_T}\right)^n\right]^{\frac{1}{r}}, & \mathcal{O} = a \\ 1, & \mathcal{O} = e, i, \Omega, \omega \end{cases}, \tag{3.11}$$

where m, n, and r are parameters, nominally set to 3, 4, and 2, respectively. The purpose of the unique form of S_a is that the Lyapunov function V_P is not, in fact, stable in the sense of Lyapunov because it approaches zero not only as the elemental errors approach zero, but also as a approaches infinity. The goal of S_a, then, is to increase the attention paid to semi-major axis error as δa grows in an effort to prevent a from growing without bound. (Implementation of the scaling function requires calculation of the derivatives of $S_{\mathcal{O}}$ with respect to the orbital elements; the necessary expressions are given in Appendix A.3.)

The desired control is found from V_P using the strategy of minimizing $\dot{V}_P$. This requires derivation of the partial derivatives of V_P with respect to each of the orbital elements; however, because some of the required derivatives are rather lengthy, the expressions themselves are omitted from the body of this thesis. Instead, a MATLAB script that utilizes MATLAB's Symbolic Toolbox to obtain the necessary derivatives is included in Appendix B.1. Once the required derivatives are obtained, the control is found as a function of the current osculating classical elements and target elements through application of (3.4).

The motivation behind the form of the Lyapunov function is that each term $\left(\frac{\delta\mathcal{O}}{\max_\nu(\dot{\mathcal{O}})}\right)^2$ is the square of the time required to change an orbital element from its current value to its target value, assuming that its rate of change were equal to $\pm\max_\nu(\dot{\mathcal{O}})$ for the duration of the transfer. Thus, rather than thinking of the Lyapunov function as a summation of weighted differences between current and target values of orbital elements, it is perhaps more natural to think of it as a summation of times required to achieve the target values of orbital elements. The goal of the control law is to drive all these times to zero.

A key feature of this approach is that each of the elemental terms of V_P will decrease not only if $\delta\mathcal{O}$ decreases but also if $\max_\nu(\dot{\mathcal{O}})$ increases. This allows the control law to take into account the fact that, for example, the optimal rate of change of inclination increases in magnitude as semi-major axis increases. Petropoulos's control law may therefore direct thrust acceleration to increase a beyond its target value, change i, then decrease a to achieve its target value.

Petropoulos discusses two strategies for introducing coast arcs into a controlled trajectory, both based on the concept of applying control acceleration only in the areas of an osculating orbit at which it is most effective to do so. The quantity absolute effectivity is defined as

$$\eta_a = \frac{\min_{\alpha,\beta}(\dot{V}_P)}{\min_{\alpha,\beta,\nu}(\dot{V}_P)}, \tag{3.12}$$

where $\min_{\alpha,\beta}(\dot{V}_P)$ is the minimum value of $\dot{V}_P$ at a given position on an osculating orbit, which is also the value of $\dot{V}_P$ obtained from (3.5). Meanwhile, $\min_{\alpha,\beta,\nu}(\dot{V}_P)$ refers to the minimum value of $\dot{V}_P$ that may be obtained by applying (3.4) at any value of ν on the current osculating orbit.

Similarly, relative effectivity is defined as

$$\eta_r = \frac{\min_{\alpha,\beta}(\dot{V}_P) - \max_{\alpha,\beta,\nu}(\dot{V}_P)}{\min_{\alpha,\beta,\nu}(\dot{V}_P) - \max_{\alpha,\beta,\nu}(\dot{V}_P)}, \tag{3.13}$$

where $\max_{\alpha,\beta,\nu}(\dot{V}_P)$ is the maximum value of $\dot{V}_P$ that may be obtained by applying (3.4) at any value of ν on the current osculating orbit.[2]

The coasting scheme, then, is to apply control acceleration only when $\dot{V}_P$ at the current value of ν yields an absolute or relative effectivity that is greater than some threshold value of either η_a or η_r. As may be expected, increasing either effectivity threshold increases the amount of time spent coasting

[2]It is important to note that this is *not* the same as the maximum value of $\dot{V}_P$ that may be obtained by any combination of α, β, and ν on the current osculating orbit.

and increases the total time required to perform a maneuver. In many (though not all) cases, this will also lead to a decrease in the amount of fuel required to perform a maneuver. Petropoulos discusses several different strategies for utilizing effectivity thresholds, including setting a constant threshold value of η_a; setting a constant threshold value of η_r; setting constant values of both η_a and η_r; and increasing the threshold value of η_a as the spacecraft nears the target orbit. However, there is no theoretical basis for selecting an appropriate threshold value for a given maneuver; the threshold must instead be selected using the discretion of the mission designer. A minimum control duration of 10° of true longitude is also imposed to prevent control on/off chatter when the effectivity is near its threshold value.[3]

Petropoulos's control law is perhaps the most complete law discussed in this thesis. The control law allows for the targeting of any subset of the classical element set; the weights for each term of the Lyapunov function are fully defined; and the law includes multiple schemes for coasting. However, Petropoulos's control law is not without its flaws. First, as mentioned in the discussion of S_0, the Lyapunov function V_P does not satisfy the conditions for Lyapunov stability. Though Petropoulos claims that the form of S_a has led to convergence to the target orbit in all numerical simulations performed [21], this lack of a completely firm theoretical footing is a cause for concern. There is no guarantee that the control law will not direct the spacecraft toward an

[3]Control on/off chatter is characterized by the controller rapidly switching back and forth between controlled arcs and coasting arcs.

infinite semi-major axis rather than toward the target orbit. Further, this is not the only scenario in which a term in the summation of V_P may be driven to zero even though the corresponding error term is not. For example, the $\delta\Omega^2$ term in V_P is multiplied by $\sin^2(i)$ and therefore goes to zero if the osculating orbit approaches an equatorial orbit.

A similar issue that may be encountered is that the complexity of the derivatives of V_P with respect to the orbital elements may produce consequences that are not obvious upon inspection of V_P. In relation to the previous example of the $\delta\Omega^2$ term of V_P, the multiplication of $\delta\Omega^2$ by $\sin^2(i)$ means that, when Ω is targeted, i will also be driven toward either 0° or 180°. Additionally, the derivatives of both the δa^2 and δi^2 terms of V_P with respect to the eccentricity are always less than zero, meaning that these two terms of V_P are always decreased by increasing e. As a result, a maneuver in which only the semi-major axis is targeted may not result in control acceleration directed only in the direction of the velocity vector, and a maneuver in which only the inclination is targeted may not result in purely out-of-plane control acceleration, as might be expected.

In addition to introducing suboptimalities, this characteristic of Petropoulos's control law can adversely affect the control profile to the point that convergence to the target orbit may not be achieved when using nominal values for all parameters, a point explored more fully in Chapter 5.

Control direction chatter is another possible source from which poor performance of the control law may arise. This is a byproduct of the dis-

cretization of the control calculation required to numerically propagate the trajectory. When multiple elements that may be changed by in-plane control acceleration are targeted, it is possible that the errors in the elements may reach values such that, at time step t_j, the control law prescribes that the majority of the in-plane control be applied to correct one element, and at time step t_{j+1}, the majority of the in-plane control be applied to correct a different element. Furthermore, it is possible that the in-plane control angles that the control law prescribes to change each of these two elements oppose one another. This can create a cycle in which the in-plane control angle changes by large amounts from time step to time step. This situation may also arise when multiple elements that may be changed by out-of-plane control acceleration are targeted. If a variable-step integration algorithm is used, the result is that the step size rapidly approaches zero and integration effectively stops, while if a fixed-step algorithm is used, propagation persists, but the spacecraft is unlikely to converge to the target orbit.

Petropoulos describes this phenomenon as occurring primarily when a and e are targeted simultaneously, and the spacecraft is very close to the target orbit. In this situation, the control directions required to change the two elements may become diametrically opposed, leading to control direction chatter. In these cases, the effectivity is generally low, so Petropoulos proposes temporarily increasing the effectivity cutoff to induce coasting until a more favorable location on the orbit is achieved – one at which control direction chatter does not occur. However, as discussed in detail in Chapter 5, this is

not the only situation in which control direction chatter may occur, and other means may be needed to counteract it.

Selection of the parameters b, m, n, r, and k used in the definition of V_P is a task that must be performed by the mission designer and requires user discretion. Though the nominal values may lead to adequate performance, it is highly unlikely that they will be optimal for all maneuvers. (In fact, some work has been done in the optimization of not only these parameters but the $W_{\mathcal{O}}$, as well, through the use of heuristic optimization techniques, including genetic algorithms and simulated annealing. Lee et al. [15] found that the modification of certain $W_{\mathcal{O}}$, as well as the parameters b, m, n, r, and k, could lead to a noticeable improvement in the performance of the control law.)

3.3.2 Joseph Control

Joseph's implementation of Petropoulos's control law differs from the original scheme in several fundamental ways [12]. First, Joseph uses the equinoctial element set rather than the classical element set. This has the advantage of eliminating the singularities caused by the use of the classical element set, but also significantly increases the difficulty of targeting any arbitrary set of classical orbital elements.

Second, Joseph's adaptation of Petropoulos's control law was published prior to the presentation of the "refined" version of Petropoulos's control law [21] and is instead based on a simpler version [20]. Therefore, the Lyapunov function on which Joseph's control law is based is

$$V_J = \sum_{\mathcal{O}} W_{\mathcal{O}} \left(\frac{\delta \mathcal{O}}{\max_\nu(\dot{\mathcal{O}})} \right)^2, \quad \mathcal{O} = a, P_1, P_2, Q_1, Q_2. \tag{3.14}$$

This form of V_J differs from the V_P given by (3.7) in that it does not take into account a penalty function and does not utilize a scaling function.

Third, Joseph uses the assumption that the derivatives of $\max_\nu(\dot{\mathcal{O}})$ with respect to all orbital elements except anomaly may be neglected. This significantly simplifies the derivation of the control law because the partial derivatives of V_J with respect to the orbital elements become

$$\frac{\partial V_J}{\partial \mathcal{O}} = \frac{2 W_{\mathcal{O}} \delta \mathcal{O}}{\left[\max_\nu(\dot{\mathcal{O}}) \right]^2}, \quad \mathcal{O} = a, P_1, P_2, Q_1, Q_2. \tag{3.15}$$

This assumption also allows for the maximum achievable rates of change over an osculating orbit of P_1 and P_2, the two equinoctial elements that may be changed by both in-plane and out-of-plane control acceleration, to be calculated numerically. Were it required that $\max_\nu(\dot{P}_1)$ and $\max_\nu(\dot{P}_2)$ be differentiated with respect to the equinoctial elements, such a numerical scheme would necessitate that the corresponding derivatives also be obtained numerically (for example, by a finite-difference approximation). This situation may be compared to that encountered in Petropoulos's control law (Section 3.3.1), in which an approximate analytical expression for $\max_\nu(\dot{\omega})$ is used to make possible the differentiation of $\max_\nu(\dot{\omega})$ with respect to the classical orbital elements.

Thus, Joseph's simplification in the calculation of $\frac{\partial V_J}{\partial \mathcal{O}}$ has the advantages of easing the derivation of the control law and facilitating an accurate numerical solution for $\max_\nu(\dot{P}_1)$ and $\max_\nu(\dot{P}_2)$, but also brings with it the disadvantage of introducing error into the calculation of the control by neglecting terms. A direct consequence of this simplification is the loss of the ability of the control law to direct "desirable overshoots" of elements, such as in the case of increasing semi-major axis to ease the burden of changing inclination. The V_J weighting terms are treated as constants, so the control law has no knowledge that changing one element will decrease the weight of another element's term in the summation of V_J.

Joseph's adoption of Petropoulos's weighting functions brings with it the lack of stability in the sense of Lyapunov caused by V_J tending toward zero as a approaches infinity. However, because Joseph's control law assumes that the derivatives of $\max_\nu(\dot{\mathcal{O}})$ with respect to all orbital elements except anomaly may be neglected, Joseph's control law is much less likely than that of Petropoulos to converge to an infinite semi-major axis rather than to the target orbit. Further, this assumption means that the "unusual" control profiles sometimes commanded by Petropoulos's control law (Section 3.3.1) are not seen in maneuvers directed by Joseph's control law, and control direction chatter is less likely to occur. As explored in Chapter 5, this has non-trivial consequences on both the optimality and robustness of the control laws of Petropoulos and Joseph.

Finally, though not strictly relevant to this thesis, it should be noted

that Joseph's control law also uses a classical proportional-integral control law to target locations within an orbit.

3.4 Naasz Control

Naasz [17] presents three control schemes for driving spacecraft to target orbits, each based on a different representation of the spacecraft state:

1. A control law based on driving spacecraft inertial position and velocity vectors to target values.

2. A control law based on driving the set of osculating equinoctial orbital elements to target values.

3. A control law based on driving the set of osculating classical orbital elements to target values.

The first strategy is not appropriate for comparison in this thesis because it generally requires the specification of a target phase within a target orbit, while this study focuses on control laws whose goal is to achieve a target orbit, regardless of phase. Furthermore, such a control scheme makes difficult the targeting of arbitrary subsets of the classical orbital elements. The second strategy presented by Naasz encounters a similar difficulty. Equinoctial elements may be transformed to classical elements and vice versa (Section 2.4), but there exists coupling between the elements that makes targeting an arbitrary set of classical elements via the equinoctial set problematic. Also, Naasz

presents no systematic method for properly weighting the errors in the different elements of either the position vector and velocity vector or the equinoctial element set for arbitrary maneuvers, meaning that further derivations or a trial-and-error approach are required when implementing either method.

Naasz's control law based on the classical element set is both more closely aligned with the aims of this thesis and more fully developed than the other two control strategies. It is based on a Lyapunov function given by

$$V_N = \frac{1}{2}\sum_{\mathcal{O}} K_{\mathcal{O}}(\delta\mathcal{O})^2, \quad \mathcal{O} = a, e, i, \Omega, \omega, M_0, \tag{3.16}$$

where the $K_{\mathcal{O}}$ are weights greater than or equal to 0 and

$$\delta\mathcal{O} = \mathcal{O} - \mathcal{O}_T, \quad \mathcal{O} = a, e, i, \Omega, \omega, M_0. \tag{3.17}$$

A systematic approach is given for the selection of the weighting functions $K_{\mathcal{O}}$. The process is begun by determining the maximum change in an orbital element that may be achieved by applying an impulsive maneuver whose change in velocity magnitude is $\Delta v = \frac{T}{m}\Delta t$, where T is the control force magnitude, m is the spacecraft mass prior to the maneuver, and Δt is the time duration for a finite-time control maneuver for which the impulsive maneuver is an approximation. For example, for semi-major axis, a maximal change Δa_{max} is achieved by applying an impulse in the direction of the velocity vector at periapsis [17, 20]; the resulting change in a is

$$\Delta a_{max} = \frac{2a^2(1+e)}{h}\frac{T}{m}\Delta t. \tag{3.18}$$

Once $\Delta\mathcal{O}_{max}$ is determined, that expression is substituted for the difference between the current osculating value of the orbital element and the target value of the element, $\delta\mathcal{O}$, in (3.4). Again using semi-major axis as an example, this gives the control dictated *only by semi-major axis error* as

$$|\boldsymbol{u}(\Delta a_{max})| = \left| -\left[\frac{2a^2(1+e\cos(\nu))}{h}\right] K_a \left[\frac{2a^2(1+e)}{h}\frac{T}{m}\Delta t\right]\right|. \tag{3.19}$$

The value of $K_{\mathcal{O}}$ is then determined by setting the expression for $|\boldsymbol{u}(\Delta\mathcal{O}_{max})|$ equal to the thrust acceleration magnitude, $\frac{T}{m}$, and solving for $K_{\mathcal{O}}$.

Naasz's application of these principles to all the elements is given by [17]

$$K_a = \frac{h^2}{4a^4(1+e)^2}\frac{1}{\Delta t} \tag{3.20}$$

$$K_e = \frac{h^2}{4p^2}\frac{1}{\Delta t} \tag{3.21}$$

$$K_i = \left[\frac{h + eh\cos(\omega + \text{asin}(e\sin(\omega)))}{p(-1+e^2\sin^2(\omega))}\right]^2 \frac{1}{\Delta t} \tag{3.22}$$

$$K_\Omega = \left[\frac{h\sin i(-1+e\sin(\omega+\text{asin}(e\cos(\omega))))}{p(1-e^2\cos^2(\omega))}\right]^2 \frac{1}{\Delta t} \tag{3.23}$$

$$K_\omega = \frac{e^2h^2}{4p^2}\left(1-\frac{e^2}{4}\right)\frac{1}{\Delta t} \tag{3.24}$$

$$K_{M_0} = \frac{a^2e^2h^2}{4b^2p^2}\left(1-\frac{e^2}{4}\right)\frac{1}{\Delta t}, \tag{3.25}$$

In order to make possible an analytical expression for K_ω, Naasz assumes that the greatest possible change in ω due to an impulsive maneuver is achieved by maneuvering purely in the $\hat{\boldsymbol{e}}_\theta$ direction near a true anomaly of $\nu = \frac{\pi}{2}$. This is not entirely correct because, uniquely among the classical elements, ω may be changed by both in-plane and out-of-plane maneuvers, and a general analytical expression for the optimal maneuver direction for changing ω taking into account both in-plane and out-of-plane maneuvering possibilities is not available [20]. Thus, the optimality of the choice of K_ω is lacking when compared with that of the other weighting functions. Furthermore, the derivations of both K_ω and K_{M_0} utilize a first-order Taylor expansion about $e = 0$ to ease the calculations. This simplification introduces further suboptimalities into K_ω and K_{M_0}, which will be most apparent when the target orbit is highly eccentric.

These expressions present several other points of interest. First, targeting a subset of the classical elements rather than all six may be accomplished by setting the $K_{\mathcal{O}}$ associated with untargeted elements to zero. Second, the algorithm prescribes that the $K_{\mathcal{O}}$ should be evaluated using the characteristics of the target orbit and held constant for the duration of the maneuver. Naasz gives no justification for this strategy, and it proves problematic when only a subset of the classical orbital elements is targeted. For example, in order to calculate K_a, the target values of a and e are required. However, if eccentricity is not targeted, then the necessary value of e is undefined. A simple workaround is to use the initial value of an orbital element whose target value

is undefined in the calculation of the $K_{\mathcal{O}}$; however, this is not mentioned by Naasz in the original presentation of the control law.

Though the presentations are somewhat different, it may be noted that the resulting expressions for Naasz's K_a and K_e are identical to the corresponding weighting terms of Petropoulos and Joseph (Section 3.3) except for a scaling – by the control acceleration magnitude in the case of Petropoulos and Joseph and by the inverse of the propagation time step in the case of Naasz. Furthermore, the expressions for K_i and K_Ω *should* be identical (disregarding the scaling); however, discrepancies arise because Naasz neglects the quadrant ambiguity presented by the inverse sine function in (3.22) and (3.23). Of course, the K_ω terms differ between the control laws due to Petropoulos and Joseph's separation of in-plane and out-of-plane control acceleration and Naasz's use of linearization.

Given this method of $K_{\mathcal{O}}$ calculation, it is interesting to think of Naasz's control law as a sort of special case of Joseph's control law in which the $K_{\mathcal{O}}$ are calculated once and held constant throughout the maneuver. And, because Naasz's $K_{\mathcal{O}}$ are constant, Naasz's strategy has the benefit of actually being stable in the sense of Lyapunov for all cases in which the semi-major axis used to calculate the $K_{\mathcal{O}}$ is not infinite. As discussed in Section 3.3, this is not the case for the control laws of Petropoulos and Joseph.

Naasz proves the stability of the system using LaSalle's Invariance Theorem [17] (Section 3.2.1). The first two conditions are seen to be met by simple inspection of (3.16). If $\boldsymbol{u}$ is chosen to satisfy (3.4), then $\dot{V}_N \leq 0$ holds because

of the form of (3.5). $\dot{V}_N$ goes to zero for $\boldsymbol{Z} = \mathbf{0}$ and may also go to zero when $\omega + \nu$ is a positive integer multiple of $\frac{\pi}{2}$. However, because true anomaly is not constant on an orbit, $\dot{V}_N$ will not remain zero unless $\boldsymbol{Z} = \mathbf{0}$. Thus, the system is globally uniformly asymptotically stable.

The fact that stability may be proven for Naasz's control law but not for Petropoulos's control law or Joseph's control law is a direct consequence of the fact that the $K_{\mathcal{O}}$ are held constant in Naasz's scheme but vary as the osculating orbital elements change in the other two. However, holding the $K_{\mathcal{O}}$ constant is also likely to lead to less fuel-optimal maneuvers than if the $K_{\mathcal{O}}$ are allowed to change as the elements of the osculating orbit change. (This is explored numerically in Chapter 5.)

It is also noteworthy that Naasz's expressions for the $K_{\mathcal{O}}$ allow for the units of the control to be those of acceleration, resulting in an intuitive output of the control law that some other control algorithms lack. Naasz uses this to prescribe a simple algorithm for incorporating coast segments into the control scheme. Because the magnitude of $\boldsymbol{u}$ output by (3.4) is itself an acceleration magnitude, it may be directly compared to the acceleration magnitude of which the spacecraft propulsion system is capable, $\frac{T}{m}$. Therefore, Naasz proposes

$$T = \begin{cases} T_{max}, & |\boldsymbol{u}| \geq \frac{T}{m} \\ 0, & |\boldsymbol{u}| < \frac{T}{m} \end{cases}. \tag{3.26}$$

A drawback of this coasting mechanism is that it may cause control on/off chatter when the commanded acceleration magnitude is nearly equal to the

available acceleration magnitude.

Naasz briefly discusses the impact of the singularities inherent in any control law based on the classical element set. If the target orbit is circular – meaning ω_T is undefined – K_ω is set to zero.

3.5 Kluever Control and Ruggiero Control

Control laws presented by Kluever [13] and Ruggiero et al. [23] are discussed together because both are based on the concept of blending the optimal control laws for changing individual classical orbital elements to create a control law capable of targeting multiple elements simultaneously.

3.5.1 Kluever Control

Kluever's scheme is capable of targeting a, e, and i. The in-plane control angle is a weighted average of the optimal control acceleration directions for changing a and e:

$$\hat{\boldsymbol{u}}_{in} = \frac{K_a \hat{\boldsymbol{u}}_a + K_e \hat{\boldsymbol{u}}_e}{|K_a \hat{\boldsymbol{u}}_a + K_e \hat{\boldsymbol{u}}_e|} = \begin{pmatrix} \sin(\alpha_{R\theta H}) \\ \cos(\alpha_{R\theta H}) \\ 0 \end{pmatrix}, \tag{3.27}$$

where $\hat{\boldsymbol{u}}_a$ is the optimal control acceleration direction for increasing a, $\hat{\boldsymbol{u}}_e$ is the optimal control acceleration direction for increasing e, and K_a and K_e are weighting functions. (Expressions for $\hat{\boldsymbol{u}}_a$ and $\hat{\boldsymbol{u}}_e$ may be obtained using the control angles derived in Sections 2.6.1 and 2.6.2 and the relation given

by (2.6).) Calculation of $\hat{\boldsymbol{u}}_i$ allows for immediate calculation of $\alpha_{R\theta H}$ using (3.27).

The out-of-plane control angle is determined solely by the optimal angle for changing i. However, Kluever modifies the expression given by (2.59) to account for the fact that it is inefficient to change inclination near $\nu+\omega = \pm\frac{\pi}{2}$ and uses instead

$$\beta_{R\theta H} = K_i \cos(\nu + \omega), \tag{3.28}$$

where K_i is a weighting function. The final control unit vector is then given by (2.6).

Kluever's method has three primary drawbacks. First, no mechanism is given for targeting Ω or ω. However, this could be remedied by adding $\hat{\boldsymbol{u}}_\omega$ and a K_ω to the calculation of $\hat{\boldsymbol{u}}_{in}$ in (3.27) and manipulating the out-of-plane control angle calculation to more closely resemble that of the in-plane control angle calculation so that

$$\hat{\boldsymbol{u}}_{out} = \frac{K_i\hat{\boldsymbol{u}}_i + K_\Omega\hat{\boldsymbol{u}}_\Omega}{|K_i\hat{\boldsymbol{u}}_i + K_\Omega\hat{\boldsymbol{u}}_\Omega|} = \begin{pmatrix} 0 \\ 0 \\ \cos(\beta_{R\theta H}) \end{pmatrix}. \tag{3.29}$$

A deficiency that is more difficult to address is the lack of a systematic approach for selecting the weighting functions K_a, K_e, and K_i. Kluever suggests expressing the weights as quadratic functions of time whose coefficients

are to be set by the mission designer using engineering judgment; however, as he himself notes [13], "simplicity is often a desired attribute of a good guidance scheme," and a robust control law should require minimal user input. Furthermore, any weighting functions that change with time are inherently problematic since the time of flight is generally unknown *a priori*.

Finally, as is the case for all control laws based on the blending of the optimal control directions for changing multiple elements, there is no theoretical basis that ensures convergence to the target orbit.

3.5.2 Ruggiero Control

The fundamental equation put forth by Ruggiero et al. gives the desired control acceleration direction unit vector as

$$\hat{\boldsymbol{u}} = \frac{\sum_{\mathcal{O}} W_{\mathcal{O}} \frac{\mathcal{O}_T - \mathcal{O}}{\mathcal{O}_T - \mathcal{O}_i} \hat{\boldsymbol{u}}_{\mathcal{O}}}{\left| \sum_{\mathcal{O}} W_{\mathcal{O}} \frac{\mathcal{O}_T - \mathcal{O}}{\mathcal{O}_T - \mathcal{O}_i} \hat{\boldsymbol{u}}_{\mathcal{O}} \right|}, \quad \mathcal{O} = a, e, i, \Omega, \omega, \tag{3.30}$$

where $\hat{\boldsymbol{u}}_{\mathcal{O}}$ is the optimal thrust direction unit vector for changing a classical element (given in Section 2.6), $\mathcal{O}_i$ is the value of an orbital element at the beginning of a maneuver, and $W_{\mathcal{O}}$ is a weighting function given by

$$W_{\mathcal{O}} = \begin{cases} 1, & \mathcal{O} \neq \mathcal{O}_T \\ 0, & \mathcal{O} = \mathcal{O}_T \end{cases}. \tag{3.31}$$

A method for introducing coast segments into the transfer trajectory is also presented, based heavily on the idea of absolute effectivity [20, 21] (see Section

3.3). As with Petropoulos's control law, however, no systematic approach for determining an appropriate value for η_a is given.

The Ruggiero control law has the advantage of being simply adaptable to the situation in which only a subset of the classical element set is targeted: the $W_{\mathcal{O}}$ of any free element is set to zero. However, the remainder of the control blending function presents problems. Beyond the $W_{\mathcal{O}}$, the weighting of the $\hat{\boldsymbol{u}}_{\mathcal{O}}$ is given by the difference between the current value of the orbital element and its target value normalized by the difference between the initial value of the orbital element and its target value. The rationale behind this strategy is that the control direction should be closer to the optimal direction for correcting elements (relatively) farther from their target values in order to ensure that all elements achieve their target values at roughly the same time. Unfortunately, such weighting leads to singularities in the case in which the target value of an element is equal to its initial value ($\mathcal{O}_T = \mathcal{O}_i$). Perhaps the simplest possible workaround for this problem is to set a lower bound on the magnitude of $\mathcal{O}_T - \mathcal{O}_i$ used to formulate $\hat{\boldsymbol{u}}$. This way, the target value of an element may still be equal to the initial value of that element, but, when used in the calculation of $\hat{\boldsymbol{u}}$, the value of $\mathcal{O}_T - \mathcal{O}_i$ is changed slightly from its true value to avoid a singularity. A drawback of this revision is that it may give an improperly large weight to an element whose target value is equal to its initial value and whose osculating value deviates from the initial/target value because of the small, non-zero value assigned to $\mathcal{O}_T - \mathcal{O}_i$.

Another disadvantage of the Ruggiero control law is that, as given, it

lacks a firm theoretical underpinning (such as Lyapunov stability theory) that guarantees convergence to the target orbit.

3.6 Bombrun Control

A control law introduced by Bombrun [5] is based on a Lyapunov function of the form

$$V_B = \sum_{i=1}^{5} K_i(\mathcal{O}_i - \mathcal{O}_{i_T})^2, \tag{3.32}$$

where the K_i are weighting functions, the $\mathcal{O}_i$ are any set of five independent parameters that may be used to define the current osculating orbit (i.e. the classical element set or the equinoctial element set), and the $\mathcal{O}_{i_T}$ are the target values of those parameters. From this general formulation, Bombrun focuses on defining V_B using the classical element set. For example, for a transfer from a geosynchronous transfer orbit to an equatorial geosynchronous orbit for which a, e, and i are targeted, the Lyapunov function is given by

$$V_{B_1} = 4\left(\frac{a}{a_{GEO}} - 1\right)^2 + 3e^2 + i^2, \tag{3.33}$$

where a_{GEO} is the semi-major axis of the equatorial geosynchronous orbit. The control is then found through application of (3.4). While V_{B_1} is certainly valid and is shown to be effective, it has the severe disadvantage of being highly

specialized to the specific problem for which it is implemented. To remedy this, Bombrun uses Lyapunov interpolation to formulate Lyapunov functions for a large set of planar orbit transfers. For these transfers, the Lyapunov function is given by

$$V_{B_2} = \cos(\phi)\left(\frac{a}{a_{GEO}} - 1\right)^2 + \sin(\phi)e^2, \tag{3.34}$$

where $\phi \in [0, \frac{\pi}{2}]$. The value of ϕ for a particular orbit transfer is determined by comparing the control commanded by the control law to the control dictated by a time-optimal transfer scheme at each time step along the time-optimal transfer trajectory. The value of ϕ is then set such that the difference between the control law's control and that of the time-optimal maneuver is minimized. Mathematically, ϕ is chosen to minimize the performance index

$$J = \frac{1}{(t_{f_{opt}} - t_{0_{opt}})} \int_{t_{0_{opt}}}^{t_{f_{opt}}} |\boldsymbol{u}_\phi(\gamma(t)) - \boldsymbol{u}(\gamma_{opt}(t))|^2 \mathrm{d}t, \tag{3.35}$$

where $t_{0_{opt}}$ and $t_{f_{opt}}$ are the initial and final times of the time-optimal transfer maneuver, respectively, $\gamma(t)$ is the transfer trajectory generated by the control law, $\gamma_{opt}(t)$ is the time-optimal transfer trajectory, $\boldsymbol{u}_\phi(\gamma(t))$ is the control acceleration vector on the trajectory $\gamma(t)$ (which is a function of ϕ), and $\boldsymbol{u}(\gamma_{opt}(t))$ is the control acceleration vector on the time-optimal trajectory.

An obvious disadvantage of Lyapunov interpolation of this kind is that the generation of V_{B_2} requires prior knowledge of the corresponding time-

optimal transfer trajectory. As the determination of arbitrary optimal low-thrust transfer trajectories can be difficult – some of the appeal of closed-loop control laws comes specifically from the fact that open-loop optimization is not required – this is a poor feature for a control law. Furthermore, the given form of V_{B_2} applies only to planar orbit transfers, and neither V_{B_1} nor V_{B_2} provides the ability to target Ω or ω.

3.7 Chang Control

Chang et al. [6] propose a control law based on targeting the angular momentum vector $\boldsymbol{h}$ and the Laplace vector $\boldsymbol{A} = \mu \boldsymbol{e}$. To this end, Chang introduces the vector $\boldsymbol{X} = (\boldsymbol{h} \quad \boldsymbol{A})^T$ and a Lyapunov function

$$V_C = \frac{1}{2} k |\delta \boldsymbol{h}|^2 + \frac{1}{2} |\delta \boldsymbol{A}|^2, \tag{3.36}$$

where $k > 0$ is a weighting function and

$$\delta \boldsymbol{h} = \boldsymbol{h} - \boldsymbol{h}_T \tag{3.37}$$

$$\delta \boldsymbol{A} = \boldsymbol{A} - \boldsymbol{A}_T. \tag{3.38}$$

Differentiating the Lyapunov function with respect to $\boldsymbol{X}$ gives

$$\frac{\partial V_C}{\partial \boldsymbol{X}} = \left(k \delta \boldsymbol{h} \quad \delta \boldsymbol{A} \right), \tag{3.39}$$

while, from the variational equations for $\boldsymbol{h}$ and $\boldsymbol{e}$,

$$\dot{\boldsymbol{X}} = \begin{pmatrix} \boldsymbol{r} \times \boldsymbol{u} \\ \boldsymbol{u} \times \boldsymbol{h} + \boldsymbol{v} \times (\boldsymbol{r} \times \boldsymbol{u}) \end{pmatrix}. \tag{3.40}$$

After some manipulation, the time derivative of the Lyapunov function may then be written as

$$\dot{V}_C = \frac{\partial V_C}{\partial \boldsymbol{X}} \dot{\boldsymbol{X}} = [k\delta\boldsymbol{h} \times \boldsymbol{r} + \boldsymbol{h} \times \delta\boldsymbol{A} + (\delta\boldsymbol{A} \times \boldsymbol{v}) \times \boldsymbol{r}]^T \boldsymbol{u}. \tag{3.41}$$

The isolation of the control $\boldsymbol{u}$ in (3.41) facilitates a nearly trivial derivation of the control that minimizes $\dot{V}_C$: The time derivative of the Lyapunov function is minimized when $\boldsymbol{u}$ is set to directly oppose the term with which it is multiplied in (3.41):

$$\boldsymbol{u} = -f[k\delta\boldsymbol{h} \times \boldsymbol{r} + \boldsymbol{h} \times \delta\boldsymbol{A} + (\delta\boldsymbol{A} \times \boldsymbol{v}) \times \boldsymbol{r}], \tag{3.42}$$

for arbitrary $f > 0$.

It may be shown, through invocation of LaSalle's Invariance Principle, that the controller given by (3.42) causes any elliptical orbit to asymptotically converge to any targeted elliptical orbit [6]. Furthermore, Chang's control law is the only one discussed in this thesis for which it is shown that an initial elliptical orbit remains an elliptical orbit throughout the orbit transfer

process. However, the proof for this requires that the maneuver be a "local" orbit transfer. A transfer between two arbitrary elliptical orbits may then be accomplished by performing multiple local transfers in succession. (See [6] for a more detailed discussion of local vs. global orbit transfers.)

While, as is shown by an example orbit transfer given in [6], this control law is not without merit, as presented, it does have several considerable shortcomings. One is associated with the parameter k. While the chosen value of k greatly influences the efficiency with which a spacecraft will reach a target orbit, no systematic approach is given for its proper selection. Moreover, it is possible that the use of multiple weighting functions would add flexibility to the method because, for the majority of orbit transfer scenarios, it is unlikely that all components of $\delta\boldsymbol{h}$ should be weighted equally and all components of $\delta\boldsymbol{A}$ should be weighted equally. Furthermore, increasing the number of weighting functions from one to six adds minimal complexity to the derivation of the control law because derivations of revised expressions for $\dot{\boldsymbol{X}} = \boldsymbol{g}(\boldsymbol{X})\boldsymbol{u}$ and $\frac{\partial V_C}{\partial \boldsymbol{X}}$ are straightforward. (See (2.47).)

A second drawback of this method is that of the coupling that exists in the transformations between the angular momentum and Laplace vectors and the classical element set. This makes it impractical to target arbitrary subsets of the classical element set with this control law.

3.8 Summary

The characteristics of the low-thrust control laws discussed in this thesis are summarized in Tables 3.1 and 3.2.

Table 3.1: Summary of low-thrust control laws.

Author(s)	Type	Targeted elements	Coasting mechanisms
Naasz	Lyapunov	any subset of a, e, i, Ω, ω, M_0	one
Petropoulos	Lyapunov	any subset of a, e, i, Ω, ω	two
Joseph	Lyapunov	any subset of a, P_1, P_2, Q_1, Q_2	zero
Kluever	Blended	any subset of a, e, i	zero
Ruggiero et al.	Blended	any subset of a, e, i, Ω, ω	one
Bombrun	Lyapunov	V_{B_1}: any subset of a, e, i; V_{B_2}: any subset of a, e	zero
Chang et al.	Lyapunov	$\boldsymbol{h}$, $\boldsymbol{A}$	zero

Table 3.2: Summary of low-thrust control law weighting parameters and selection methods.

Author(s)	Weighting parameters	Selection method
Naasz	one per element	$\mathcal{O}_T$
Petropoulos	two per element	$\mathcal{O}$
Joseph	one per element	$\mathcal{O}$
Kluever	one per element	polynomial functions of time
Ruggiero et al.	one per element	$\mathcal{O}_i$, $\mathcal{O}$, $\mathcal{O}_T$
Bombrun	one per element	V_{B_1}: $\mathcal{O}$, $\mathcal{O}_T$; V_{B_2}: time-optimal trajectory
Chang et al.	one	no method given

Note: For Lyapunov-type control laws, weighting refers to the weighting of element errors; for blended-type control laws, weighting refers to the weighting of control directions. $\mathcal{O}_i$ refers to the initial orbit, $\mathcal{O}$ refers to the osculating orbit, and $\mathcal{O}_T$ refers to the target orbit.

Chapter 4

Numerical Simulation of Low-Thrust Control Laws

4.1 Introduction

This chapter describes the methods used to numerically model three of the control laws described in Chapter 3. The method of trajectory propagation is presented, and modifications made to each of the three control laws to improve performance are discussed. Three methods used to introduce coast arcs into trajectories are described, and, finally, the problem of measuring convergence to the target orbit is discussed.

4.2 Control Laws Modeled

Of the seven control laws discussed in depth in Chapter 3, three are implemented in numerical simulations in order to obtain a quantitative comparison: Naasz's control law, Petropoulos's control law, and Joseph's control law. These control laws are selected for two primary reasons:

1. All three present methods with firm theoretical bases for weighting the error terms of their Lyapunov functions.

2. Naasz's control law and Petropoulos's control law allow for the targeting of arbitrary subsets of the classical element set, and Joseph's control law may be made to do so with straightforward modifications.

Ruggiero's control law also meets these criteria (although in this case the weighting is of the blended control directions rather than of the terms of a Lyapunov function). However, the severe problems with the weighting functions discussed in Section 3.5.2 preclude the control law's use in many practical scenarios. Therefore, Ruggiero's control law is not modeled.

Bombrun's control law, Kluever's control law, and Chang's control law are not modeled primarily because of the lack of a systematic method for selecting the values of weighting parameters.

4.3 Spacecraft State Propagation

For all maneuvers, the primary method of spacecraft state propagation is numerical integration of Gauss's form of the Lagrange Planetary Equations (see (2.26)) using variable-step-size Adams methods [10]. The state vector is

$$\mathbf{x} = \begin{pmatrix} a \\ e \\ i \\ \Omega \\ \omega \\ \nu \\ m \end{pmatrix}. \tag{4.1}$$

$\boldsymbol{\mathfrak{X}}$ is integrated in time, with the time derivative of the spacecraft mass given by

$$\dot{m} = -\frac{T}{g_0 I_{sp}}, \tag{4.2}$$

where T is the thrust force magnitude, g_0 is the reference gravitational acceleration at Earth's surface, and I_{sp} is the specific impulse of the spacecraft's propulsion system.

Because control direction chatter can cause a variable-step integration scheme to take step sizes so small that propagation effectively stops, the fixed-step propagation method employed by Naasz [17] is also implemented. This method is invoked only in the case that the primary integrator requires the evaluation of the derivatives of the state at $10,000$ time steps in a 100-second time span. If this condition is met, the fixed-step propagation method is used for a time span of up to one day, at which point integration duties are returned to the primary propagation scheme. The fixed step size used is 3 seconds.[1] A detailed description of Naasz's propagation method is given in Appendix A.4.

Only one control law and one of the maneuvers simulated numerically required the use of fixed-step propagation (Section 5.4).

[1]Note that the criterion for switching to the fixed-step propagation method is problem-dependent, as is the fixed step size itself.

4.4 Modifications to Control Laws

Several modifications are made to the three modeled control laws in order to improve the numerical properties of the simulations. First, in order to avoid singularities in the classical element set, threshold values are set on eccentricity and inclination. If it is desired to begin a maneuver at a value of e or i (or target a value of e or i) near a value that produces a singularity in the variational equations or in the equations used to calculate the control, the initial (or target) value is changed so that it is different from the value that produces the singularity by the threshold value. Additionally, if, during the course of a maneuver, the osculating elements of the transfer orbit near a value of e or i that would cause a singularity, the offending element is held constant at the threshold value until the rate of change of the element becomes such that the element will begin to move away from the singularity [21]. Mathematically, the singularity-avoidance procedure may be written as

$$\mathcal{O} = \begin{cases} \mathcal{O}, & \mathcal{O} \geq \epsilon_{\mathcal{O}} \\ \epsilon_{\mathcal{O}}, & \mathcal{O} < \epsilon_{\mathcal{O}} \end{cases}, \quad \mathcal{O} = e, i, \tag{4.3}$$

for some $\epsilon_{\mathcal{O}} > 0$. For all simulations performed in the completion of this thesis, $\epsilon_{\mathcal{O}}$ is set such that $\epsilon_e = 5 \times 10^{-3}$ and $\epsilon_i = 10^{-4}$ rad. The relatively large value of ϵ_e is used because the calculation of the control in Petropoulos's control law requires exponentiating the eccentricity with large negative values.

4.4.1 Modifications to Naasz Control

Several changes are made to the Lyapunov function for the form of Naasz's control law implemented in this thesis. First, because phasing is not considered here, the value of K_{M_0} is always set to zero; error in the mean anomaly at epoch therefore does not contribute to the Lyapunov function. Second, the error functions for Ω and ω are changed slightly to the form presented by Petropoulos [21], given by (3.8). Also, the expressions for K_i and K_Ω given by Naasz – which do not account for the quadrant ambiguity inherent in invoking the inverse sine function – are replaced by expressions that do take this into consideration:

$$K_i = \left[\frac{h\left(\sqrt{1-e^2\sin^2(\omega)} - e|\cos(\omega)|\right)}{p}\right]^2 \frac{1}{\Delta t} \tag{4.4}$$

$$K_\Omega = \left[\frac{h\sin(i)\left(\sqrt{1-e^2\cos^2(\omega)} - e|\sin(\omega)|\right)}{p}\right]^2 \frac{1}{\Delta t}. \tag{4.5}$$

Finally, the minimum-periapsis-distance penalty function used by Petropoulos (see (3.10)) is introduced into Naasz's Lyapunov function so that it becomes

$$V_{N_{mod}} = \frac{1}{2}(1 + W_P P)\sum_{\mathcal{O}} K_{\mathcal{O}}(\delta\mathcal{O})^2, \quad \mathcal{O} = a, e, i, \Omega, \omega. \tag{4.6}$$

Further modifications are made in the calculation of the $K_{\mathcal{O}}$. First and foremost, the issue of undefined $K_{\mathcal{O}}$ in the case of an only partially defined

target orbit (discussed in Section 3.4) is circumvented by prescribing that, should the target value of an untargeted orbital element be required to calculate the $K_{\emptyset}$, the initial value of that element is used instead. Also, because Naasz gives no theoretical basis for calculating the $K_{\emptyset}$ on the target orbit and holding them constant for the duration of the maneuver, two other possibilities are investigated:

1. Calculate $K_{\emptyset}$ on the initial orbit and hold constant.

2. Calculate $K_{\emptyset}$ by evaluating the orbital elements at a simple average of the initial and target values and hold constant. (The continuity of Ω and ω at values of 0 and 2π is taken into account.)

It would also be natural to calculate the $K_{\emptyset}$ using the osculating orbital elements and thereby continuously revise the weights of the terms of the Lyapunov function. However, such a strategy would make Naasz's weighting terms identical to those of Petropoulos and Joseph. Therefore, this method is not examined as a separate case of Naasz's control law.

4.4.2 Modifications to Joseph Control

For implementation in this thesis, the Lyapunov function used by Joseph is altered so that the error terms are written in terms of the classical element set rather than the equinoctial element set in order to allow for the targeting of arbitrary subsets of the classical element set. Furthermore, the modifications made by Petropoulos [21] to the Lyapunov function originally presented in [20]

are incorporated into Joseph's Lyapunov function. (This includes the use of the penalty function used to enforce a minimum periapsis distance.) Thus, the Lyapunov function implemented for Joseph's control law is equivalent to that which is implemented for Petropoulos's control law. The difference between the two control laws, then, is in the calculation of the derivatives of the Lyapunov function with respect to the classical orbital elements (see Sections 3.3.1 and 3.3.2).

4.4.3 Modifications to Petropoulos Control

No substantive modifications are made to Petropoulos's control law.

4.5 Coast Segments

Introducing coast segments into a trajectory is accomplished by simply setting the control acceleration magnitude to zero at a given time step in the numerical integration if the control law dictates the existence of a coast segment. This determination is made one of four ways:

1. Control acceleration is applied under all circumstances.
2. Control acceleration is applied if absolute effectivity is greater than a constant threshold value (see Section 3.3.1).
3. Control acceleration is applied if relative effectivity is greater than a constant threshold value (see Section 3.3.1).

4. Control acceleration is applied if the magnitude of requested control acceleration is greater than the magnitude of available control acceleration (see Section 3.4). (Only applicable to Naasz's control law.)

While Petropoulos [21] presents simulations that use multiple values of η_a for a single trajectory and others that use both absolute effectivity and relative effectivity thresholds for a single trajectory, these strategies are not used in the simulations presented in this thesis. Furthermore, while the effectivity concept is not explicitly mentioned by either Naasz or Joseph, its extension to these two control laws is natural and straightforward. On the other hand, Naasz's coasting scheme may not be so easily applied to the control laws of Petropoulos and Joseph because it relies on comparison of the requested control acceleration magnitude with the maximum value available to the spacecraft. Such a comparison is meaningless for the other two control laws because the units of the control they output are not those of acceleration.[2] For this reason, Naasz's coasting strategy is implemented only for the corresponding control law.

The determination of absolute and relative effectivity is done numerically. Because the only optimization variable in the calculations is true anomaly, the numerical procedure presents no large difficulty. On the first calculation of an effectivity, the control dictated by a control law is calculated

[2]In the SI system, the units are $[\boldsymbol{u}] = \frac{[s]^3}{[m]}$. The control must be unitized and scaled by the magnitude of the available control acceleration to make physical sense.

at half-degree increments of true anomaly between $\nu = 0^\circ$ and $\nu = 360^\circ$ on the current osculating orbit. From this, the approximate minimum and maximum time rates of change of the Lyapunov function on the current osculating orbit are calculated. The minimum value of the time rate of change of the Lyapunov function is used to calculate absolute effectivity, while both the minimum and maximum values are used to calculate relative effectivity. When effectivities are calculated at subsequent time steps, a sequential quadratic programming (SQP) algorithm [24] is used to calculate the minimum and maximum time rates of change of the Lyapunov function over true anomaly. The initial guess of true anomaly required by the algorithm is set to the corresponding optimized value from the previous time step. (The lack of knowledge regarding an accurate initial guess is the reason the SQP algorithm is not used at the first time step). If for any reason the SQP algorithm fails at a given time step, the method used to calculate the effectivities at the first time step is used instead.

The SQP algorithm requires the derivatives of the objective function (the time rate of change of the Lyapunov function) with respect to the optimization variable (true anomaly). From (3.5) and the forms of the Lyapunov functions used by the control laws modeled, the only derivatives that must be taken are those of the elements of (2.36) with respect to true anomaly. The necessary expressions are given in Appendix A.1.

In order to minimize control on/off chatter, Petropoulos's strategy of requiring a minimum control application duration of 10° of true longitude is applied to all coast methods. The implementation is such that a controlled arc

begins when the criterion for control is first met and must continue at least until the minimum duration is reached. It is likely more optimal to center the controlled arc around the time at which the criterion for control is first met, but any attempt to do so would require knowledge of the control criterion at future values of time. This would require that the maneuver be propagated iteratively. Because the goal of closed-loop control laws is to prescribe a control using only the current and target values of the spacecraft state, no such scheme is used.

4.6 Defining Convergence

Each of the three implemented control laws is based on Lyapunov control theory, the goal of which is to drive the spacecraft to the target orbit *asymptotically*. A consequence of this is that, as the spacecraft nears the target orbit, the rate of approach decreases ($\dot{V}$ approaches zero). Because of this, the Lyapunov function will not achieve a value of precisely zero in finite time, and a mission designer must choose some other criteria with which to determine arrival on the target orbit. A natural strategy is to pronounce a maneuver complete when the value of the Lyapunov function becomes less than some threshold value. However, several issues complicate this method. First, because different control laws utilize different Lyapunov functions, a different threshold value must be set for each to achieve similar results. Second, even when using a single control law, tolerable error for two maneuvers may correspond to different values of the Lyapunov function, meaning that the threshold

value must be tuned for every maneuver analyzed.

Another difficulty arises from the fact that the state and control are (necessarily) evaluated at discrete points in the maneuver evolution. Like all CLFD control laws, those modeled in this thesis rely on the difference between the current value of a state and its target value to prescribe the control. As a state approaches its target value, at some point it will begin to oscillate about the target value because the combination of the magnitude of the control and the size of the step between consecutive points in the numerical propagation results in a control that is unable to change rapidly enough to avoid overshooting the target. (For this reason, smaller control magnitudes and smaller propagation steps generally result in tighter convergences.) When a variable-step-size integration scheme is used to perform the numerical propagation, this phase of the maneuver is generally characterized by rapidly shrinking step sizes, often to the point that the propagation effectively stops. At this point, convergence must be pronounced, as further improvement is not possible unless the propagation scheme is changed.

In an effort to avoid these problems, the control law algorithms implemented in this thesis deem a maneuver complete when the differences between the osculating values of targeted orbital elements and their target values are all less than threshold values simultaneously. The threshold values for the individual maneuvers performed are specified in Chapter 5. Options for obtaining a maneuver that achieves the final orbit more exactly include (1) decreasing the control acceleration magnitude and (2) targeting specific elements individually

after other elements have achieved acceptable values.

Chapter 5

Numerical Results

5.1 Introduction

Three maneuvers are simulated using the methodology presented in the preceding chapters. The maneuvers are selected for two reasons: first, to represent a realistic set of maneuvers a spacecraft may be expected to perform, and, second, to showcase both the strengths and weaknesses of the control laws modeled. For each maneuver, the results obtained from the control laws of Petropoulos, Joseph, and Naasz are compared against one another using a variety of absolute and relative effectivity control cutoff values. Additionally, the results obtained from implementation of two other methods of calculating Naasz's weighting values and from the use of Naasz's coasting strategy are presented. Table 5.1 summarizes abbreviations used in the discussion of all maneuvers.

Table 5.1: Control law abbreviations.

Abbreviation	Meaning
P	Petropoulos's control law
J	Joseph's control law
N_0	Naasz's control law, weights evaluated on target orbit
N_1	Naasz's control law, weights evaluated on initial orbit
N_2	Naasz's control law, weights evaluated using average of initial orbit and target orbit

For all maneuvers, the Earth is taken to be the central body. Thus, $g_0 = 9.80665\ \frac{\mathrm{m}}{\mathrm{s}^2}$ and $\mu = 3.9860049\ \frac{\mathrm{km}^3}{\mathrm{s}^2}$.

5.2 Equatorial Orbit to Polar Orbit Transfer

The characteristics of a maneuver from an equatorial orbit ($i \approx 0°$) to a polar orbit ($i = 90°$) are given in Tables 5.2 and 5.3. Note that, when the maneuver is performed using Petropoulos's control law, a penalty function of the form given by (3.10) with $k = 100$ and $r_{p_{min}} = 6578$ km is used in order to prevent the spacecraft from impacting the Earth.

Table 5.2: Equatorial orbit to polar orbit maneuver elements.

Orbit	a (km)	e	i (deg)	Ω (deg)	ω (deg)	ν (deg)
Initial	10000	0.005	5.73×10^{-3}	0	0	0
Target	10000	0.005	90	free	free	free

Note: The initial inclination value corresponds to $\epsilon_i = 10^{-4}$ rad. (See Section 4.4.)

Table 5.3: Equatorial orbit to polar orbit maneuver characteristics.

Thrust (N)	Initial mass (kg)	I_{sp} (s)
1	300	3100

The convergence tolerances for this maneuver are given in Table 5.4.

Table 5.4: Equatorial orbit to polar orbit maneuver convergence tolerances.

Element	Tolerance
a	1 percent relative error (100 km)
e	0.01
i	0.1°

The results of the maneuvers commanded by the control laws are summarized in Tables 5.5 - 5.8. Table 5.5 also includes a comparison to a maneuver obtained using Edelbaum's orbital averaging scheme [4, 8]. (A description of Edelbaum's method is given in Appendix A.5.)

Table 5.5: Equatorial orbit to polar orbit maneuver comparisons: continuous control application.

Coasting Criterion	Control Law	Flight time (days)	Propellant mass (kg)
None	P	33.5683	95.4027
	J	42.2917	120.1949
	N_0, N_1, N_2	42.2917	120.1949
	Edelbaum	35.8779	101.9668

Table 5.6: Equatorial orbit to polar orbit maneuver comparisons: absolute effectivity coasting criteria.

Coasting Criterion	Control Law	Flight time (days)	Propellant mass (kg)
$\eta_a = 0.33$	P	34.5671	89.9121
	J	45.6516	106.3174
	N_0, N_1, N_2	45.6516	106.3174
$\eta_a = 0.67$	P	73.1551	71.4029
	J	57.6863	93.7575
	N_0, N_1, N_2	57.6863	93.7575
$\eta_a = 0.90$	P	153.3137	68.0399
	J	92.8495	86.7943
	N_0, N_1, N_2	92.8495	86.7943

Table 5.7: Equatorial orbit to polar orbit maneuver comparisons: relative effectivity coasting criteria.

Coasting Criterion	Control Law	Flight time (days)	Propellant mass (kg)
$\eta_r = 0.33$	P	84.8553	73.1519
	J	45.6968	106.1905
	N_0, N_1, N_2	45.6516	106.3174
$\eta_r = 0.67$	P	167.0590	69.4826
	J	57.7153	93.7625
	N_0, N_1, N_2	57.7211	93.7523
$\eta_r = 0.90$	P	278.7106	67.9010
	J	92.7500	86.8024
	N_0, N_1, N_2	92.7940	86.8013

Table 5.8: Equatorial orbit to polar orbit maneuver comparisons: Naasz coasting criterion.

Coasting criterion	Control Law	Flight time (days)	Propellant mass (kg)
Naasz	N_0, N_1, N_2	42.2917	120.1938

In all scenarios, the results for Joseph's control law and all three implementations of Naasz's control law are identical except for numerical imprecision. This is to be expected: The initial and final values of semi-major axis and eccentricity are identical, and inclination does not appear in the expressions for Naasz's K_a, K_e, or K_i, so N_0, N_1, and N_2 should all produce identical trajectories. (See (3.20).) Joseph's control law produces the same control profile, as well, because of the similarities between Joseph's control law and Naasz's control law discussed in Section 3.4. Initially, the errors in semi-major axis and eccentricity are zero, so all control is directed toward correcting the inclination error. In Joseph's control law and Naasz's control law, this is accomplished through out-of-plane control application only, which has no effect on semi-major axis or eccentricity. Therefore, the control for both laws is directed purely out of plane for the entirety of the maneuvers, thereby creating identical transfer trajectories.

The maneuver directed by Petropoulos's control law, however, is markedly different, and the lower propellant mass requirements shown in Tables 5.5 - 5.7 clearly display the utility of differentiating the full form of the Lyapunov

function rather than using Joseph's approximation or Naasz's constant $K_\mho$ values. As shown in Figure 5.1, Petropoulos's control law increases a to a peak of approximately five times its initial and target value to decrease the fuel expenditure required to change i. The time evolution of i shown in Figure 5.2 confirms that i begins its increase more slowly when Petropoulos's control law is used, but quickly increases its rate of change as a grows.

Another difference between the maneuvers is that Petropoulos's control law causes the eccentricity to increase to a maximum value greater than 0.6 before decreasing to its target value, while the control laws of Joseph and Naasz leave the eccentricity constant for the duration of the maneuver, as illustrated in Figure 5.3.[1] As previously discussed, Joseph's control law and Naasz's control law direct the control acceleration purely out of plane for the duration of the maneuver, and this accounts for the lack of change in eccentricity. The large eccentricity change dictated by Petropoulos's control law is due to the fact that the derivatives of the a and i terms of V_P with respect to e are always less than zero, meaning that control acceleration is applied to increase e in order to decrease these terms. (See (2.54), (2.61), and (3.7).)

For all three control laws, increasing either the absolute or relative effectivity control-application threshold results in longer flight times and less

[1] In fact, the large changes in e commanded by Petropoulos's control law are the reason a minimum-periapsis-distance penalty function is implemented for this control law. Without the penalty function, the control causes the spacecraft to impact the central body. Further, the large eccentricity change plays a large role in Petropoulos's control law achieving the target orbit is less time than Edelbaum's averaging method, which assumes a quasi-circular orbit for the duration of the maneuver.

propellant mass expenditure. For all cases, Petropoulos's control law produces the maneuver that requires the least propellant mass.

Naasz's coasting strategy, on the other hand, is seen to be less effective. When comparing the results of Table 5.8 to those of Table 5.5, it is notable that Naasz's coasting scheme produces only miniscule changes in both the flight time and propellant usage. This is because the control acceleration "requested" by Naasz's control law is significantly greater than the control acceleration that the spacecraft propulsion system is capable of producing for the duration of the maneuver until the spacecraft has very nearly achieved the target orbit. This is typical of Naasz's coasting strategy for most maneuvers and makes it less effective at introducing intermediate coast arcs than Petropoulos's effectivity cutoff coasting criterion, which, as shown in Tables 5.6 and 5.7, produces significant propellant savings for the cases tested.

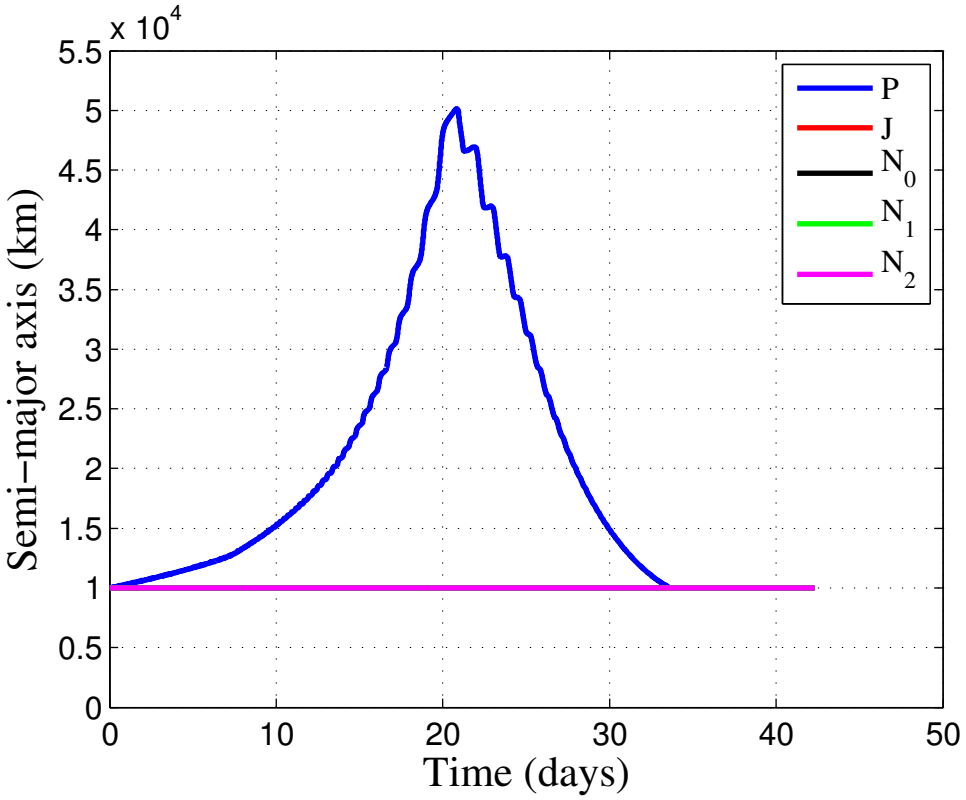

Figure 5.1: Equatorial orbit to polar orbit maneuver comparisons: semi-major axis evolution, continuous control application. Note: Only two curves are visible because all evolutions but P are identical.

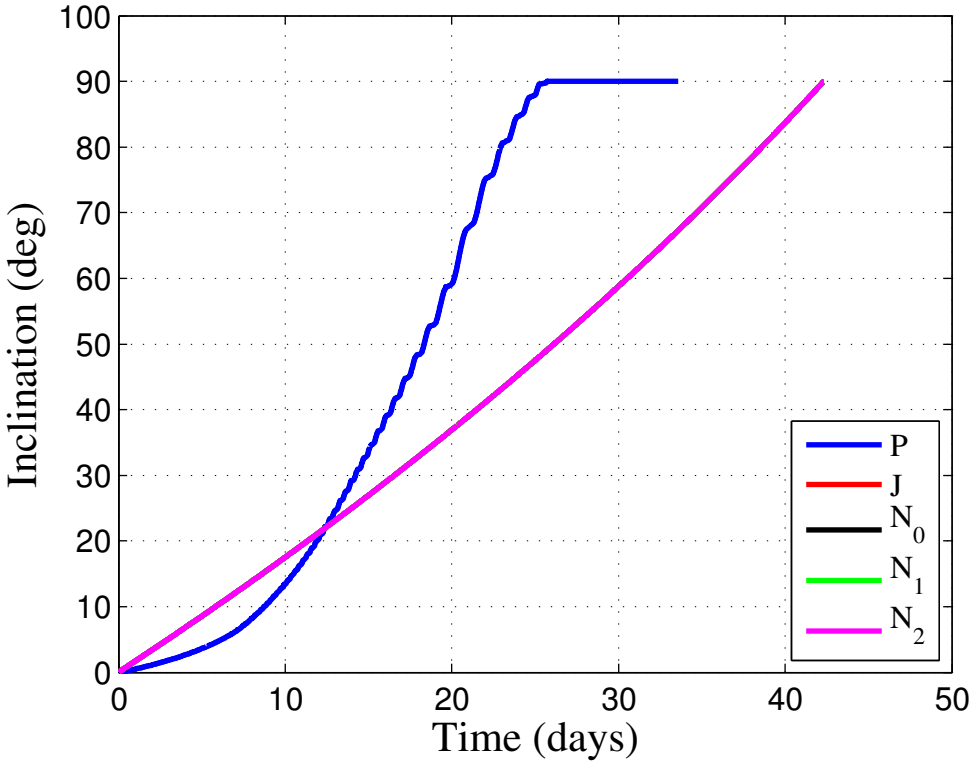

Figure 5.2: Equatorial orbit to polar orbit maneuver comparisons: inclination evolution, continuous control application. Note: Only two curves are visible because all evolutions but P are identical.

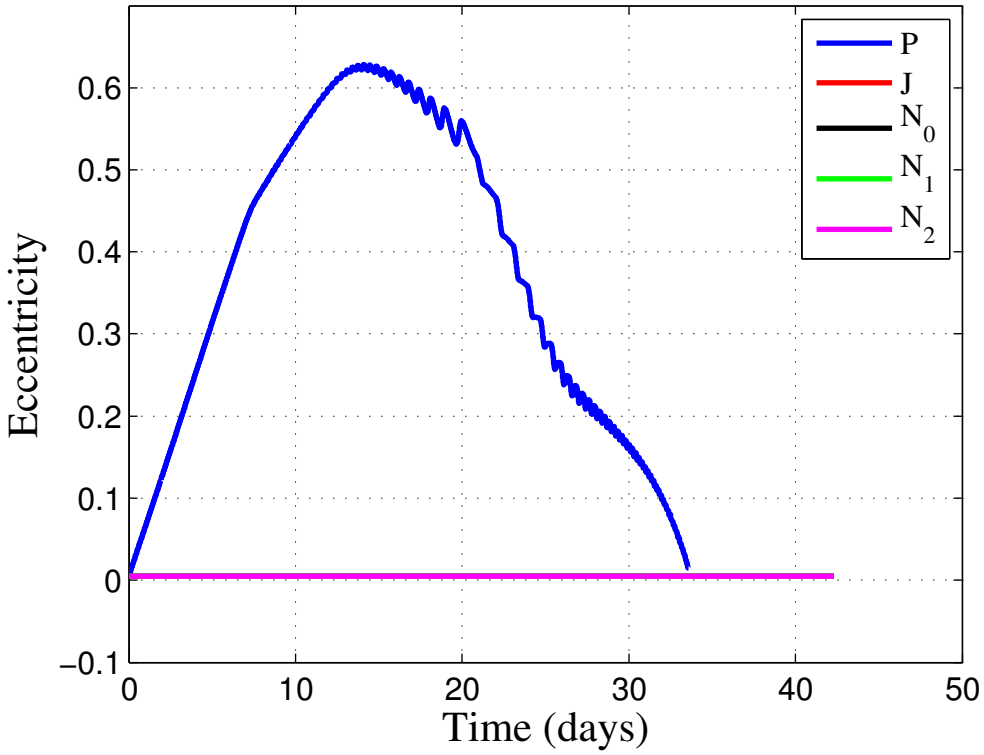

Figure 5.3: Equatorial orbit to polar orbit maneuver comparisons: eccentricity evolution, continuous control application. Note: Only two curves are visible because all evolutions but P are identical.

5.3 Low-Earth Orbit to Geosynchronous Orbit Transfer

The characteristics of a maneuver from an inclined low-earth orbit (LEO) to an equatorial geosynchronous orbit (GEO) are given in Tables 5.9 and 5.10. (Note that the initial and target orbits of this maneuver are identical to those given in Example 5.2.2 of [17].) No penalty function is used for any of the control laws.

Table 5.9: LEO-to-GEO maneuver elements.

Orbit	a (km)	e	i (deg)	Ω (deg)	ω (deg)	ν (deg)
Initial	6700	0.005	28.4	0	0	0
Target	42100	0.005	5.73×10^{-3}	free	free	free

Table 5.10: LEO-to-GEO maneuver characteristics.

Thrust (N)	Initial mass (kg)	I_{sp} (s)
1	300	3100

The convergence tolerances for this maneuver are given in Table 5.11.

Table 5.11: LEO-to-GEO maneuver convergence tolerances.

Element	Tolerance
a	1 percent relative error (421 km)
e	0.01
i	1°

The results of the maneuvers commanded by the control laws are sum-

marized in Tables 5.12 - 5.15. Table 5.12 also includes a comparison to a maneuver obtained using Edelbaum's orbital averaging scheme [4, 8].

Table 5.12: LEO-to-GEO maneuver comparisons: continuous control application.

Coasting Criterion	Control Law	Flight time (days)	Propellant mass (kg)
None	P	19.9236	56.6239
	J	18.7072	53.1667
	N_0	22.1400	62.9231
	N_1	20.9178	59.4495
	N_2	19.3472	54.9857
	Edelbaum	17.4850	49.6933

Table 5.13: LEO-to-GEO maneuver comparisons: absolute effectivity coasting criteria.

Coasting Criterion	Control Law	Flight time (days)	Propellant mass (kg)
$\eta_a = 0.33$	P	23.7188	54.2818
	J	18.6887	52.2052
	N_0	23.5116	63.5711
	N_1	20.9282	56.8857
	N_2	19.3056	54.4658
$\eta_a = 0.67$	P	38.9664	47.2680
	J	19.8495	50.5170
	N_0	29.5532	63.2015
	N_1	22.3310	54.7301
	N_2	22.3773	54.2060
$\eta_a = 0.90$	P	76.1887	43.4002
	J	25.4583	48.8086
	N_0	44.1076	62.3083
	N_1	26.3796	53.5839
	N_2	33.9606	53.6883

Table 5.14: LEO-to-GEO maneuver comparisons: relative effectivity coasting criteria.

Coasting Criterion	Control Law	Flight time (days)	Propellant mass (kg)
$\eta_r = 0.33$	P	30.3854	50.8810
	J	29.5660	48.7295
	N_0	30.0463	63.9392
	N_1	68.4873	56.6051
	N_2	26.9641	53.5172
$\eta_r = 0.67$	P	49.6030	45.3285
	J	49.4097	46.5574
	N_0	61.0475	62.9216
	N_1	115.3438	49.2048
	N_2	40.5521	53.1342
$\eta_r = 0.90$	P	95.7326	42.8495
	J	87.1921	45.9463
	N_0	148.3495	62.2314
	N_1	191.8079	45.4384
	N_2	73.5463	53.0624

Table 5.15: LEO-to-GEO maneuver comparisons: Naasz coasting criteria.

Coasting criterion	Control Law	Flight time (days)	Propellant mass (kg)
Naasz	N_0	22.1400	62.9231
	N_1	20.9178	59.4495
	N_2	19.3472	54.9857

Though still a circle-to-circle transfer, the LEO-to-GEO maneuver reveals several characteristics of the control laws not seen in the example of Section 5.2. For example, the differences between the three implementations

of Naasz's control law are readily apparent. As shown in Figures 5.4 and 5.7, N_1 increases the semi-major axis more quickly than any of the other control laws, while N_2 and N_0 successively increase the time required to achieve the target semi-major axis. This is caused by the fact that K_a in Naasz's control scheme is *constant* and proportional to a^{-3}, meaning that a larger a value used in the calculation of K_a results in a smaller K_a value and a longer time required to achieve the target semi-major axis. Examination of the forms of K_e and K_i reveal similar causes for the differences between the evolutions of these elements, as well.

The differences between Petropoulos's control law and Joseph's control law caused by Joseph's differentiation approximation create interesting effects in the evolution of the orbital elements for this maneuver. For example, the overshoot in semi-major axis directed by Petropoulos's control law when no coast arcs are permitted (Figure 5.4) actually causes the maneuver to take *more* time and therefore use more fuel than the maneuver that uses Joseph's control law. However, as the effectivity threshold increases, the propellant mass required by Petropoulos's control law decreases not only absolutely, but also relative to the propellant mass required by Joseph's control law, such that, at higher effectivity threshold values, Petropoulos's control law requires less fuel mass than Joseph's control law (Figure 5.10). The suboptimal semi-major axis overshoot gradually disappears and the vast majority of the inclination change is postponed until the tail end of the maneuver, when it is more optimal to change inclination due to the larger semi-major axis (Figures 5.7 - 5.9).

In the majority of cases, Petropoulos's control law and Joseph's control law create maneuver profiles that are more fuel-optimal than those produced by any of the three implementations of Naasz's control law. This is to be expected, as the inability to vary the weights of the error terms that make up the Lyapunov function as the maneuver progresses is a strong limitation of Naasz's control law.

As in the previous example, Naasz's coasting scheme produces nearly no change in maneuver characteristics because the magnitude of the acceleration requested remains significantly greater than the magnitude of the acceleration available to the spacecraft until the spacecraft approaches convergence to the target orbit (Table 5.15).

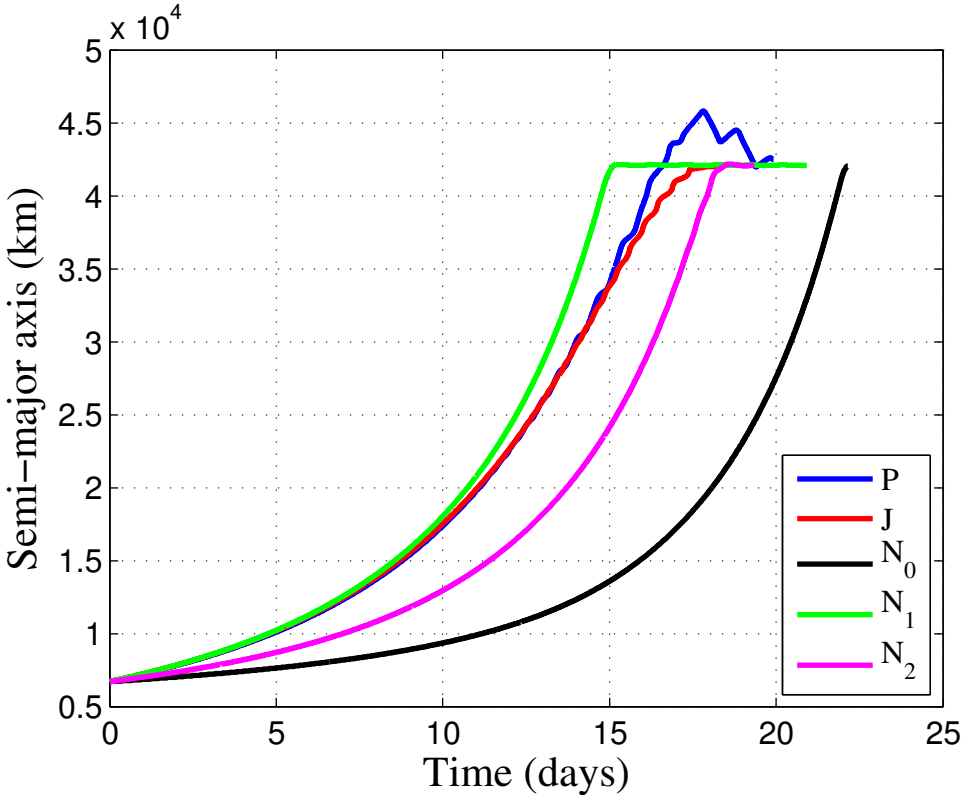

Figure 5.4: LEO-to-GEO maneuver comparisons: semi-major axis evolution, continuous control application.

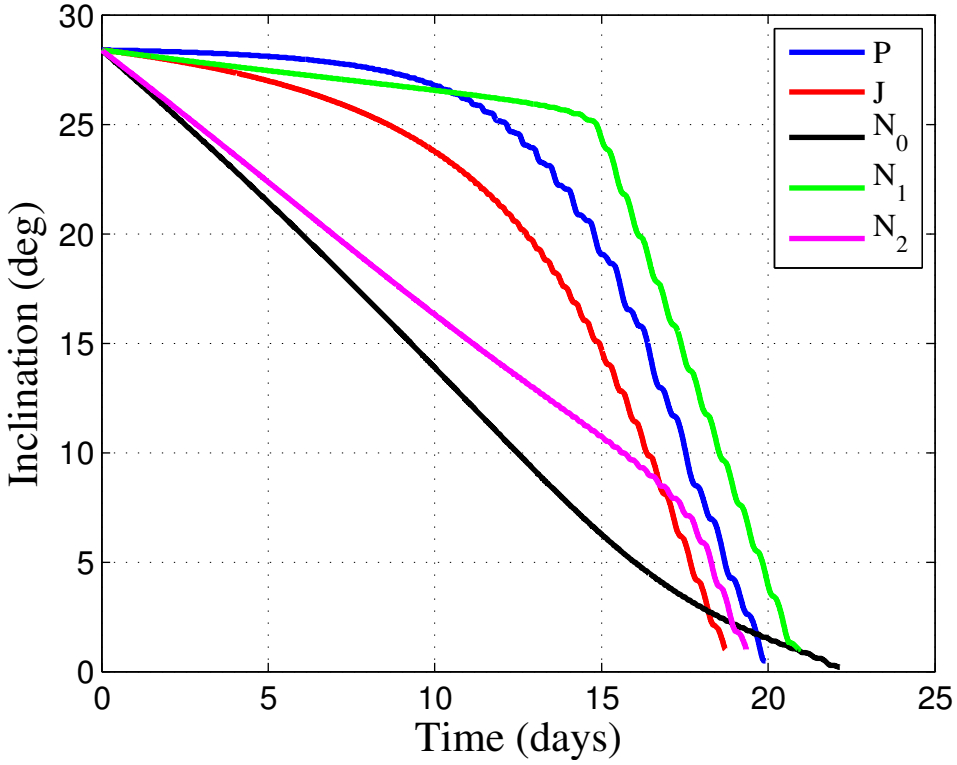

Figure 5.5: LEO-to-GEO maneuver comparisons: inclination evolution, continuous control application.

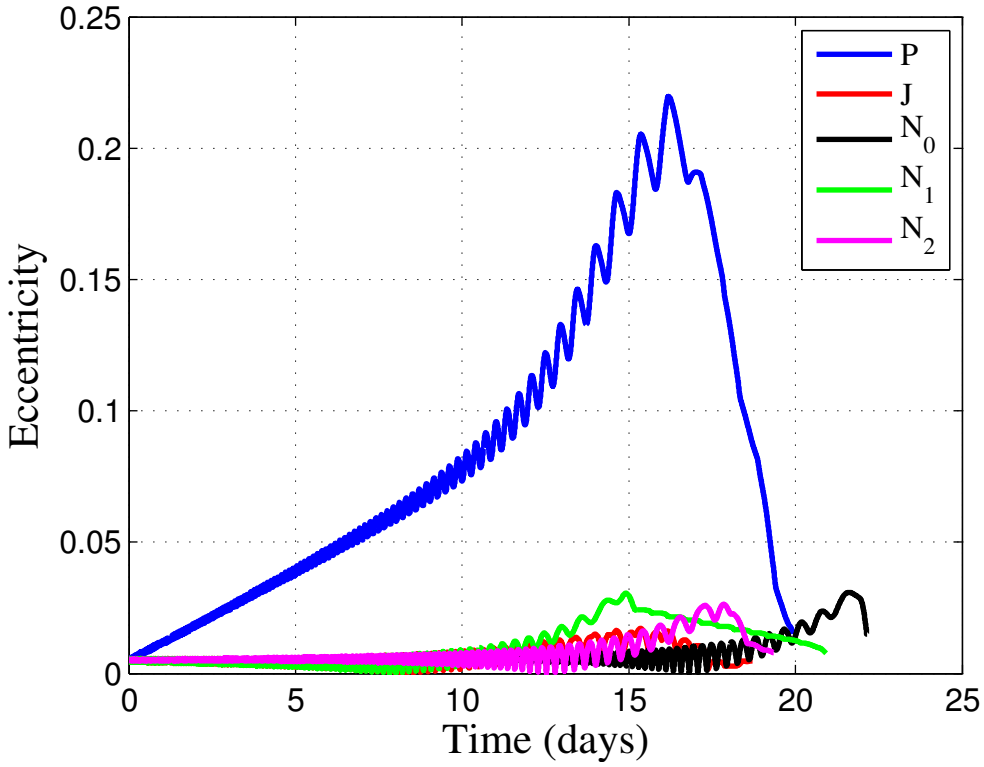

Figure 5.6: LEO-to-GEO maneuver comparisons: eccentricity evolution, continuous control application.

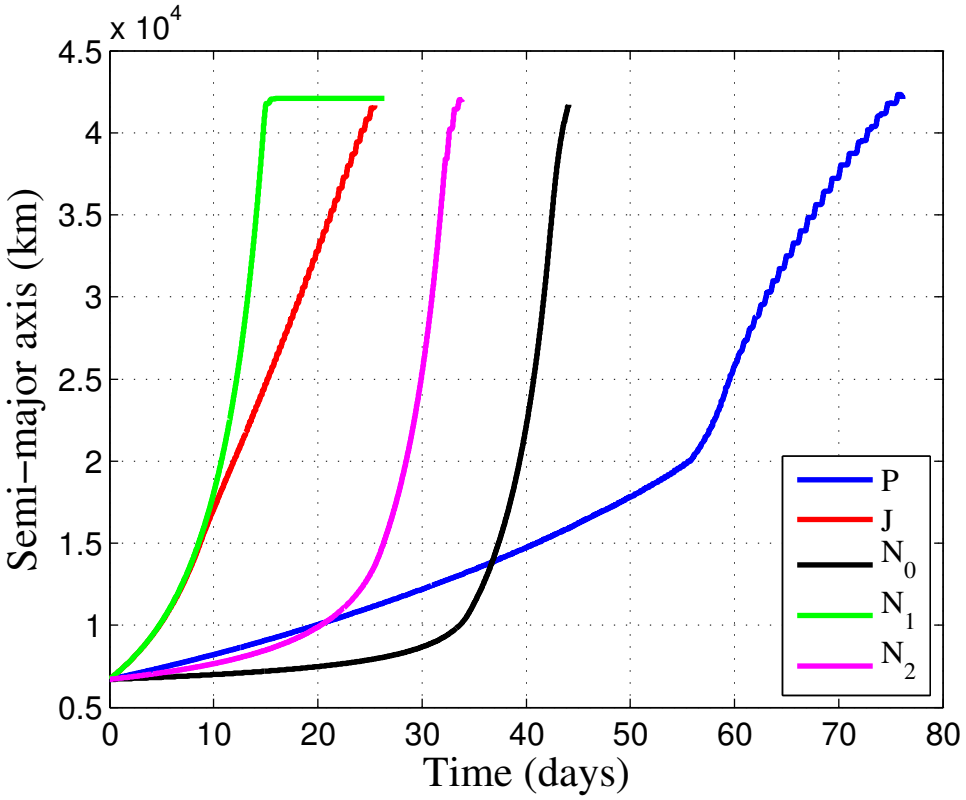

Figure 5.7: LEO-to-GEO maneuver comparisons: semi-major axis evolution, $\eta_{a_{threshold}} = 0.9$.

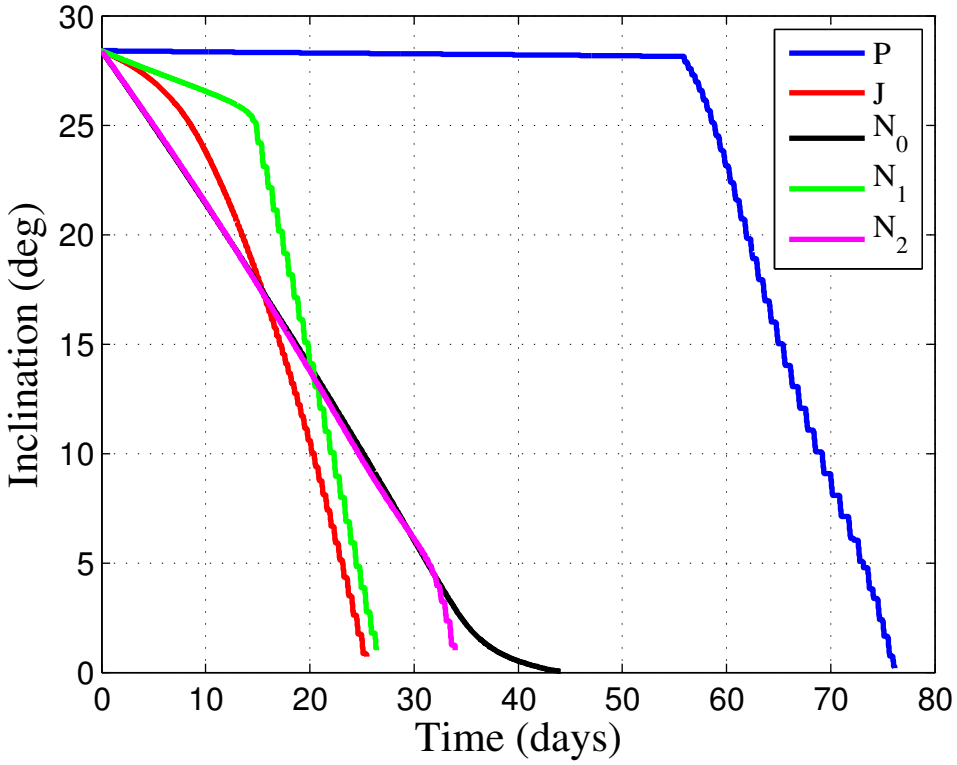

Figure 5.8: LEO-to-GEO maneuver comparisons: inclination evolution, $\eta_{a_{threshold}} = 0.9$.

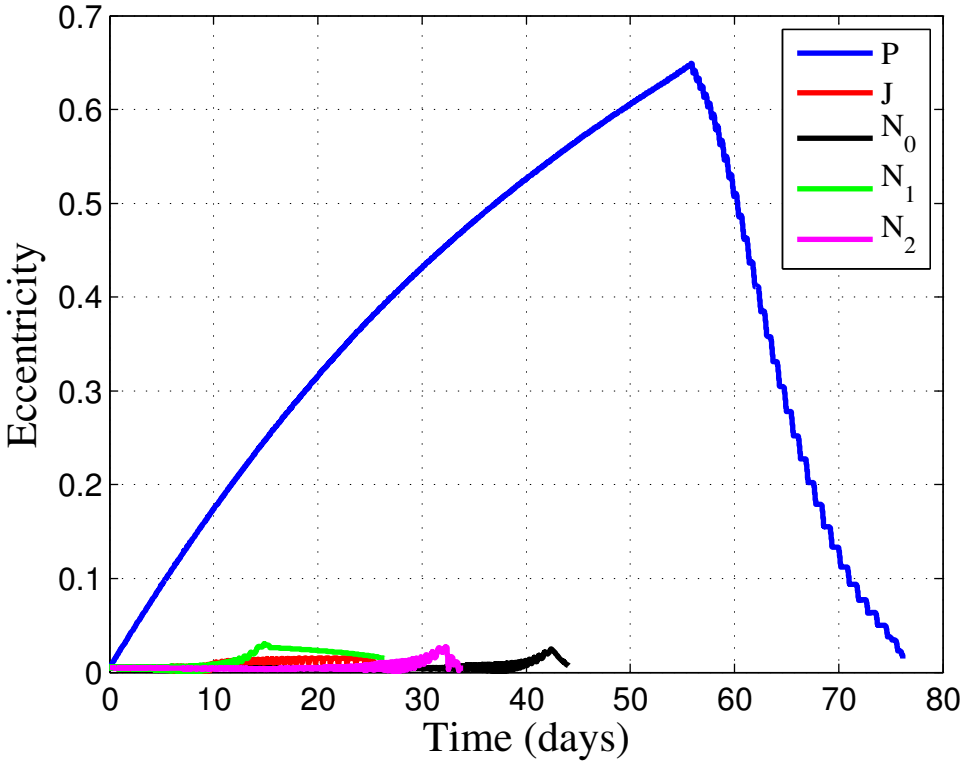

Figure 5.9: LEO-to-GEO maneuver comparisons: eccentricity evolution, $\eta_{a_{threshold}} = 0.9$.

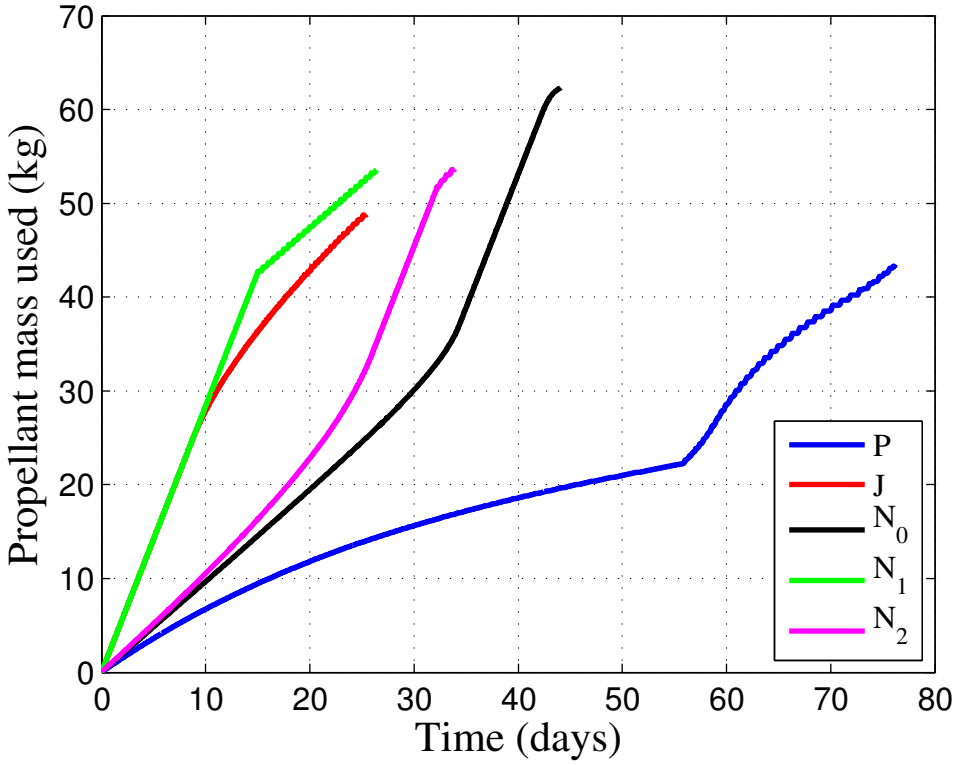

Figure 5.10: LEO-to-GEO maneuver comparisons: propellant mass usage evolution, $\eta_{a_{threshold}} = 0.9$.

5.4 Geostationary Transfer Orbit to Molniya Orbit Transfer

The characteristics of a maneuver from a geostationary transfer orbit (GTO) to a Molniya-type orbit are given in Tables 5.16 and 5.17. (Note that the initial and target orbits of this maneuver are identical to those given in Case E of [21].[2]) Because of the highly eccentric nature of both the initial and target orbits, Petropoulos's minimum-periapsis-distance penalty function is used to augment all control laws modeled in order to prevent the spacecraft from impacting the Earth. (See (3.7) and (3.10).) The parameters used to define the penalty function are $k = 100$ and $r_{p_{min}} = 6578$ km.

Table 5.16: GTO-to-Molniya maneuver elements.

Orbit	a (km)	e	i (deg)	Ω (deg)	ω (deg)	ν (deg)
Initial	24505.9	0.725	0.06	0	0	0
Target	26500	0.7	116	180	270	free

Table 5.17: GTO-to-Molniya maneuver characteristics.

Thrust (N)	Initial mass (kg)	I_{sp} (s)
2	2000	2000

The convergence tolerances for this maneuver are given in Table 5.18.

[2]It must be noted that the results for Petropoulos's control law presented here do not match those given in [21]. However, the results presented here have been confirmed by multiple independent third parties, and correspond to the control law derived and implemented as described in this thesis.

Table 5.18: GTO-to-Molniya maneuver convergence tolerances.

Element	Tolerance
a	1 percent relative error (265 km)
e	0.01
i	1°
Ω	1°
ω	1°

Further modifications are made to the N_1 control law due to unacceptably poor performance by the default formulation. The N_1 control law experiences difficulties because of the small initial i and ω values and the large initial e value. For this control law, the weight attached the $\delta\Omega$ term of the Lyapunov function is given by

$$K_\Omega = \left[\frac{h\sin(i)\left(\sqrt{1-e^2\cos^2(\omega)}-e|\sin(\omega)|\right)}{p}\right]^2 \frac{1}{\Delta t}. \tag{5.1}$$

Because the values of i and ω at which K_Ω is evaluated are 0.06° and 0°, respectively, for N_1, K_Ω takes on such a low value that the error in Ω is never corrected. As a workaround, K_Ω is scaled by 10^4, a value determined through trial and error.

Petropoulos's control law also requires modifications. When using a variable-step integration scheme with nominal values for all parameters and continuous control application, propagation ceases after less than a day of maneuver time because of chatter in the out-of-plane control angle. In order to

obtain a better idea of the maneuver evolution for this case, a fixed-step integration scheme (Appendix A.4) was also used to propagate the trajectory, with a step size of 10 seconds. The set of initial and target elements and the forms of the gradients of the $K_{\mathcal{O}}$ with respect to the orbital elements lead to nonconvergence to the target orbit. The majority of the magnitude of the Lyapunov function is initially contributed by the δi term of the summation. In order to increase the efficiency of changing i, the control law commands increases in both a and e. However, a grows to millions of kilometers, and e approaches 1, despite the presence of the scaling function S_a intended to prevent a from growing without bound. This causes the δi term of the Lyapunov function to decrease because K_i decreases, but the actual inclination value itself never increases significantly – δi remains near its initial value. The inclination remains near zero because $\frac{\partial V_P}{\partial i}$ is much greater than zero for the vast majority of the maneuver, meaning that the control law attempts to drive i down in order to decrease V_P. This, in turn, is due to the fact that the gradients of the $\delta\Omega$ and $\delta\omega$ terms of the Lyapunov function summation with respect to i are, together, significantly more positive than the gradient of the δi term with respect to i is negative. The cause of these large positive gradients with respect to i is readily apparent upon inspection of (2.64), (2.72), and (3.7): The $\sin^2(i)$ terms in the maximum rates of change of Ω and ω due to out-of-plane control acceleration mean that these terms of the Lyapunov function approach zero as $\sin^2(i)$ approaches zero. Therefore, the target orbit is never achieved even though V_P decreases continuously.

In order to force convergence to the target orbit for the case of continuous control application, the weights of V_P are modified such that $W_\Omega = W_\omega = 10^{-2}$. Even with these modifications, control direction chatter is still encountered, and use of the hybrid variable/fixed-step integration technique described in Section 4.3 is required to fully propagate the trajectory. Also, this modification does not lead to convergence for nonzero absolute or relative effectivity thresholds because of the renewed presence of chatter in the out-of-plane control angle. No other straightforward modification of the tunable parameters of Petropoulos's control law is found that leads to convergence to the target orbit. The strategy of temporarily increasing the effectivity threshold in order to induce coast arcs when control direction chatter is encountered [21] is similarly not found to lead to convergence in this case.

The results of both the variable-step propagation and fixed-step propagation reflect poorly on the robustness of Petropoulos's control law when multiple elements that may be changed by out-of-plane acceleration are targeted.[3] Petropoulos claims that control direction chatter is most commonly seen in the in-plane control angle when both a and e are targeted [21]; this maneuver, however, demonstrates a scenario in which control direction chatter occurs in the out-of-plane control angle early in a maneuver. This is a case in which Joseph's control law – which does *not* take into account the derivatives of the $K_\mathfrak{O}$ with respect to the orbital elements when differentiating the Lyapunov function – may produce useful results more reliably.

[3] If only one of i, Ω, and ω is targeted for this maneuver, convergence is readily achieved.

The results of the simulations are given in Tables 5.19 - 5.22.

Table 5.19: GTO-to-Molniya maneuver comparisons: continuous control application.

Coasting Criterion	Control Law	Flight time (days)	Propellant mass (kg)
None	P	103.3885	910.8890
	J	100.5208	885.6235
	N_0	85.7338	755.3445
	N_1	115.4664	1017.2995
	N_2	108.0532	951.9867

Table 5.20: GTO-to-Molniya maneuver comparisons: absolute effectivity coasting criteria.

Coasting Criterion	Control Law	Flight time (days)	Propellant mass (kg)
$\eta_a = 0.33$	P	N/A	N/A
	J	104.9039	819.0864
	N_0	84.4236	659.7969
	N_1	130.4074	934.4736
	N_2	113.0787	890.1130
$\eta_a = 0.67$	P	N/A	N/A
	J	120.0938	622.0207
	N_0	96.8993	589.3837
	N_1	181.5185	830.5341
	N_2	139.7315	733.7799
$\eta_a = 0.90$	P	N/A	N/A
	J	181.7199	543.6037
	N_0	145.6042	531.1991
	N_1	270.7650	749.9020
	N_2	241.1782	659.9646

Table 5.21: GTO-to-Molniya maneuver comparisons: relative effectivity coasting criteria.

Coasting Criterion	Control Law	Flight time (days)	Propellant mass (kg)
$\eta_r = 0.33$	P	N/A	N/A
	J	106.2465	764.0672
	N_0	87.6632	627.7959
	N_1	130.7442	913.1253
	N_2	149.3275	703.2975
$\eta_r = 0.67$	P	N/A	N/A
	J	129.2083	590.2332
	N_0	106.2419	564.9858
	N_1	185.3264	821.5054
	N_2	149.3275	703.2975
$\eta_r = 0.90$	P	N/A	N/A
	J	198.9549	537.6985
	N_0	166.2407	512.1025
	N_1	283.5961	752.6686
	N_2	257.2894	642.6833

Table 5.22: GTO-to-Molniya maneuver comparisons: Naasz coasting criteria.

Coasting criterion	Control Law	Flight time (days)	Propellant mass (kg)
Naasz	N_0	85.7338	755.3446
	N_1	115.4664	1017.2995
	N_2	108.0532	951.9867

An interesting result of the inclusion of effectivity-based coast arcs is that, in the case of the N_0 control law, the time of flight for the maneuver with an absolute effectivity threshold of 0.33 is less than that of the maneuver during

which control acceleration is applied continuously. This clearly shows the suboptimality of trajectories produced by CLFD control laws because optimal application of continuous control acceleration may be shown to produce the minimum-time transfer maneuver [19].

The behavior of the maneuvers in the flight-time-propellant-mass plane is similar as either the absolute effectivity threshold or relative effectivity threshold is varied. The N_0 control law requires less fuel than Joseph's control law for all cases. However, this result is due primarily to a fortuitous combination of target orbital elements and is not to be generally expected.

Like the maneuvers discussed in Sections 5.2 and 5.3, Naasz's coasting criterion produces a negligible effect for the N_0, N_1, and N_2 maneuvers.

Figures 5.11 - 5.15 clearly demonstrate a significant drawback of the method used to achieve convergence with Petropoulos's control law. Despite the fact that a is increased significantly to accommodate the large required change in i, the vast majority of the change in i occurs before a reaches its peak value. Furthermore, the majority of the required changes in Ω and ω occur after i approaches its target value – where it is much less efficient to change Ω and ω than at values of i where $\sin^2(i)$ is near zero. Both of these unfortunate maneuver characteristics are caused by the small values used for W_Ω and W_ω.

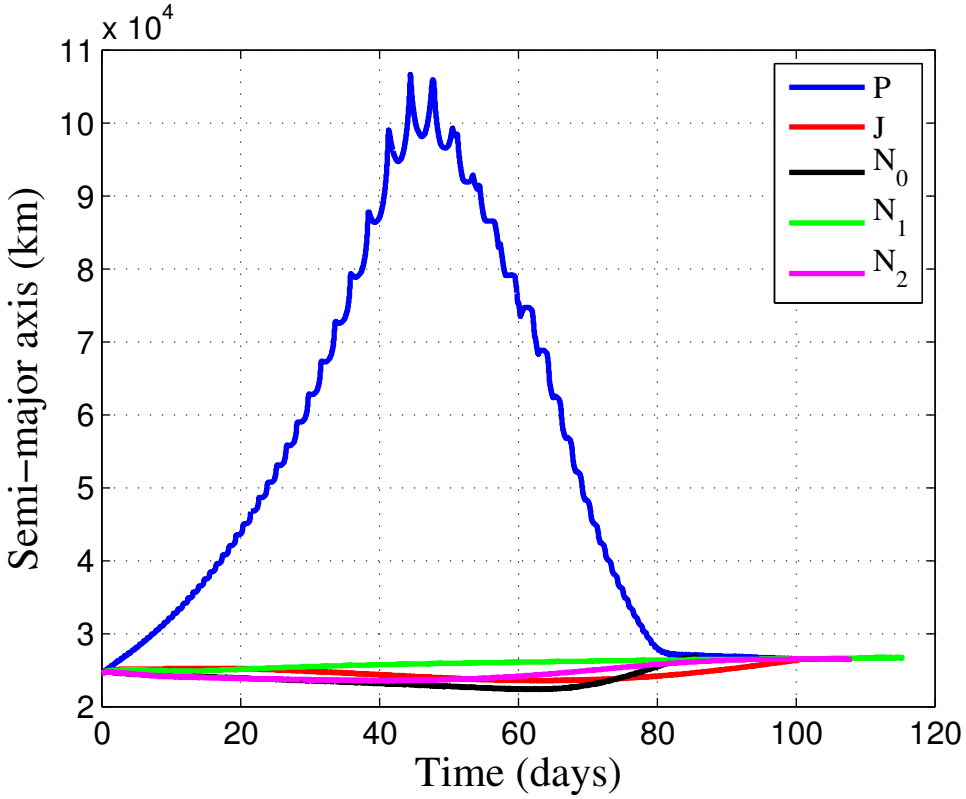

Figure 5.11: GTO-to-Molniya maneuver comparisons: semi-major axis evolution, continuous control application.

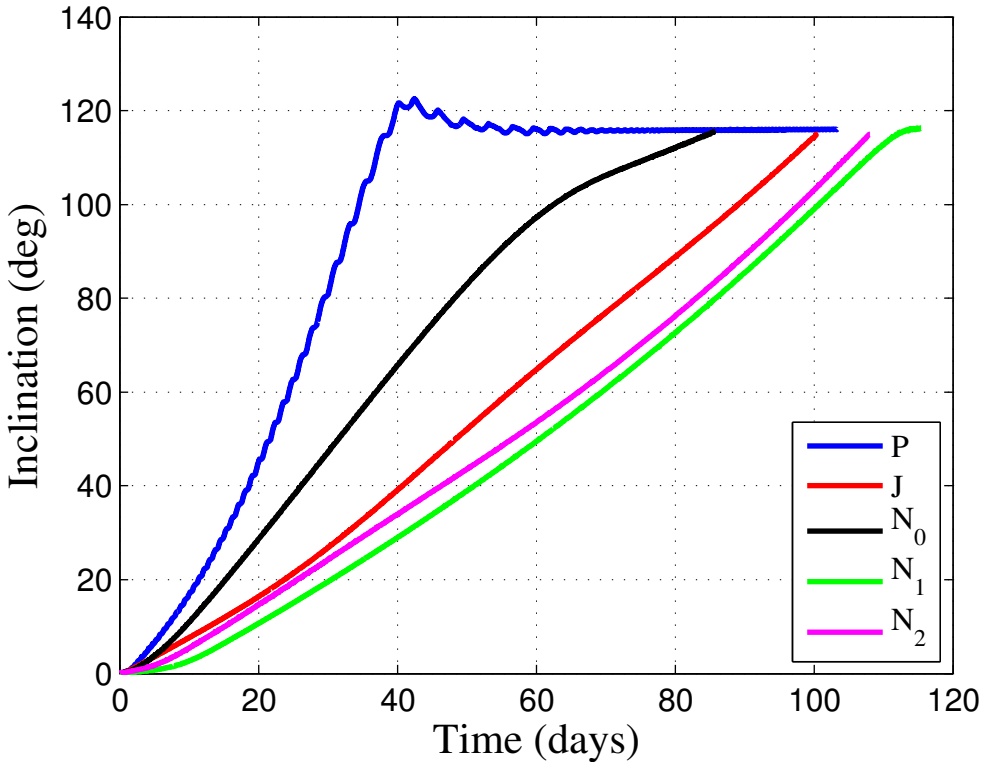

Figure 5.12: GTO-to-Molniya maneuver comparisons: inclination evolution, continuous control application.

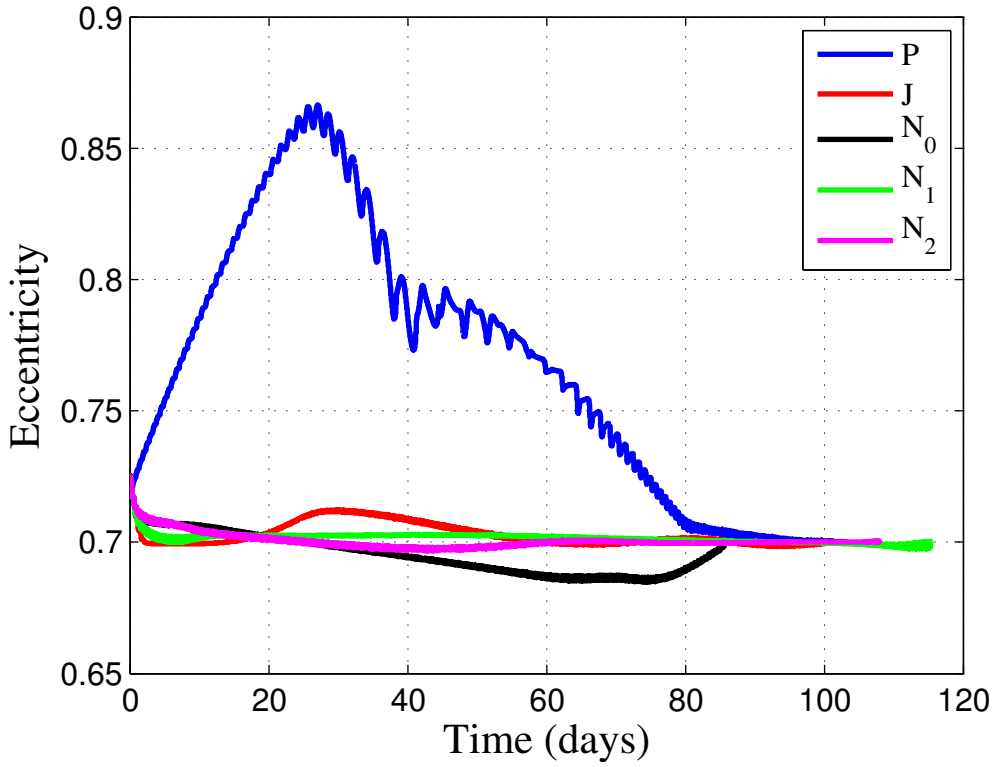

Figure 5.13: GTO-to-Molniya maneuver comparisons: eccentricity evolution, continuous control application.

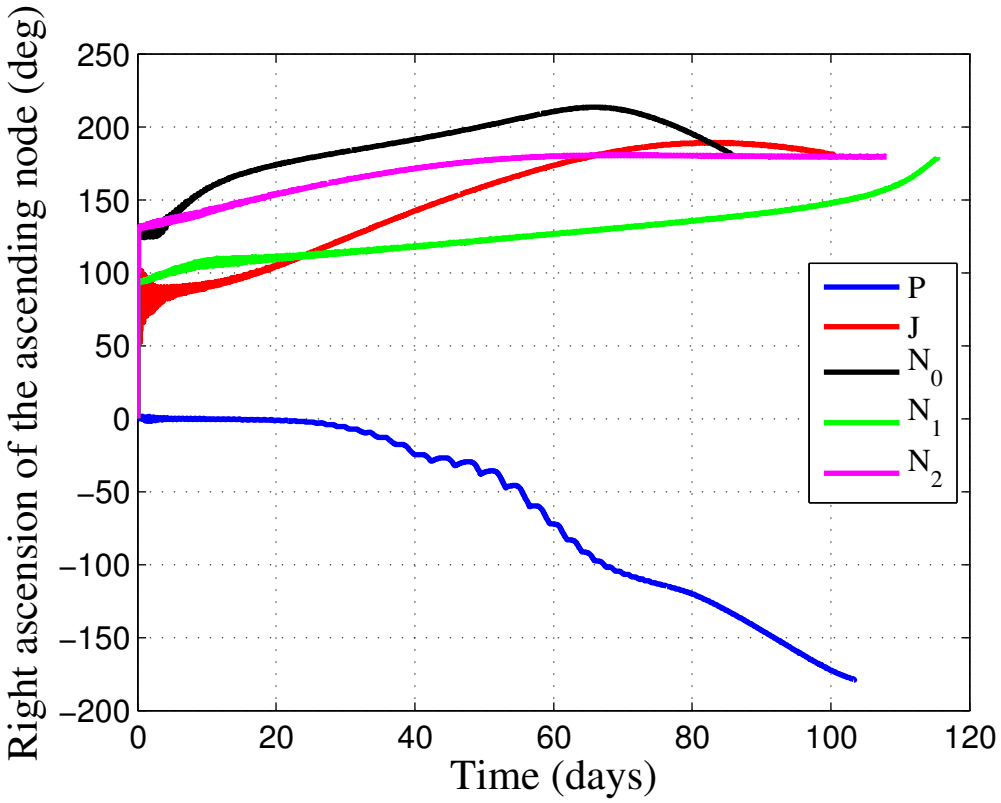

Figure 5.14: GTO-to-Molniya maneuver comparisons: right ascension of the ascending node evolution, continuous control application. Note that Petropoulos's control law yields convergence to $\Omega = -180°$, which is equivalent to $\Omega = 180°$.

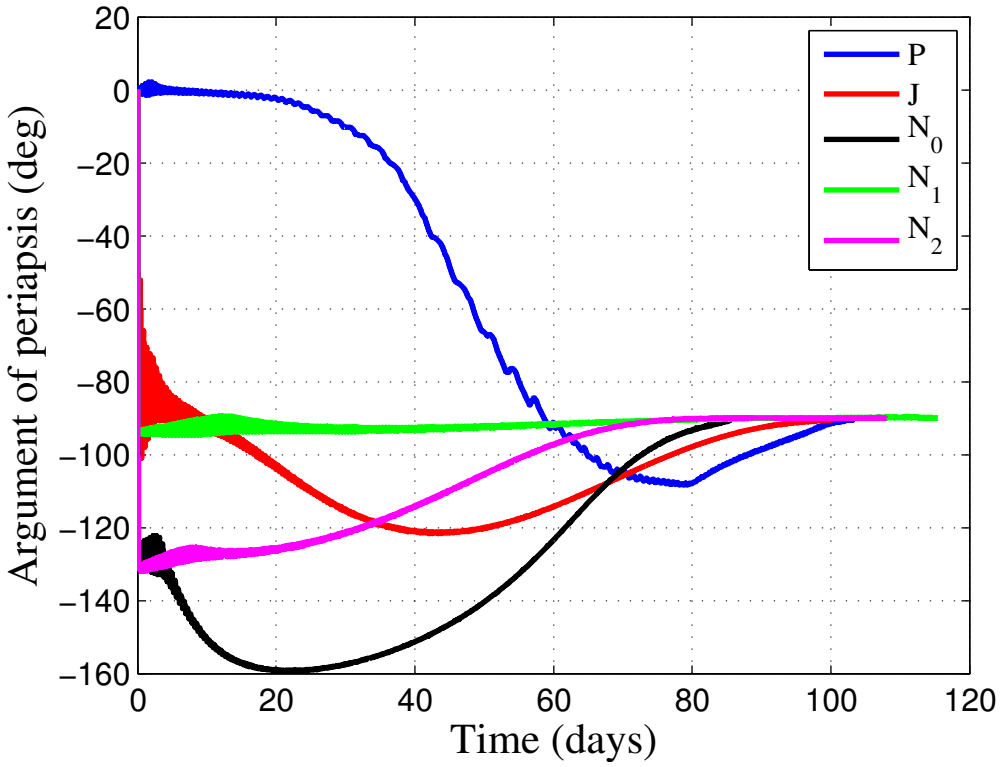

Figure 5.15: GTO-to-Molniya maneuver comparisons: argument of periapsis evolution, continuous control application.

5.5 Summary

Three maneuvers are simulated numerically using Petropoulos's control law, Joseph's control law, and three implementations of Naasz's control law. The results of an equatorial-to-polar transfer confirm that Joseph's control law and Naasz's control law behave identically when inclination is the only element to be changed because only out-of-plane control is dictated by either of the control laws. Identical performance would therefore also be obtained were right ascension of the ascending node the only element to be changed. The results of Petropoulos's control law for this maneuver are strikingly different, however, due to its use of gradient information of the weighting functions of the Lyapunov function with respect to the orbital elements. (Both Joseph's control law and Naasz's control law only consider the gradients of the error functions of the Lyapunov function.) Petropoulos's control law commands increases in the semi-major axis and eccentricity in order to more efficiently accomplish the large inclination change, yielding smaller fuel mass requirements than Joseph's control law or any of the three implementations of Naasz's control law.

A LEO-to-GEO transfer clearly shows the differences between the three implementations of Naasz's control law, and also provides an example for which an element overshoot commanded by Petropoulos's control law actually results in a *less* fuel-optimal maneuver than may be achieved by using only the gradient information of the element error functions of the Lyapunov function.

A GTO-to-Molniya transfer in which all five orbital elements are targeted reveals problems that may arise when using the control laws tested. Tar-

geting multiple elements that may be changed by in-plane control acceleration or multiple elements that may be changed by out-of-plane control acceleration may lead to control direction chatter, a situation characterized by rapid, discontinuous changes in the control direction. Additionally, when a fixed-step integration scheme is used to propagate through control direction chatter, the GTO-to-Molniya transfer represents a case for which the use of Petropoulos's control law with all nominal parameters leads to non-convergence to the target orbit due in part to the possibility of terms of the summation of the Lyapunov function approaching zero despite the corresponding elements not approaching their target values.

The GTO-to-Molniya transfer also explicitly reveals the problems that may arise from setting the Lyapunov function weights to constant values, as is done by Naasz's control law. The N_1 implementation requires that K_Ω be scaled by 10^4 to achieve convergence to the target orbit because of this.

Despite the problems exhibited by Petropoulos's control law and Naasz's control law, Joseph's control accomplishes the maneuver using all nominal values, suggesting that it may be the most robust of the three methods tested.

For all three maneuvers simulated, Naasz's coasting mechanism does not lead to the inclusion of intermediate coast arcs because the magnitude of the acceleration requested by the control law is much greater than the magnitude of the acceleration available to the spacecraft until the spacecraft closely approaches the target orbit. Thus, Naasz's coasting mechanism is quite ineffective for the maneuvers simulated, particularly when compared

to the effectivity-based coasting criterion, which is found to effectively introduce intermediate coast arcs into the trajectories dictated by all three control laws tested. As either the absolute or relative effectivity threshold for control application is increased, the fuel mass required to perform any of the three maneuvers is found to generally decrease for all control laws tested: Higher effectivity thresholds generally yield longer flight times and more fuel-optimal maneuvers.

Due to problems of the type encountered by the N_1 control law when applied to the GTO-to-Molniya transfer, it is clear that using the initial orbital elements to calculate the $K_{\mathcal{O}}$ for Naasz's control law has a significant and detrimental effect on the robustness of the method. The N_0 and N_2 methods of calculating $K_{\mathcal{O}}$ are more robust. However, it cannot be said that one or the other is generally superior; that determination must be made on a manuever-by-maneuver basis.

Chapter 6

Conclusions and Recommendations for Further Study

6.1 Conclusions

This thesis presents a qualitative and quantitative comparison of modern closed-loop, feedback-driven (CLFD) low-thrust spacecraft control laws.

Control laws whose error functions are calculated based on the classical orbital element set, the equinoctial orbital element set, and the angular momentum vector and Laplace vector are discussed. While the latter two orbit representations have the advantage of lacking the singularities that can occur when using the classical element set, other factors must also be considered when choosing the best representation to use in a CLFD control law. Importantly, the transformations between the three representations are coupled, with the result that, in many cases, changing one element of one representation results in changing multiple elements in another representation. This presents problems if only a subset of the elements of a target orbit is specified because, in a different representation, the target orbit is likely to be unnecessarily constrained. To avoid this issue, and since orbits are most often specified using the classical element set, it is concluded that the classical element set is a

preferred representation in which to write control law error functions.

Based on the qualitative comparisons performed, it is concluded that CLFD control laws based on Lyapunov control theory are generally preferable to those based on the blending of multiple control laws, each designed to optimally change one orbital element. This is primarily because there exists a sound theoretical framework for choosing the control that minimizes the time rate of change of the Lyapunov function at each step of the maneuver and because a control law based upon a well-chosen Lyapunov function may be theoretically proven to force a spacecraft to asymptotically approach a target orbit.

For Lyapunov-based control laws, the most important factor in the determination of the effectiveness of the control law is the weights of the error terms, or the K_i in

$$V = \sum_{\mathcal{O}} K_i \delta \mathcal{O}_i^2. \tag{6.1}$$

The control law of Chang et al. gives no strategy for the selection of appropriate K_i, a drawback that significantly increases the amount of user interaction required to obtain acceptable performance. Bombrun's control law, on the other hand, requires knowledge of the corresponding time-optimal maneuver in order to set its K_i. This creates difficulties since optimal low-thrust trajectories are very difficult to determine, a fact that is a major motivation for the development of CLFD control laws. Thus, it is concluded that these

two control laws require heavy modification to reach the utility of the other Lyapunov-based control laws discussed in this thesis: those of Petropoulos, Joseph, and Naasz.

It is shown that, by assuming that the osculating orbital elements (other than anomaly) remain constant between the discrete time steps of a numerical propagation scheme, Joseph's control law is a significant simplification of Petropoulos's control law. However, this simplification comes at a price: Joseph's control law is unable to command "scheduled overshoots" in one element in order to ease the changing of another, as confirmed by the results of the numerical examples performed.

It is also shown that, though derived independently, Naasz's control law may be thought of as a special case of Joseph's control law, in which the maximum rate of change of each orbital element – used in the formulation of the Lyapunov function – is calculated using the parameters of the target orbit and held constant for the duration of the maneuver rather than calculated on the current osculating orbit and varied continuously. This comparison holds for all terms of the Lyapunov function except for argument of periapsis, for which Naasz uses a linearization about $e = 0$ to approximate the maximum rate of change of ω on an orbit.

Improvements to both the Joseph and Naasz control laws are presented, which increase the robustness of each. Naasz's control law is altered to account for the quadrant ambiguity present in the calculation of the maximum rates of change of inclination and right ascension of the ascending node and to account

for the continuity of right ascension of the ascending node and argument of periapsis at values of 0 and 2π. Further changes are made to Naasz's control law to make it more impervious to singularities and to address issues that may arise due to the method of calculation of the weights of the terms of the Lyapunov function.

Because Naasz gives no rationale for his choice of calculating the weights of his Lyapunov function using the target orbital elements, two other possibilities are explored: calculation using the elements of the initial orbit and calculation using a simple arithmetic mean of the elements of the initial and target orbits. Calculation on the initial orbit is shown to be ineffective in certain situations, while calculation using the target elements and calculation using the averaged elements are shown to lead to results whose quality is heavily dependent on the specific maneuver modeled.

Joseph's control law, meanwhile, is altered so that it utilizes the classical element set rather than the equinoctial element set in the formulation of its Lyapunov function for reasons discussed earlier in this section.

Both the Joseph and Naasz control laws are updated to include the minimum-periapsis-radius penalty function included in Petropoulos's control law, the utility of which is confirmed in the numerical simulations presented.

The Lyapunov functions upon which the control laws of Petropoulos and Joseph are based are shown to not be globally asymptotically stable in the sense of Lyapunov for all possible targeting subsets of the classical ele-

ment set. The results of a GTO-to-Molniya orbit transfer numerical example indicate that the use of gradient information related to the Lyapunov function weights – an attribute unique to Petropoulos's control law among those tested numerically – may cause Petropoulos's control law to be more susceptible to nonconvergence to the target orbit than Joseph's control law due to this lack of stability. Nevertheless, the advantage of using the aforementioned gradient information (as opposed to only using gradient information related to the differences between the osculating element values and the target element values) is shown in an equatorial-to-polar orbit transfer example and a LEO-to-GEO orbit transfer example. In both cases, Petropoulos's control law produces trajectories that require less fuel mass than those generated by the control laws of Joseph and Naasz.

The possibility of poor performance, or even complete failure, of the control laws presented due to control direction chatter at consecutive time steps of numerical propagation is discussed. When using a variable-step integration scheme, this generally causes the numerical propagation to come to a complete standstill. A fixed-step integration scheme, on the other hand, is capable of integrating through regions of chatter, but the resulting maneuver is likely to be either highly suboptimal or not converge to the target orbit at all.

All three numerical examples performed indicate that the coasting scheme suggested by Naasz is generally ineffective at introducing mid-maneuver coast arcs into orbit transfer trajectories because the magnitude of the acceler-

ation "requested" by the control law tends to remain significantly greater than the magnitude of the control acceleration available to the spacecraft until the spacecraft very nearly converges to the target orbit.

The effectivity-based coasting criterion of Petropoulos, on the other hand, is shown to be capable of introducing coast arcs that can result in significant propellant mass savings, at the cost of increasing the required flight time. The numerical examples confirm that this coasting method is applicable also to the control schemes of Joseph and Naasz and, indeed, to any Lyapunov-based control law.

Analysis of the theoretical foundations and the numerical simulations performed indicate that Naasz's control law is the least effective of the three control laws tested numerically. This is unsurprising given that Naasz's control law may be thought of as a simplification of Joseph's control law in which the weights of the Lyapunov function are evaluated once and held constant for the duration of the maneuver, while Joseph's weights and Petropoulos's weights are continuously varied using the elements of the current osculating orbit. The relative effectiveness of Petropoulos's control law and Joseph's control law, however, is more difficult to define. While Petropoulos's control law is capable of producing more fuel-optimal results, Joseph's control law is shown to be more robust in certain situations, particularly those in which multiple elements that may be changed by out-of-plane acceleration are targeted simultaneously. Without a more exhaustive numerical comparison, the only conclusion that may be made is that each has its uses, but, as with all CLFD control laws,

analyst discretion is required.

6.2 Recommendations for Further Study

A myriad of options exist for extending the work presented in this thesis. Perhaps most obviously, the development of new Lyapunov functions or new weighting schemes for blended control algorithms may produce control laws capable of outperforming those currently in use. Beyond this, there are four key areas in which work may be performed based on already-derived control laws.

First, the incorporation of effective methods of eliminating or ameliorating the consequences of control-direction chatter into CLFD control laws could have a strongly positive effect on the robustness of the laws. Possible areas of investigation include setting a maximum value on the change in the control angle between consecutive time steps or temporarily "untargeting" one or more targeted elements to eliminate the control law's confusion as to the direction in which control should be applied.

Second, the fidelity of the model used to derive and implement the control laws may be improved. As detailed in Section 1.2, the control laws discussed in this thesis are developed for use in a simple two-body gravitational force field that does not take into account any of the other forces that act on spacecraft, like the gravitational attraction of third bodies, non-spherical central body effects, solar radiation pressure, and, for low-altitude spacecraft, atmospheric drag. All of the control laws discussed in this thesis model the

motion of a spacecraft subjected to a disturbing acceleration, namely, a control acceleration. However, the disturbing acceleration may just as easily include other effects, as well, and (2.25) may be rewritten as

$$\ddot{\boldsymbol{r}} + \frac{\mu}{r^3}\boldsymbol{r} = \boldsymbol{a}_c + \boldsymbol{a}_o, \tag{6.2}$$

where $\boldsymbol{a}_c$ is the control acceleration and $\boldsymbol{a}_o$ is a term combining all other disturbing accelerations to be modeled. It is then straightforward to determine Gauss's form of the variational equations in this new model and thus propagate the spacecraft state. Less simple, however, may be the determination of the control. For example, the control laws of Petropoulos, Joseph, and Naasz all require that the maximum rate of change of the orbital elements over an orbit be calculated, which requires differentiation of Gauss's equations with respect to the control angles and true anomaly. While it is unlikely that $\boldsymbol{a}_o$ will depend on the control direction, it is possible that $\boldsymbol{a}_o$ will have some dependency on true anomaly, and this must be taken into account when implementing any of these control laws in the presence of disturbing accelerations. Some work in this area has been performed by Maddock and Vasile [16], who adapted Joseph's control law to account for the effects of solar radiation pressure and the presence of a third body.

A third method by which control laws may be improved is the optimization of the parameters and functions which help to define them. The inclusion of non-unity scaling functions – similar to Petropoulos's S_a – for other orbital

elements may be able to improve the robustness of control laws by forcing convergence to the target orbit in cases in which terms of the Lyapunov function summation approach zero even though the orbit does not approach the target orbit (Section 3.3.1). In addtion, the terms of the summations of the Lyapunov functions used in the control laws of Petropoulos, Joseph, and Naasz are each multiplied by a weighting parameter (e.g. the W_0 in (3.7)). Each parameter is nominally set to unity if the orbital element corresponding to that term is targeted and zero if it is free. However, it is very likely that setting each of the weights of the targeted elements to positive values *not* equal to unity will result in improved performance. (And, as shown in Chapter 5, this is sometimes *required* to simply achieve convergence to the target orbit.) Further, the nominal values for heuristic parameters such as those used in the definition of S_a in Petropoulos's control law (3.11) are also highly unlikely to be optimal for all maneuvers. The optimization of these parameters to, for example, minimize fuel usage, provides a means by which the trajectory calculated by the control law may more closely approximate the true optimal trajectory. Lee et al. [15] used heuristic optimization techniques to optimize the parameters that make up the Lyapunov function introduced by Petropoulos, and found that significant fuel savings could be achieved in this manner. Future work may look into the use of optimization of the parameters of the other control laws presented in this thesis – particularly the weights used in the blended control laws.

Finally, further work may focus on the use of the trajectories gen-

erated by control laws as initial guesses for iterative optimization routines. Petropoulos and Lee [22] have performed some work in this area, utilizing Petropoulos's control law – both using nominal parameter values and using heuristically optimized parameter values – to determine initial guesses for the direct optimization algorithm Mystic [22, 25, 26]. For the maneuvers modeled, it was found that use of the control law to create the initial guess could significantly decrease the computational time required to determine the optimal trajectory. Much work may still be done in this area, however. The optimization was performed only for fixed-flight-time maneuvers; free-flight-time maneuvers may also be investigated. Also, the use of an indirect optimization method is not considered, and the extent to which the use of a CLFD control law may improve the performance of an indirect algorithm has not yet been determined.

Appendices

Appendix A

Supplemental Expressions

A.1 Derivatives of Classical Element Variational Equations with Respect to True Anomaly

As introduced in (2.36), Gauss's form of the variational equations for the classical element set may be represented in matrix-vector form by

$$\begin{pmatrix} \dot{a} \\ \dot{e} \\ \dot{i} \\ \dot{\Omega} \\ \dot{\omega} \\ \dot{M}_0 \end{pmatrix} = \boldsymbol{A}\boldsymbol{a}_d. \tag{A.1}$$

In the implementation of several control laws, it is necessary to obtain the derivatives of the elements of the first five rows of the matrix $\boldsymbol{A}$ with respect to true anomaly. These expressions are given by

$$\frac{\partial \boldsymbol{A}_{1,1}}{\partial \nu} = \frac{2a^2 e \cos(\nu)}{h} \tag{A.2}$$

$$\frac{\partial \boldsymbol{A}_{1,2}}{\partial \nu} = -\frac{2a^2 e \sin(\nu)}{h} \tag{A.3}$$

$$\frac{\partial \boldsymbol{A}_{1,3}}{\partial \nu} = 0 \tag{A.4}$$

$$\frac{\partial \boldsymbol{A}_{2,1}}{\partial \nu} = \frac{p \cos(\nu)}{h} \tag{A.5}$$

$$\frac{\partial \boldsymbol{A}_{2,2}}{\partial \nu} = \frac{r \sin(\nu)[-2e \cos(\nu) - 2 - e^2 \cos^2(\nu) + e^2]}{h[1 + e \cos(\nu)]} \tag{A.6}$$

$$\frac{\partial \boldsymbol{A}_{2,3}}{\partial \nu} = 0 \tag{A.7}$$

$$\frac{\partial \boldsymbol{A}_{3,1}}{\partial \nu} = 0 \tag{A.8}$$

$$\frac{\partial \boldsymbol{A}_{3,2}}{\partial \nu} = 0 \tag{A.9}$$

$$\frac{\partial \boldsymbol{A}_{3,3}}{\partial \nu} = \frac{re \sin(\omega) \cos(\omega + \nu)}{h[1 + e \cos(\nu)]} - \frac{r \sin(\omega + \nu)}{h} \tag{A.10}$$

$$\frac{\partial \boldsymbol{A}_{4,1}}{\partial \nu} = 0 \tag{A.11}$$

$$\frac{\partial \boldsymbol{A}_{4,2}}{\partial \nu} = 0 \tag{A.12}$$

$$\frac{\partial \boldsymbol{A}_{4,3}}{\partial \nu} = \frac{re \sin(\nu) \sin(\omega + \nu)}{h \sin(i)[1 + e \cos(\nu)]} + \frac{r \cos(\omega + \nu)}{h \sin(i)} \tag{A.13}$$

$$\frac{\partial \boldsymbol{A}_{5,1}}{\partial \nu} = \frac{p \sin(\nu)}{he} \tag{A.14}$$

$$\frac{\partial \boldsymbol{A}_{5,2}}{\partial \nu} = \frac{r \sin^2(\nu)}{h[1 + e \cos(\nu)]} + \frac{(p + r) \cos(\nu)}{he} \tag{A.15}$$

$$\frac{\partial \boldsymbol{A}_{5,3}}{\partial \nu} = -\left(\frac{re \cos(i) \sin(\nu) \sin(\omega + \nu)}{h \sin(i)[1 + e \cos(\nu)]} + \frac{r \cos(i) \cos(\omega + \nu)}{h \sin(i)} \right). \tag{A.16}$$

A.2 Derivatives of Petropoulos's Penalty Function with Respect to the Classical Orbital Elements

The penalty function used by Petropoulos [21] to enforce a minimum-periapsis-distance constraint is

$$P = \exp\left[k\left(1 - \frac{r_p}{r_{p_{min}}}\right)\right], \tag{A.17}$$

where k is a parameter nominally set to 100. Periapsis distance may be expressed as $r_p = a(1-e)$, so the penalty function depends only on semi-major axis and eccentricity; therefore, derivatives with respect to the other orbital elements are zero.

$$\frac{\partial P}{\partial a} = \frac{-k(1-e)\,\exp\left[k\left(1 - \frac{a(1-e)}{r_{p_{min}}}\right)\right]}{r_{p_{min}}} \tag{A.18}$$

$$\frac{\partial P}{\partial e} = \frac{ka\,\exp\left[k\left(1 - \frac{a(1-e)}{r_{p_{min}}}\right)\right]}{r_{p_{min}}} \tag{A.19}$$

A.3 Derivatives of Petropoulos's Scaling Function with Respect to the Classical Orbital Elements

The scaling functions used by Petropoulos are [21]

$$S_{\mathcal{O}} = \begin{cases} \left[1 + \left(\frac{a-a_T}{ma_T}\right)^n\right]^{\frac{1}{r}}, & \mathcal{O} = a \\ 1, & \mathcal{O} = e, i, \Omega, \omega \end{cases}, \tag{A.20}$$

where m, n, and r are parameters nominally set to 3, 4, and 2, respectively. Therefore, the only non-zero derivative is that of S_a with respect to semi-major axis:

$$\frac{\partial S_a}{\partial a} = \frac{n\left[1+\left(\frac{a-a_T}{ma_T}\right)^n\right]^{\left(\frac{1}{r}-1\right)}\left[\frac{a-a_T}{ma_T}\right]^n}{r(a-a_T)}. \tag{A.21}$$

A.4 Naasz's Fixed-Step State Propagator

Naasz's method [17] of fixed-step spacecraft state propagation uses the state vector

$$\boldsymbol{\mathcal{X}} = \begin{pmatrix} \boldsymbol{r} \\ \boldsymbol{v} \\ m \end{pmatrix}, \tag{A.22}$$

where $\boldsymbol{r}$ is the spacecraft position vector in the CBCI coordinate system, $\boldsymbol{v}$ is the spacecraft velocity vector in the CBCI coordinate system, and m is the spacecraft mass. Naasz's method approximates the continuous control acceleration as a sequence of instantaneous $\Delta\boldsymbol{v}$ maneuvers uniformly separated by time spans Δt. At each maneuver, $\boldsymbol{\mathcal{X}}$ is discontinuously changed such that

$$\boldsymbol{\mathcal{X}}^+ = \boldsymbol{\mathcal{X}}^- + \begin{pmatrix} \mathbf{0} \\ \frac{T^-}{m^-}\hat{\boldsymbol{u}}^-\Delta t \\ -\frac{T^-}{g_0 I_{sp}}\Delta t \end{pmatrix}, \tag{A.23}$$

where the superscript $(-)$ represents the time immediately prior to the discontinuity, the superscript $(+)$ represents the time immediately following the discontinuity, $\hat{\boldsymbol{u}}$ is the control application direction unit vector, g_0 is the reference gravitational acceleration, and I_{sp} is the spacecraft propulsion system's specific impulse. Propagation from time t to time $t + \Delta t$ is then accomplished analytically via solution of Kepler's problem [7]. This propagation method provides adequate accuracy for sufficiently small values of Δt.

A.5 Edelbaum's Low-Thrust Orbit Transfer Analysis

Edelbaum's analysis [1, 4, 8] linearizes the orbital element variational equations about a circular orbit ($e \approx 0$) in order to obtain an analytical solution for a low-thrust orbit transfer between two circular orbits with (generally) different semi-major axes and inclinations. The following assumptions and restrictions apply:

1. The osculating orbit is quasi-circular for the duration of the maneuver.
2. The control acceleration is constant, and there are no coast arcs.
3. The in-plane control acceleration is tangential. (There is no control acceleration in the $\hat{\boldsymbol{e}}_u$ direction.)
4. The magnitude of the out-of-plane control angle is constant over an orbit revolution and switches signs at the orbit antinodes.

5. The difference between the initial and final inclinations must be less than 114.59°.

For such a transfer, Edelbaum gives the required Δv as

$$\Delta v = \sqrt{v_1^2 + v_2^2 - 2v_1 v_2 \cos\left(\frac{\pi \Delta i}{2}\right)}, \tag{A.24}$$

where v_1 is the magnitude of the initial circular velocity, v_2 is the magnitude of the final circular velocity, and Δi is the difference between the initial and final inclinations (in radians). From this, the fuel mass required to perform the transfer may be determined using the Tsiolkovsky rocket equation [14].

$$m_f = m_0 \exp\left(-\frac{\Delta v}{g_0 I_{sp}}\right) \tag{A.25}$$

$$m_{fuel} = m_0 - m_f, \tag{A.26}$$

where m_0 is the initial mass of the spacecraft, m_f is the final mass of the spacecraft, and m_{fuel} is the fuel mass required. Furthermore, the time required to perform the maneuver may be calculated by

$$\Delta t = \frac{m_{fuel} g_0 I_{sp}}{T}, \tag{A.27}$$

where T is the control force magnitude. (It should be noted that this calculation assumes constant control *force* magnitude, while Edelbaum's analysis

assumes constant control *acceleration* magnitude. The prior assumption is used in the calculations performed in this thesis to provide a better point of comparison for the results obtained using other control laws, which operate under a constant-thrust-force assumption.)

Appendix B

MATLAB Scripts

B.1 Petropoulos Control: Derivatives of V_P with Respect to the Classical Element Set

The derivatives of V_P with respect to the classical orbital elements are in many cases quite lengthy and are therefore not included explicitly in this thesis. However, the following script, which utilizes the MATLAB Symbolic Toolbox, may be used to obtain the required expressions. Because the required derivatives of the minimum-periapsis-constraint penalty function are given explicitly in Appendix A.2, it is excluded from V_P in the calculation of these derivatives. It should be noted that this script returns the derivatives of *each term* of the summation of V_P with respect to each orbital element to ease the calculation of derivatives when one or more orbital elements are not targeted.

```
%%%%%%%%%%%%%%%%%%%%%%%%%%%%%%%%%%%%
% Script calculates the derivatives of the Lyapunov function of
% Petropoulos's control law with respect to semi-major axis,
% eccentricity, inclination, right ascension of the ascending
% node, and argument of periapsis symbolically.
```

```
%%%%%%%%%%%%%%%%%%%%%%%%%%%%%%%%%%%

% Declare symbolic variables
syms v dvdt % Lyapunov function and its time derivative
syms mu % gravitational parameter of central body
syms f % magnitude of control acceleration
syms fr ftheta fh % components of control acceleration in
% R-theta-H system
syms h p r % osculating values of: angular momentum
% magnitude, semi-latus rectum, and position vector
% magnitude
syms sma e inc ape ran tru % osculating orbital elements
syms sma_t e_t inc_t ape_t ran_t % target orbital elements
syms vsma ve vinc vape vran % terms of Lyapunov function
% summation
syms smadotxx edotxx incdotxx randotxx apedotxxi apedotxxo
syms apedotxx cosvxxo rxxo distape distran m_petro n_petro
syms r_petro b_petro
% ^^^ maximum rates of change of each element over
% osculating orbit and other variables used in their calculation
syms dvdcoe % 5x5 array holding derivatives of each term of
% Lyapunov function with respect to each orbital element
```

```
% put h, p, r in terms of orbital elements
p = sma*(1-e^2);
h = sqrt(mu*p);
r = p/(1+e*cos(tru));
% maximum values of rates of change of orbital elements over
% control acceleration angles and true anomaly
% semi-major axis
smadotxx = 2*f*sqrt((sma^3*(1+e))/(mu*(1-e)));
% eccentricity
edotxx = (2*p*f)/h;
% inclination
incdotxx = (p*f)/(h*(sqrt(1-e^2*(sin(ape))^2)-e*abs(cos(ape))));
% right ascension of the ascending node
randotxx = (p*f)/(h*sin(inc)*(sqrt(1-e^2*(cos(ape))^2)- ...
    e*abs(sin(ape))));
% argument of periapsis: in-plane
cosvxxo = (((1-e^2)/(2*e^3)) + ...
    sqrt((1/4)*((1-e^2)/e^3)^2+(1/27)))^(1/3) - ...
    (((-(1-e^2)/(2*e^3))) + ...
    sqrt((1/4)*((1-e^2)/e^3)^2+(1/27)))^(1/3) - (1/e);
rxxo = p/(1+e*cosvxxo);
apedotxxi = (f/(e*h))*sqrt(p^2*cosvxxo^2 + (p+rxxo)^2* ...
    (1-cosvxxo^2));
```

```
% argument of periapsis: out-of-plane
apedotxxo = randotxx*abs(cos(inc));
% NO PENALTY FUNCTION
% build Lyapunov function term by term
% semi-major axis term also has scaling function:
s_sma = (1+((sma-sma_t)/(m_petro*sma_t))^n_petro)^(1/r_petro);
% semi-major axis term
vsma = s_sma*(((sma - sma_t)/smadotxx)^2);
% eccentricity term
ve = ((e - e_t)/edotxx)^2;
% inclination term
vinc = ((inc - inc_t)/incdotxx)^2;
% right ascension of the ascending node term
distran = acos(cos(ran - ran_t));
vran = (distran/randotxx)^2;
% argument of periapsis term
distape = acos(cos(-ape_t + ape));
apedotxx = (apedotxxi+b_petro*apedotxxo)/(1+b_petro);
vape = (distape/apedotxx)^2;
% differentiate each term with respect to all orbital elements
dvdcoe(1,1) = diff(vsma, sma);
dvdcoe(1,2) = diff(vsma, e);
dvdcoe(1,3) = diff(vsma, inc);
```

```
dvdcoe(1,4) = diff(vsma, ran);
dvdcoe(1,5) = diff(vsma, ape);

dvdcoe(2,1) = diff(ve, sma);
dvdcoe(2,2) = diff(ve, e);
dvdcoe(2,3) = diff(ve, inc);
dvdcoe(2,4) = diff(ve, ran);
dvdcoe(2,5) = diff(ve, ape);

dvdcoe(3,1) = diff(vinc, sma);
dvdcoe(3,2) = diff(vinc, e);
dvdcoe(3,3) = diff(vinc, inc);
dvdcoe(3,4) = diff(vinc, ran);
dvdcoe(3,5) = diff(vinc, ape);

dvdcoe(4,1) = diff(vran, sma);
dvdcoe(4,2) = diff(vran, e);
dvdcoe(4,3) = diff(vran, inc);
dvdcoe(4,4) = diff(vran, ran);
dvdcoe(4,5) = diff(vran, ape);

dvdcoe(5,1) = diff(vape, sma);
dvdcoe(5,2) = diff(vape, e);
```

```
dvdcoe(5,3) = diff(vape, inc);

dvdcoe(5,4) = diff(vape, ran);

dvdcoe(5,5) = diff(vape, ape);
```

Bibliography

[1] Barbee, Brent W. Mission Design with MATLAB, Lecture 6: Edelbaum's Low-Thrust Transfer Problem Algorithm. NASA-GSFC Mission Design Class Summer 2011, 2011.

[2] Bate, Roger R., Mueller, Donald D, and White, Jerry E. *Fundamentals of Astrodynamics*. Dover Publications, Inc., 1971.

[3] Battin, Richard H. *An Introduction to the Mathematics and Methods of Astrodynamics, Revised Edition*. American Institute of Aeronautics and Astronautics, Inc., Reston, Virginia, 1999.

[4] Beeker, Gregory L. Continuous, Low Thrust Orbit Transfers with Varying Eccentricity. Master's thesis, Air Force Institute of Technology, 1988.

[5] Bombrun, Alex. Efficient Feedback for Low Thrust Orbital Transfers. In *57th International Astronautical Congress*, 2006.

[6] Chang, Dong Eui, Chichka, David F., and Marsden, Jerrold E. Lyapunov-Based Transfer Between Elliptic Keplerian Orbits. *Discrete and Continuous Dynamical Systems–Series B*, 2(1):57–67, 2002.

[7] Curtis, Howard D. *Orbital Mechanics for Engineering Students*. Elsevier Ltd., Burlington, MA, 2005.

[8] Edelbaum, T. N. Optimum Power-Limited Orbit Transfer in Strong Gravity Fields. *AIAA Journal*, 3(5):921–925, 1965.

[9] Hedrick, J. K. and Girard, A. *Control of Nonlinear Dynamic Systems: Theory and Applications*. Berkeley Press, 2005.

[10] Hindmarsh, Alan C. Serial Fortran Solvers for ODE Initial Value Problems. `http://www.llnl.gov/CASC/odepack` [cited 31 July 2012].

[11] Hull, David G. *Optimal Control Theory for Applications*. Springer-Verlag New York, Inc., 2003.

[12] Joseph, Benjamin E. Lyapunov Feedback Control in Equinoctial Elements Applied to Low Thrust Control of Elliptical Orbit Constellations. Master's thesis, Massachusetts Institute of Technology, 2006.

[13] Kluever, Craig A. Simple Guidance Scheme for Low-Thrust Orbit Transfers. *Journal of Guidance, Control, and Dynamics*, 21(6):1015–1017, 1998.

[14] Larson, Wiley J. and Wertz, James R., editor. *Space Mission Analysis and Design, Third Edition*. Microcosm Press and Springer, 1999.

[15] Lee, Seungwon, Petropoulos, Anastassios, and von Allmen, Paul. Low-Thrust Orbit Transfer Optimization with Refined Q-Law and Multi-Objective Genetic Algorithm. In *AAS/AIAA Astrodynamics Specialists Conference*, 2005.

[16] Maddock, C. and Vasile, M. Extension of the proximity-quotient control law for low-thrust propulsion. In *59th International Astronautical Congress*, 2008.

[17] Naasz, Bo J. Classical Element Feedback Control for Spacecraft Orbital Maneuvers. Master's thesis, Virginia Polytechnic Institute and State University, 2002.

[18] Ocampo, Cesar. Conversion of Position and Velocity Vectors to Classical Element Set. Unpublished course notes for ASE 387P6: Optimal Spacecraft Trajectories, The University of Texas at Austin, Spring 2011.

[19] Ocampo, Cesar. Introduction To The Optimal Control Problem. Unpublished course notes for ASE 387P6: Optimal Spacecraft Trajectories, The University of Texas at Austin, Spring 2011.

[20] Petropoulos, Anastassios E. Simple Control Laws for Low-Thrust Orbit Transfers. In *AAS/AIAA Space Astrodynamics Specialists Conference*, 2003.

[21] Petropoulos, Anastassios E. Refinements to the Q-law for low thrust orbit transfers. In *15th AAS/AIAA Space Flight Mechanics Conference*, 2005.

[22] Petropoulos, Anastassios E. and Lee, Seungwon. Optimisation of Low-Thrust Orbit Transfers Using the Q-Law for the Initial Guess. In *AAS/AIAA Astrodynamics Specialists Conference*, 2005.

[23] Ruggiero, A., Pergola, P., Marcuccio, S., and Andrenucci, M. Low-Thrust Maneuvers for the Efficient Correction of Orbital Elements. In *32nd International Electric Propulsion Conference*, 2011.

[24] VF13AD. `http://www.hsl.rl.ac.uk/archive/hslarchive/packages.new/vf13/vf13.pdf` [cited 31 July 2012].

[25] Whiffen, G. J. Optimal Low-Thrust Orbit Transfers around a Rotating Non-Spherical Body. In *AAS/AIAA Space Flight Mechanics Meeting*, 2004.

[26] Whiffen, G. J. and Sims, J. A. Application of a Novel Optimal Control Algorithm to Low-Thrust Trajectory Optimization. In *AAS/AIAA Space Flight Mechanics Meeting*, 2001.